Optimization of tools for multiplexed super resolution imaging of the synapse

Dissertation

for the award of the degree
Doctor rerum naturalium
of the Georg-August-Universität Göttingen

within the doctoral program IMPRS for Molecular Biology
of the Georg-August University School of Science (GAUSS)

submitted by
Shama Sograte Idrissi

born in
Casablanca, Morocco

Göttingen, 2019

Members of the Thesis Advisory Committee:

Prof. Dr. Silvio O. Rizzoli
Institute for Neuro-and Sensory Physiology, University Medical Center Göttingen

Prof. Dr. Peter Rehling
Institute for Cellular Biochemistry, University Medical Center Göttingen

Prof. Dr. Blanche Schwappach-Pignataro
Institute for Molecular Biology, University Medical Center Göttingen

Further members of the Examination Board:

Prof. Dr. Henning Urlaub
Bioanalytical Mass Spectrometry Group, Max Plank Institute for Biophysical Chemistry

Prof. Dr. Dieter Klopfenstein
Third Institute of Physics, Dept. of Biophysics, University of Goettingen

Dr. Sarah Adio
Department of Molecular Structural Biology, Institute for Microbiology and Genetics, University of Goettingen

Date of oral examination:
16.10.2019

Declaration

I hereby declare that this thesis has been written independently and with no other sources and aids than quoted.

Shama Sograte Idrissi

Göttingen, 1st September, 2019

Contents

1. Abstract:

The synapse is the major site of neurotransmission in the brain. Even though the synapse has been extensively studied, artefact-free imaging tools are still necessary for its correct investigation. With the resolution of modern techniques approaching the molecular size, the main current limitations are the few available affinity probes targeting synaptic proteins and the limited multiplexing abilities of most microscopy techniques. Camelid single-domain antibodies (also called nanobodies) are a superior alternative to conventional antibodies for super resolution microscopy applications. Nanobodies have a significantly smaller size than conventional antibodies; they are monovalent binders, they can reach buried epitopes and can be expressed recombinantly in prokaryotic systems. However, nanobodies against just a few targets are available and their selection is laborious. In this thesis, I first established a pipeline that allows selection, production, and validation of nanobodies against various synaptic proteins. Next, I characterized nanobodies binding selectively to primary antibodies (secondary nanobodies) and compared them in immunofluorescences performed with conventional secondary antibodies. Finally, I also established a protocol for coupling a single-stranded DNA to nanobodies using click chemistry. As a proof of principle, I used this procedure to implement a triple color super resolution Exchange PAINT with an automated microfluidic setup. Altogether, this thesis gives rise to a set of tools that allows the characterization of the neuronal synapses with fewer technical constrains at super resolution scales and minimal artefacts.

2. General introduction

2.1 Synapse characterization

Unraveling the basic principles of brain function is at the center of current scientific research. The *Human Brain Project*, started in 2013 by the European Union, is a billion Euro initiative that aims to advance our understanding of the brain. Its American counterpart, the *Brain Initiative*, has already precisely catalogued the cells of the brain and its connectome. The *JNPD* (The EU Joint Programme – Neurodegenerative Disease Research) engages in the eradication of neurodegenerative diseases. These are just a few examples of the efforts made in understanding the brain, illustrating the imminence of explaining brain mechanisms. To reach this goal, the subcellular level of the brain needs to be equally understood. To do so, purified hippocampal neurons from rodents are commonly used. This primary cell culture is a simplified model to mimic the neural tissue they come from. It is relatively homogenous in its composition, forms synaptic networks and shows consistent characteristics from one lab to another (Benson, Watkins, Steward, & Banker, 1994). This type of primary neuronal culture has been used for the past thirty years because they enable easy manipulations, observation under various microscopy techniques, and a variety of labelling and biochemical tools are readily available to investigate it. Primary hippocampal neurons are therefore a good simplified model to understand basic neuronal functions, communication and how those are altered by neurological impairments.

The synapse is the element that allows communication between neurons. In a standard chemical synapse, the presynaptic side releases neurotransmitters that bind to receptors on the postsynaptic side and trigger a signal in the postsynaptic neuron. This mechanism is mediated through synaptic vesicles that store neurotransmitters and release them by fusing to the cell plasma membrane at the active zone of the presynapse. Synaptic vesicles, after fusing to the plasma membrane, are then retrieved back by endocytosis fused to early endosomes and bud once again as synaptic vesicle. This process is known as the synaptic vesicle cycle and it has been studied in great detail (Rizzoli, 2014). The study of the synaptic architecture and neurotransmitter release mechanism has been performed through a variety of methods. One relevant method for the task has been imaging. Initially electron microscopy provided important

insights such as models of synaptic vesicle recycling (Takei, Mundigl, Daniell, & De Camilli, 1996), More recently, fluorescent imaging, which exhibit good experimental flexibility with sufficient resolution, has been used for example to obtain the quantitative molecular description of the synaptic bouton (Wilhelm et al., 2014) and the molecular organization and distribution of proteins in chemical synapse (Dani, Huang, Bergan, Dulac, & Zhuang, 2010).

2.2 Detection of proteins of interest

Proteins are involved in multiple essential functions in the synapse: they provide structural stability, transport material and are responsible for a variety of different steps in the synaptic vesicle cycle. Endogenous mammalian proteins are *per se* non-visible to the human eye nor to the different light microscopy techniques. In order to image them with fluorescent microscopy, they are usually tagged with a detectable element such a recombinant fluorescent protein or an organic dye.

2.2.1 Recombinant proteins

The green fluorescent protein (GFP) was the first naturally-occurring fluorescent protein that was discovered back in the nineties (Chalfie, Tu, Euskirchen, Ward, & Prasher, 1994). The so-called “green revolution” allowed many biological discoveries by enabling the observation of location and expression of proteins fused to GFP. However, the original GFP suffered from homo-oligomerization, slow folding properties and limited brightness leading to poor signal to noise ratio (Shashkova & Leake, 2017). Variants of this original fluorescent protein have been discovered and designed to improve brightness and photostability (Thastrup et al., 1995), to enhance folding kinetics (Pédelacq et al., 2006), to reduce self-oligomerization and to emit at different wavelengths on the light spectrum (Zacharias et al., 2002). Currently, there are more than five hundred variants of fluorescent proteins with different characteristics (Lambert, 2019). Recently, other types of proteins have been engineered to become fluorescent upon ligand binding. Those are the so-called “self-labelling proteins”: SNAP tag (Keppler et al., 2003), HALO tag (Los et al., 2008) and CLIP tag (Gautier et al., 2008). They are modified enzymes that are fused to the target of interest and will then form a covalent bond with their substrate carrying an organic dye once it is added.

Usually, the use of fused tags, either fluorescent of self-labelling requires the transient overexpression of the protein construct. This has been shown to alter the original endogenous location and behavior of the targeted protein (T. J. Gibson, Seiler, & Veitia, 2013). To overcome these artefacts, stable transfection and direct modification of the endogenous protein with a system like CRISPR-Cas (Jinek et al., 2012) could be used.

2.2.2 Standard immunostaining:

Immunostaining is a common technique that circumvents the modification of the original protein and the potential problems suggested above. It is important to point out that with this approach, in order to label intracellular targets, permeabilization of the cell is necessary and therefore live imaging is difficult.

Conventional immunostaining uses antibodies, mainly immunoglobulin G (IgG), to bind specifically to the protein of interest. IgGs are a heterotetratmeric structure, composed of two identical heavy chain and two identical light chain connected by disulfide bridges. They have two binding identical sites (the paratopes) recognizing a specific sequence of the targeted protein (the epitope). The paratope is composed of a combination of a variable domain of a light chain (V_L) and a variable domain of the heavy chain (V_H). Those two domains are not connected and therefore the minimal functional antigen binding part contains also constant domains of the light and heavy chain (C_L and C_H1) connected by disulfide bonds. This fragment is referred to as antigen binding fragment (Fab) in contract to the rest of the antibody called the fragment crystallizable domain (Fc). The Fc domain of IgGs is composed of four constant domains (C_H2 and C_H3, for each of the two copy of the heavy chain) and is the site of post-translational modification (PTM). The presence of PTM on IgG is a hindrance to cheap fast and simple manufacturing of antibody, since it impedes its production in bacterial hosts and requires mammalian cells host (Lee & Jeong, 2015).

Since antibodies are also *per se* non-fluorescent, they have to be directly coupled to a reporter (such as an organic dye), in this case the process is called direct immunostaining. Otherwise, in a method called indirect immunostaining, a primary antibody raised in a particular animal species binds to the protein of interest and a secondary antibody carrying a reporter (such as a

fluorophore) binds in a specie-specific fashion the primary antibody. The indirect variant of immunostaining is cheaper and more convenient because secondary antibodies targeting every species are commercially available. Another advantage is that multiple secondary antibodies bind a single primary antibody, thereby creating an amplification of the signal obtained, which might be useful in some applications, for example, when the amount of the targeted protein is low.

Antibodies can be either polyclonal or monoclonal. Polyclonal antibodies are produced by different B cell lineage within the animal. They are therefore a mixture of different antibodies targeting different epitopes, allowing further signal amplification (Lipman, Jackson, Trudel, & Weis-Garcia, 2005). In contrast, monoclonal antibodies target a single epitope since they are derived from a single B cell which is then proliferated by creating a hybridoma cell line (Köhler & Milstein, 1975). The use of monoclonal antibodies minimizes batch-to-batch variation and increases consistency in experiments, when compared to the effects of polyclonal antibodies (M. Baker, 2015; Bradbury & Plückthun, 2015). However, the majority of the secondary antibodies used are polyclonals, due to their faster, less expensive and less technical skills required for their production (Lipman et al., 2005).

Standard immunostaining involves a series of limitations. The size of the IgGs (~150 kDa and ~15 nm for, might even double in case of indirect immunostaining) have been shown to hinder the penetration into thick sample and the access to buried epitopes. Their size also increases the distance between the targeted protein and the reporter leading to the imaging of a bigger structure. The latter is known as linkage error or fluorophore delocalization and has been shown to decrease achievable resolution in super resolution microscopy (described below). The bivalency (binding two identical epitopes) and the potential polyclonality of the antibodies might cluster the targeted protein, leading to artefacts like probe-induced clustering. Finally, the reporter (such as an organic dye) is usually linked to the antibody using N-hydroxysuccinimide (NHS) ester coupling chemistry. The reporter reacts with the free secondary amino groups on lysines at the surface of the antibody resulting in an uncontrolled labeling strategy, which can also alter the epitope recognition site (Mattson et al., 1993). The last disadvantage of indirect immunofluorescence is the limited multiplexing capability, i.e. the ability to image different

targets at the same time. In fact, in the same sample, the primary antibodies need to come from different species in order that the secondary antibody used does not cross-react on the different targets. Despites of the pitfalls of conventional immunostaining, it is a well- and long-established method and therefore thousands of antibodies are currently commercially available.

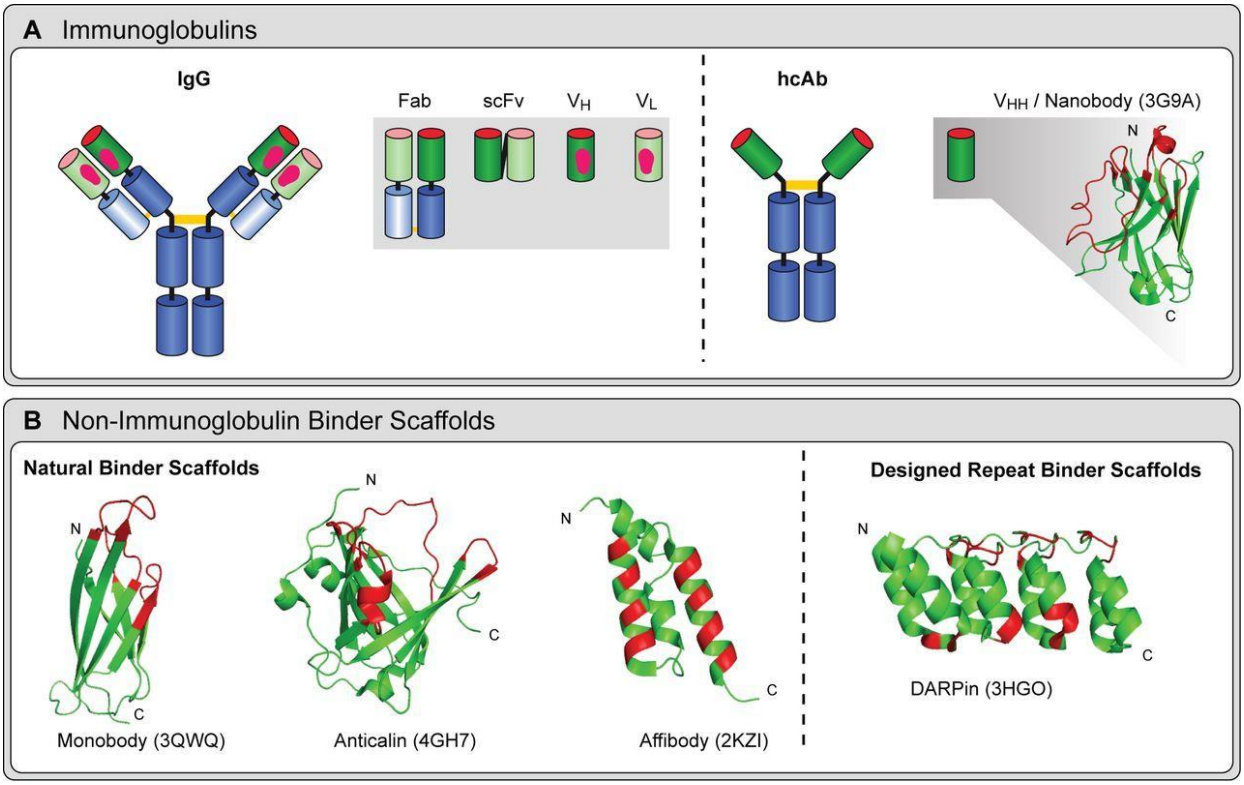

Figure 2.1: Different affinity binders are used to target proteins in immunostaining. (**A**) Immunoglobulin based affinity binders. Conventional antibodies (IgG) and recombinant antibody fragments (left). Heavy chain antibody and recombinant antigen binding domain V_HH or nanobody. Blue blocks are constant domains; green blocks are variable domains. Light chain is in lighter color. (**B**) Non immunoglobulin-based binders. Between brackets the PDB accession number. "N", "C" are N terminus and C terminus, respectively. Adapted from (Helma, Cardoso, Muyldermans, & Leonhardt, 2015).

2.2.3 Alternative probes for staining biological samples

Other types of affinity probes have been developed to overcome some of the limitations of standard antibodies. To reduce the size of the IgG to its minimal binding functional entity is to

get rid of the Fc region. This can be done with the enzyme Pepsin and obtain a Fab2 fragment (i.e. the two Fab regions which stays connected by disulfide bonds), or with Papain to obtain a Fab fragment, a monovalent probe of around 50 kDa and 9 nm in length (Porter, 1959). Fab fragments are composed of four domains (see Fig.2.1): two constant domains C_H and C_L and two variable domains V_H and V_L where L and C stand for light chain and heavy chain respectively. A further attempt to reduce the size of this construct is to form a single chain variable fragment (scFv) which consist of the V_L and V_H connected by an engineered polypeptide linker leading to an affinity probe of ~30 kDa and 6 nm in size (Huston et al., 1988). Optimization of recombinant scFv is complicated in the design of the short peptide linker that needs to maintain the light and heavy chain conformation to be able to recognize the epitope. These antibody fragments are definitely reducing the size of the probe, however, their expression in recombinant form in bacteria is complicated due to the inability of the disulfide bonds to form ensuring proper folding (Vaks & Benhar, 2014).

Other affinity probes not based on immunoglobulin scaffolds have been developed by using other naturally existing scaffolds where random mutagenesis is performed on the binding surface. For example, Affibodies are binders based on the Z domain of staphylococcal protein A (a natural binder to immunoglobulins) and they have a size of 6 kDa and 2 nm (Nord et al., 1996). These probes have been used in many applications such as *in vivo* molecular imaging for tumor diagnosis (Nilsson & Tolmachev, 2007) and super resolution microscopy (Gomes de Castro et al., 2019). Along the same line, Adnectins, also known as Monobodies, were formed by the framework of the extracellular domain of human fibronectin III (Koide & Koide, 2007). They were modified and used as a FRET sensor for imaging intercellular junctions (Limsakul et al., 2018). Other examples are Anticalin (~30 kDa) or DARPins (~14 kDa) both derived from modified scaffolds of naturally binding proteins (Plückthun, 2015; Skerra, 2008). Affimers are derived from a synthetic protein called the Adhiron scaffold (Tiede et al., 2014) and were used to increase the resolution power of single molecule localization microscopy (Schlichthaerle et al., 2018). Nucleic acids have also been explored for their ability to be used as affinity probes. For instance, aptamers, or their higher affinity binding versions Somamers, are single-stranded DNA or RNA based probes, *in vitro* selected through systematic evolution of ligands by exponential enrichment methods (SELEX) (Gupta et al., 2011). They recognize their target

through their three-dimensional structure. Thanks to their small size (~15 kDa), they can penetrate tissues and bind previously inaccessible epitopes and clearly define cellular structures in the context of super resolution microscopy (Opazo et al., 2012; Strauss et al., 2018).

2.2.4 Nanobodies

One type of alternative small probes that deserves particular attention are the single-domain antibodies also known as nanobodies® (trademark by the company *Ablynx*). Nanobodies are derived from a peculiar type of antibodies that are devoid of light chains, thus termed heavy chain antibody (hcAb) and can be found in camelid like camels, llamas alpacas and interestingly also in sharks (Greenberg et al., 1995; Hamers-Casterman et al., 1993). In camelids, the hcAbs coexist with the conventional IgGs that are named IgG1. In the hcAbs, the antigen binding part is composed of a single domain, the variable domain of the hcAbs (V_HH) and is linked directly to the constant domains (to the C_H2) by the hinge region. The different length of this hinge region gives rise to two isotypes of hcAbs: the IgG2 and the IgG3. Because of the simplicity and lack of post-translational modification, the V_HH can be expressed as a recombinant protein in bacteria (Muyldermans, 2001). In this thesis, the V_HH expressed as recombinant binding domain will be called nanobody or Nb, as it is also commonly referred to in the literature. Nanobodies have a size of 15 kDa and 2-3 nm. They do not have a light chain, which might be interpreted as reduction of binding surface and therefore render lower affinity to their targets when compared to the conventional antibodies. However, the affinity of the V_HH to its cognate antigen is not necessarily lower, in fact, affinities in the low picomolar range have been measured (Götzke et al., 2019; Soler, Fortuna, de Marco, & Laio, 2018). This is attributed to their complementarity determining regions (CDRs) which are in average longer than in a classical antibody and thus increasing the interacting surface to the antigen. The CDRs of nanobodies form protruding loops that have also been associated with reaching buried or convex epitopes, which are inaccessible to conventional IgG. This peculiarity gave a wide range of special applications to the nanobodies such as inhibition of enzymes by binding to their catalytic site (Chaikuad et al., 2014; Lauwereys et al., 1998), or the inhibition of viral infection by competing for the host receptor (Desmyter et al., 2013). In addition, nanobodies have been used as crystallization chaperones (Lam, Pardon, Korotkov, Hol, & Steyaert, 2009), in medical diagnosis and *in vivo* imaging (D'Huyvetter et al., 2014).

Nanobodies have also been used in super resolution imaging and have been shown to increase the resolution obtained (Maidorn, Olichon, Rizzoli, & Opazo, 2019; Ries, Kaplan, Platonova, Eghlidi, & Ewers, 2012). They are easily conjugable to moieties such as fluorophores in a site-directed manner (Pleiner et al., 2015).

The classical route to generate nanobodies against specific target needs the immunization of a camelid with the specific antigen. Naive libraries (obtained from not-immunized animals) and synthetic libraries (variability comes from synthetically produced nanobodies with randomized sequences on their CDRs) have also been used to screen for target-specific nanobodies (Kumaran, MacKenzie, & Arbabi-Ghahroudi, 2012; Yan, Li, Hu, Ou, & Wan, 2014; Zimmermann et al., 2018). To identify nanobodies against a specific target, those libraries are screened by different display techniques (Liu et al., 2018). Phage display, one of the most used screening methods, permits the selection of antigen-specific binding molecules from a library of different binders expressed as fusion proteins with a bacteriophage coat protein (Smith, 1985). This method uses bacteriophages to create a physical linkage between the genotype, the encapsulated DNA coding for the binder, and the phenotype, the displayed protein fused to a surface phage protein able to bind the intended target. Recently, an alternative method uses next generation sequencing (NGS) and mass spectrometry to establish this gene-protein link (Fridy et al., 2014).

2.3 Fluorescence imaging and super resolution microscopy

Fluorescent microscopy is currently the most commonly used method to image cells. It beats its *competitor* methods such as electron microscopy and scanning probe microscopy by its ability to introduce molecular targeted contrast and its possibility of live imaging. The resolution of fluorescent microscopes (i.e. its ability to separate two different objects) is however limited by the diffraction of light. This is described by Abbe (Abbe, 1873) putting the resolution as a function of the numerical aperture of the microscope and the wavelength used to excite the object. In ideal settings, this number reaches around 200 nm for the visible spectrum in the lateral dimension (i.e. in the direction perpendicular to the light propagation) which is bigger than the subcellular structures we are interested in imaging in the synapse. For example, synaptic

vesicles are around 40 nm in diameter (Qu, Akbergenova, Hu, & Schikorski, 2009) and therefore cannot be resolved by diffraction-limited microscopy.

With the advent of super resolution microscopy that it has been in continues development during the last fifteen years, the diffraction limit has been not only overcome, but subcellular elements smaller than 5 nanometers could be imaged (Schermelleh et al., 2019). The super resolution microscopy techniques rely on the control or switching "off" and "on" the fluorescence emission. This modulation allows neighboring fluorescent objects to be resolved independently of the light diffraction. This control has been exercised mainly in two different ways leading to two different categories of super resolution microscopy. One of such categories controls spatially the status of the fluorophore. The most commonly used technique that matches this category is Stimulated emission depletion (STED) microscopy (Hell & Wichmann, 1994). In STED microscopy, the illumination pattern is controlled by scanning the sample with two overlapping beams. One beam excites the fluorophore while the other beam has a doughnut shape and depletes the emitted fluorescence (STED depletion beam). The fluorescent emission of only the center of the doughnut is then recorded (Fig.2.2)

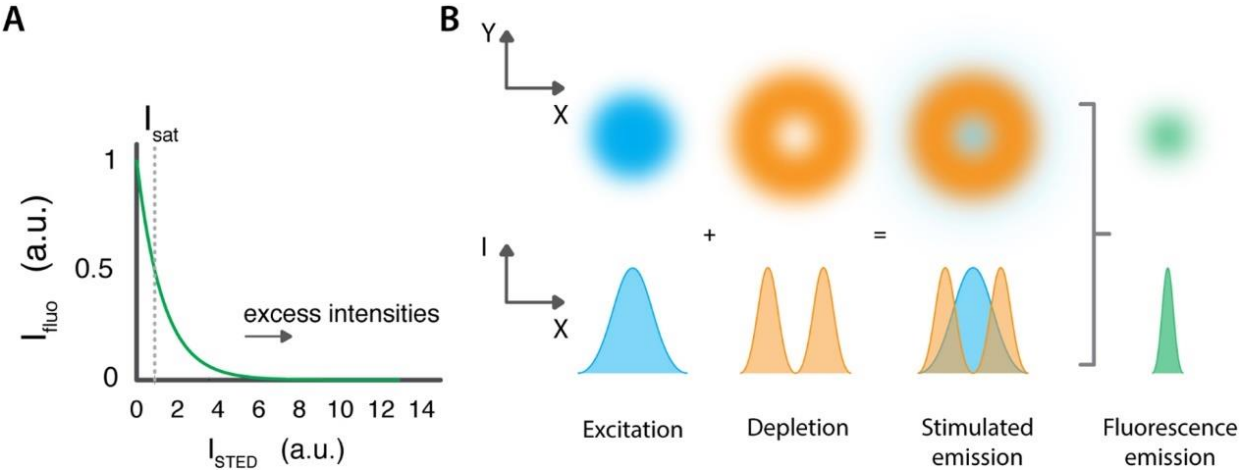

Figure 2.2: The basic principle of STED microscopy. (A**)** Probability of the fluorophore to emit (I_{fluo}) as a function of the intensity of the STED depletion beam (I_{STED}). After a certain threshold (I_{sat}) the molecule ability to emit is reduced to 50 %. (**B**) The excitation beam overlaps with a doughnut shaped beam that depletes the fluorescence locally. The resulted recorded fluorescence has a narrower diffraction pattern. Adapted from (Vangindertael et al., 2018)**.**

The second group of techniques controls the status of the emitter temporally. This group of techniques falls under the name of single molecule localization microscopy (SMLM).
Members of this group are Photo-activated localization microscopy (PALM) (Betzig, 2015) and stochastic optical reconstruction microscopy (STORM) (Rust, Bates, & Zhuang, 2006). Switching the emitter "off" and "on" in a stochastic manner creates a "blinking" pattern that is recorded over thousands of frames. The individual, separated localized signals can be fitted with a Gaussian and its center position can be precisely calculated. The image is then reconstructed from the position of the individual fluorescent molecules. It is worth mentioning a very recently developed technique that combines the properties of both STED microscopy and PALM/STORM: MINFLUX (Balzarotti et al., 2017). Here, photo switchable fluorophores are used and are located through a doughnut-shaped excitation beam. The localization of the emitter is determined by the position of the laser, since when located in the center the emission is zero, reducing drastically the need of photons required and therefore reaching up to one nanometer localization precision (Balzarotti et al., 2017).

The above-mentioned approaches are dependent on the photophysical properties of the fluorophores, such as blinking, quantum yield, dark state recovery or bleaching properties. Another SMLM technique, termed DNA-points accumulation for imaging in nanoscale topography (DNA-PAINT), managed to overcome this dependence (Jungmann et al., 2010). In fact, in this approach, the "blinking" pattern is obtained by repetitive transient binding of a fluorophore diffusing in the sample solution. A short single-stranded DNA called the imager strand carries the fluorophore. The imager strand is complementary to a short single strand DNA called the docking strand that is attached to the target (or to an affinity probe binding the target) (Jungman et al., 2010) (Fig 2.3). This approach allows 1) overcoming the risk of photobleaching of the fluorophore since there is a constant replenishment of fluorophore brought by the repetitive binding of the imager strand diffusing freely in the solution 2) fine-tuning of the blinking kinetics. The binding duration can be controlled by modulating the stability of the DNA duplex formed by imager and docking strand (by modulating GC content, salinity of the imaging buffer etc.). While the binding frequency can be controlled by the influx rate of imager strand (Schnitzbauer, Strauss, Schlichthaerle, Schueder, & Jungmann, 2017). To overcome the potential compromise of the fluorescent background of the unbound imager strand in solution,

the imaging is typically done with a selected plane illumination such as Highly inclined thin illumination (HILO), Total internal reflection fluorescence (TIRF), or with a spinning disk confocal microscope (Schueder et al., 2017). All of these diffraction unlimited fluorescence microscopy techniques enable the localization and study of proteins at high resolution necessary for the analysis of synaptic components.

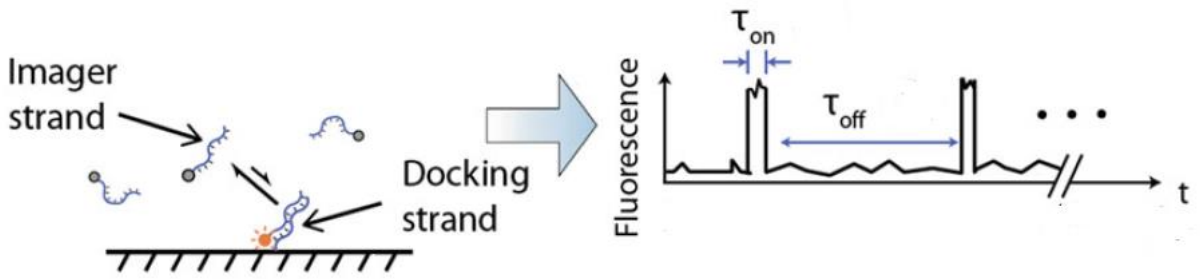

Figure 2.3: The principle of DNA-PAINT. The imager strand carrying the fluorophore diffuses in solution and bind transiently to the docking strand present on the target. This binding is detected as "blinking": an increase in fluorescence in time. Adapted from (Dai, 2017).

2.4 Multiplexed imaging

To be able to study the molecular organization of the synapse, there is a need for an imaging technique with multiplexing (also known as multicolor) capabilities i.e. imaging several different targets of interest in the same sample. This simultaneous detection of targets is extremely beneficial because it allows the study of inter-molecular interactions and provides contextual information by using markers of structural/functional areas. Limitations of the multiplexing capabilities of microscopy techniques lie mainly in the spectral overlaps of multiple dyes, the physical limits of the microscope (such as the available filters), and the limitations of the affinity probe (Stack, Wang, Roman, & Hoyt, 2014). In the following sections, I will outline the fundamentals of these limitations and how they have been partially overcome.

2.4.1 True multicolor imaging

Organic dyes and fluorescent proteins used in fluorescence microscopy have each of them specific emission spectrum. The spectra of different dye in the same sample needs to be

separated in order to unambiguously identify them. Therefore, in fluorescent microscopy, the choice of fluorophores is limited to combinations that do not overlap in their emission spectra. Most microscopes are able to separate up to 4 different dyes (Stack et al., 2014). To reduce overlap of the emission spectra of the different target, quantum dots have been used. Quantum dots (QDs), are semiconductor nanocrystals that have a higher brightness and photostability than organic dyes (Walling, Novak, & Shepard, 2009). QDs provide the advantage of having a narrower emission peak compared to the standard organic dyes enabling better spectral separation (Zrazhevskiy & Gao, 2013). However, their cellular toxicity have been the subject of debates (Hardman, 2006). Even if the quantum dots are in the nanometer range, they require to be conjugated to other molecules in order to target them to the protein or the affinity probe that increases their intrinsic size (Weng & Ren, 2006). Spectral overlaps can also be separated thanks to spectral imaging and linear unmixing. This can be done with a standard fluorescent microscope equipped with a multispectral camera. The spectra of the fluorophores are registered in a library before imaging. The intensity of the fluorophores is then extracted from the multispectral data by linear unmixing (Mansfield, Vet Pathology 2014).

Multiplexing is an even more difficult topic when it comes to the super resolution microscopy approaches. In fact, PALM/STORM microscopy and derivative techniques that rely on switching organic dyes or fluorescent proteins are limited by the requirements of the fluorophore (high photon yield and short “on” state to ensure high resolution) and the buffers necessary for the blinking. These conditions tend to vary drastically from one fluorophore to another and therefore imaging has been limited to 4 super resolved colors in exceptional works (Dempsey et al., 2011). STED microscopy suffers from the needs of multiple laser lines to function. For a single super-resolved color, both an excitation and a depletion laser are needed, reducing the number of available channels for other dyes. STED has been successfully expanded to three colors by discriminating the specific lifetime associated to each particular dyes, using dyes with a large Stoke shift (emission farther than normal in respect to the excitation wavelength) (Sidenstein et al., 2016).

2.4.2 Sequential staining-imaging

All of the above-mentioned techniques achieve a limited number of targets that can be potentially imaged at the same time. To increase this number, cycles of staining and imaging have been performed. Between cycles, targeted bleaching, high pH, peroxides, or alkaline buffers (Lin et al., 2016) eliminate the fluorescence. The images of the different staining cycles are later superimposed. This sequential labelling and imaging strategy are a time-consuming methodology. In addition, the sample integrity might be compromised and the inactivation of the previous dye might not be completed, leading to artefactual signal cross talk. Recently, a protocol has been established to maintain sample integrity and reduce reactive oxygen species production, but still guaranteeing proper elution of antibodies (Gut et al., 2018)

To overcome the sequential staining, other approaches have been developed, where the fluorescent moiety is introduced during the imaging process. One example was done by Schweller et al., who used dynamic DNA COMPLEXES to sequentially add and remove the fluorescence to the targets associated with DNA strands by strand displacement. However, the strand displacements required are long reactions, and to “erase” the fluorescence of each target, an overnight reaction is needed (Schweller et al., 2012). Another example is an extension of the DNA PAINT technique, to what is known as Exchange PAINT (Jungmann et al., 2014). This approach relies on the sequential imaging of the different targets by introduction and removal of a specific imager strand to the solution. In this way, the different “imager strands” targeting the different “docking strands” can carry the same fluorophore. By using the same fluorophore, chromatic aberrations can be avoided and the limits due to the availabilities of dyes with different emission spectrum can be removed. This expands the targets that can be imaged to virtually infinite numbers (Schueder et al., 2017b). This approach has been successfully applied for up to 10 targets on a single cell (Agasti et al., 2017). A more recent variant of this technique introduced in addition to a DNA sequence barcoding, a kinetic barcoding. Meaning that different targets are tagged with different docking strands recognized by the same imager having however different frequency and duration of *blinking* according to the docking strand length of the target. In this way, Wade et al. could recognize 124 different DNA origami structure with 97 % accuracy (Wade et al., 2019). This method was however not yet applied to a complex sample such as a cell or tissue.

2.5 Aim of this work

This work primarily aims to establish the basics to study the molecular composition of a neuronal synapse in multiplexed super resolution microscopy. In particular, I aim to 1) bypass some of the current limitations of conventional probes used for labeling synaptic targets 2) enable the use of alternative probes in highly multiplexed imaging methods.

To reach these objectives, I first focus on the development of nanobodies targeting the synapse and establish a pipeline for their discovery, selection, and validation. To enlarge the number of synaptic targets that can be studied, I also aim to characterize systematically the use of secondary nanobodies and their advantage over conventional secondary antibodies. Finally, I aim to establish a protocol for site targeted conjugation of a single-stranded DNA to nanobodies in order to be used for Exchange-PAINT.

3. Synaptosome-immunized alpacas lead to Nanobodies targeting synaptic proteins

Shama Sograte-Idrissi[1,2,3,], Karine Villa Real[2], Manuel Maidorn[1,2,3], Nora Baligacs[2], Felipe Opazo[1,2,*]

[1]Institute of Neuro- and Sensory Physiology, University Medical Center Göttingen, 37073 Göttingen, Germany

[2]Center for Biostructural Imaging of Neurodegeneration (BIN), University of Göttingen Medical Center, 37075 Göttingen, Germany

[3] International Max Planck Research School for Molecular Biology, Göttingen, Germany

[*] Corresponding Author: fopazo@gwdg.de

3.1 Abstract

Single domain antibodies (also called nanobodies) derive from camelid heavy chain antibodies (hcAbs) have been proven a better alternative to conventional antibodies for the detection of proteins. However, the current availability and target diversity of nanobodies are limited due to the long and laborious production necessary. Here we optimized a pipeline for the production of nanobodies targeting different neuronal synaptic proteins. We immunized alpacas with a synaptosome preparation enabling potential immune reaction of the alpacas against a wide range of synaptic proteins. To assess the generation of hcAbs against a specific protein, we established an enzyme-linked immunosorbent assay based protocol. Based on the outcome of this protocol we performed phage display selection for those targets. Using this selection approach, we successfully generated nanobodies with different binding abilities toward rat Vesicle-associated membrane protein 2 (VAMP2), human and mice 2',3'-Cyclic-nucleotide 3'-phosphodiesterase (CNPase), rat Bassoon, rat Homer1 and rat Synaptotagmin 1 (Stg1).

Graphical abstract

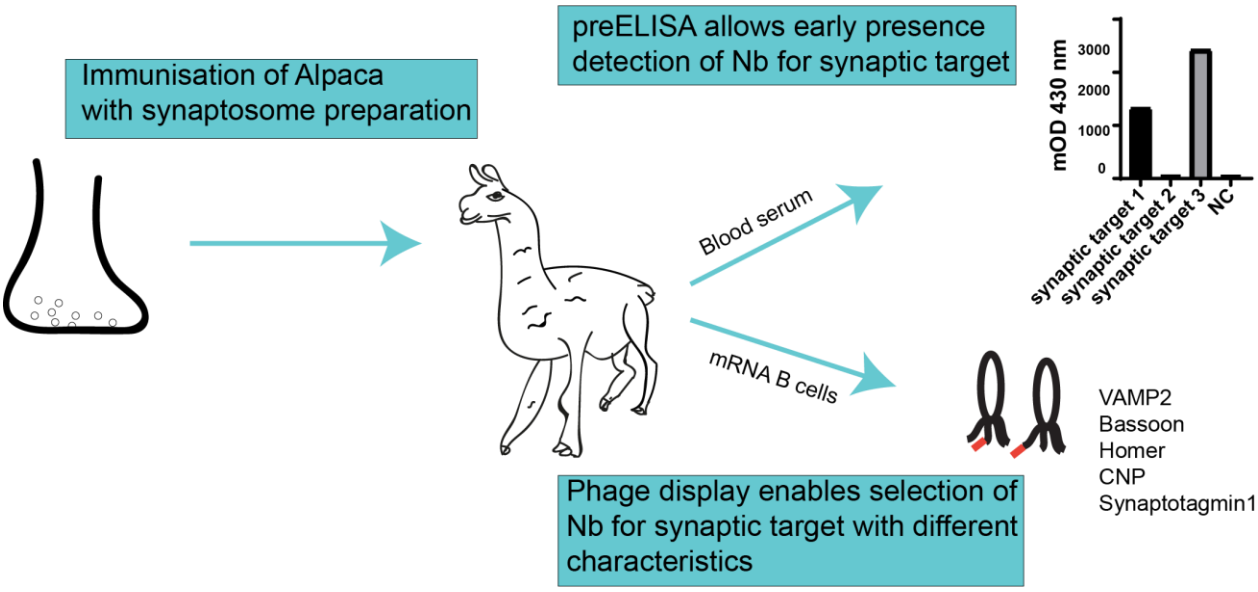

3.2 Introduction

The synapse is an essential component of the nervous system necessary for the transmission of signals. To study synapse in depth, we need probes to target their components. Up to now, a wide range of probes has been used to target the synaptic proteins. In particular, antibodies targeting synaptic proteins keeps enabling different scientific achievement. An example is the quantification of synaptic proteins by imaging and biochemical methods (Wilhelm et al., 2014) using antibodies. However, antibodies have also been shown to be not ideal probes because of their large size, bivalency or limited access to hidden epitopes (Maidorn, Rizzoli, & Opazo, 2016). Nanobodies are single domain antibodies originating from camelid heavy chain antibodies (hcAbs) (Hamers-Casterman et al., 1993) that have been shown to overcomes some of the limitations present in conventional antibodies. Thanks to their small size, high solubility and monovalent nature nanobodies allow quantitative labeling, lower linkage error and consequent higher imaging resolution and decreased probe-induced clustering (Maidorn et al., 2016; Mikhaylova et al., 2015).

Nanobodies targeting synaptic proteins were able to reveal a previously unobserved population of the Soluble NSF Attachment protein Receptor (SNARE) proteins (Maidorn et al., 2019) and were used as tools to inhibit neurotransmitter receptors (Schenck et al., 2017). Due to the scarce availability of nanobodies for specific targets, previous studies used nanobodies against fluorescent proteins to investigate the neuronal processes. For example, nanobodies against GFP were used to measure neurotransmitter receptor dynamics (Modi, Higgs, Sheehan, Griffin, & Kittler, 2018) or to study synaptic vesicle redistribution (Seitz & Rizzoli, 2019). However, utilizing fluorescent proteins through genetic engineering of cell lines is long and laborious. Also, using the fastest transient transfection can impair the endogenous function and localization of the protein of interest (Wiedenmann, Oswald, & Nienhaus, 2009).

To overcome those limitations, we immunized two alpacas (Alp1 and Alp2) with a rat synaptosome preparation. This strategy should avoid single immunizations of single purified antigens and gives the theoretical potential to generate nanobodies against all synaptic targets present in the synaptosomes. When immunizing animals with a complex antigen like synaptosomes, it is challenging to predict which proteins present in the synaptosome preparation were more or less immunogenic, thus creating an unknown factor for the next step of the

discovery phase. For this reason, we established a protocol based on an enzyme-linked immunosorbent assay (ELISA) which assesses the presence or absence of hcAbs (nanobody precursor) for specific targets by using the immunized animal serum, before starting the full *in vitro* phage-display process. We termed this assay preELISA and the shortage of available nanobodies, and we decided to create a pipeline to identify many different nanobodies against different synaptic proteins. To then select nanobodies, we tried a recently published protocol claiming to produce a large repertoire of nanobodies against a given antigen by using a combination of Next Generation Sequencing (NGS) and Mass spectrometry (MS) (Fridy et al., 2014). The proof of concept showed by Fridy and colleagues, seemed successful when using a single very immunogenic antigen at a time. In fact, they immunized the animal with GFP and RFP, which are both very immunogenic proteins not endogenously present in mammals. However, we found this approach unsuitable for finding nanobodies in complex immunizations like ours using full rat synaptosomes. Several proteins might be too close to the alpacas´ endogenous proteins, and therefore they might not produce an immune response to avoid generating an auto-immune reaction in the animal. We therefore decided to use the conventional approach of phage display. To do so we first generated a nanobody library fused in a customized phagemid called here the “minimal phagemid”. This phagemid has a short sequence of 2800 bp that guarantees high transformation efficiency and therefore produces nanobody libraries with high diversity. We selected nanobodies against rat Vesicle-associated membrane protein 2 (VAMP2), human and mice 2',3'-Cyclic-nucleotide 3'-phosphodiesterase (CNPase), rat Bassoon, rat Homer1 and rat Synaptotagmin 1 (Stg1) all of them exhibiting different binding characteristics.

3.3 Results

3.3.1 PreELISA for assessment of presence of nanobodies

Two alpacas were immunized with a synaptosome preparation to allow the selection of nanobodies against synaptic proteins. To assess the presence of hcAbs, before starting the selection process such as phage display and NGS-MS combination, we established a preELISA. As depicted in Fig 3.1 A, the general procedure of preELISA requires a small amount of the specific protein of interest, a small amount of serum from the immunized animal, and an antibody set coupled to the enzyme horseradish peroxidase (HRP) detecting alpaca antibodies. The protein of interest was either immobilized on a 96 well plate in a purified form or by using directly the cell lysate of cells expressing the protein of interest. The serum was enriched in hcAbs (isoform IgG2 and IgG3) or depleted from the conventional antibodies (isoform IgG1) by affinity chromatography. We injected the full serum into a Protein G column. After extensive washes, we sequentially eluted the bound fractions with pH 3.5 and pH 2.7 that resulted in two distinct peaks, as shown in the chromatogram (Fig. 3.1 B). Those two peaks, according to the literature, were expected to contain the majority of IgG3 and IgG1, respectively. We collected the flow through and injected it on a Protein A column. Again, a sequential elution at pH 4.0 and pH 2.7 resulted in two distinct peaks expected to be IgG2 and IgG1, respectively. We then ran on ab SDS-PAGE the collected fractions. The fractions eluted at pH 2.7 showed the presence of two bands: a band at 30 kDa that corresponds to the light chain with an expected molecular weight (MW) of 25 kDa), and a band at 60 kDa that corresponds to the heavy chain with expected MW of 50 kDa. These bands confirm the nature of those fractions as IgG1 isoforms and where therefore discarded. The fact that the bands in SDS-PAGE showed always a higher molecular weight than expected was observed throughout this project and probably came from using a ladder displaying expected size not fully optimized to our SDS-PAGE setup. The fractions eluted at pH 3.5 and pH 4.0 showed a band running lower than the IgG1 heavy chain that corresponds to the heavy chains of IgG3 and IgG2 with and expected MW of 45 and 43 kDa, respectively confirming the isotype of these fractions (Fig. 3.1 B). In the IgG3 mainly enriched fractions, we could observe a light chain contamination, which was further depleted by incubation with beads, conjugated to antibody anti llama light chain, however traces of contaminant remained (data not shown).

Before measuring the actual presence or absence of hcAbs against a specific target, we performed a series of negative control experiments. We measured the background signal absorbed at 430 nm, which is the wavelength at which the preELISA is revealed, generated by the different elements used in the preELISA (Fig. 3.1 C). Then we compared these background signals to the absorption at 430 nm of the positive control (PC). The PC consisted of coated cell lysate (CL) of cells expressing a control construct detected by an anti-GFP antibody fused to HRP. The control construct was composed of the tags, which were fused to the antigens of interest: GFP, twin strep-Tag (tst) and HA tag. When analyzing the different negative controls, we observed that the incubation on the wells of the anti mouse-HRP alone (NC1) and in combination with the mouse anti llama antibody (NC2) displayed low levels of absorption compared to the PC. Later during the course of the project, we obtained an antibody anti llama directly conjugated to HRP which also showed low background signal compared to the PC (data not shown). We also observed that the incubation of CL of cells expressing no exogenous proteins or expressing the control construct (NC3 and NC4) displayed low absorption. We also tested the stickiness of the enriched serum, to confirm that only the antigen-bound hcAbs will be detected by our preELISA (NC5 and NC6).

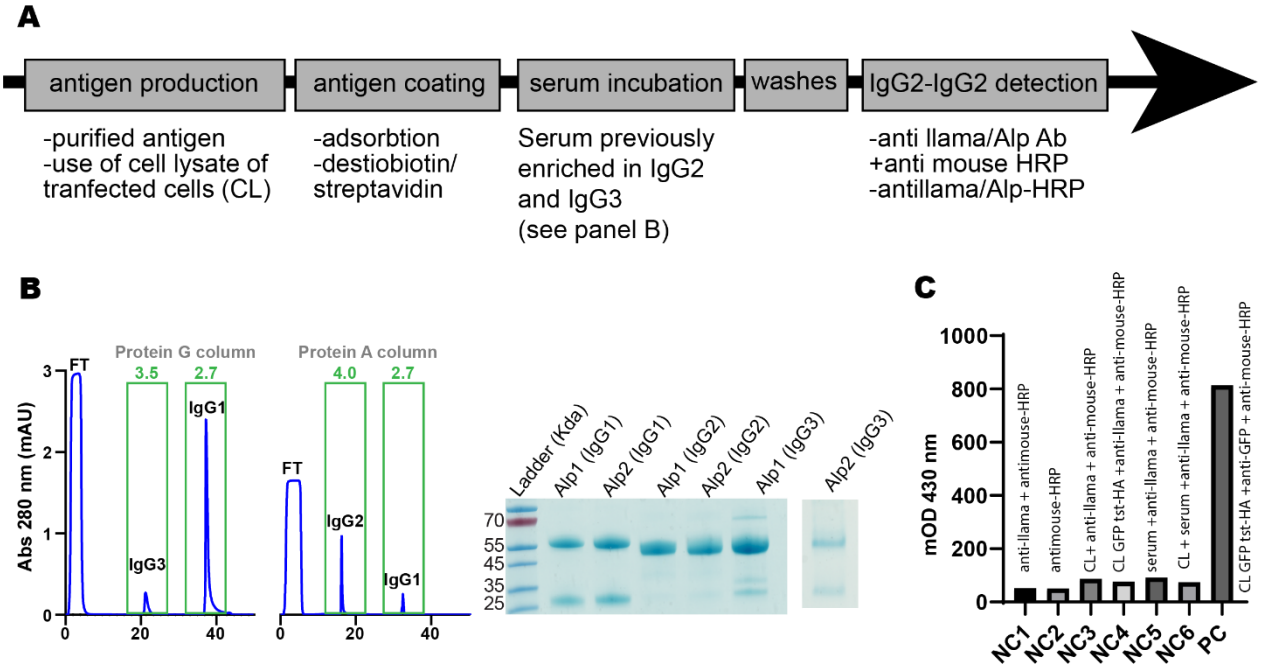

Figure 3.1. preELISA assesses the presence/absence of Nanobody against specific synaptic target before starting the selection process. (**A**)Schematic representation of the preELISA and different options (**B**) HPLC chromatogram of serum enrichment through Protein G and Protein A column and elution at different pH depicted in green. *FT*: Flowthrough i.e. unbound fraction; the expected IgG isoform is depicted on the top of the chromatogram peaks. SDS PAGE shows that expected isoform are the main component of the collected fractions. (**C**) preELISA preliminary negative controls shows low background absorbance at 430 nm and evident difference to positive control. CL= cell lysate, tst= twin Strep-Tag, HA= HA tag, serum= enriched serum, NC= negative control, PC= positive control.

3.3.2 Alternative nanobodies selection through NGS-MS approach

We tested an NGS-MS approach as an alternative to the conventional phage display method to select nanobodies. We created a database containing the nanobody sequences from the immunized alpacas. To do so we extracted the peripheral blood cells of the animals, isolated their mRNA and retrotranscribed the binding domain of the hcAbs (the nanobodies) into cDNA by using specific primers. We then performed NGS and *in silico* translated the data into protein sequence database (Fig. 3.2 A upper line). After several NGS runs the database was composed of 10^6 non-redundant nanobodies sequences from the two animals. In parallel, we immobilized antigens to select nanobodies able to bind specifically to the antigen of interest; the bound fraction was then submitted to MS. (Fig. 3.2 A lower lane). We then determined the sequence by matching the peptides revealed by MS to the previously ensemble nanobody database (at the protein sequence level).

We tested this approach for the antigens VAMP2 and Phosphatidylinositol-4-phosphate 3-kinase C2 domain-containing alpha polypeptide (PIK3C2a) that showed positive preELISA (Fig. 3.2B). To reduce the number of non-relevant flying peptides in the MS, which could mask the peptides necessary for identification, we digested the hcAbs of the enriched serum with the IdeS enzyme. The IdeS enzyme is a cysteine protease which specifically cuts IgGs at their hinge region (Von Pawel-Rammingen, Johansson, & Björck, 2002). The previously observed band at 50 kDa of the enriched serum (Fig. 3.1 B, SDS PAGE) was not detected, and we could observe

a smear of bands ranging between 35 and 15 kDa (Fig. 3.2 C). These bands represent the FC domains of the hcAbs and the binding domain with different hinge region lengths. We then performed the affinity selection of the nanobodies by incubating the digested hcAbs to immobilized antigen. We immobilized on streptactin-coated beads the antigens in two different conformations: the native one and the one the antigen is expected to be detected in immunostaining i.e. cross-linked by chemical fixation (4% PFA). After binding of the hcAbs to the antigen and extensive washing (<2 hours) we eluted the bound nanobodies. For eluting the bound nanobodies, we tested different approaches. We eluted either by addition of biotin (EB), by denaturation (ED) and in the case of the fixed antigen elution by acidic pH (EA). We compared the bands obtained on SDS-PAGE (Fig. 3.2 C). As expected, we observed the band representing the antigen when eluting by denaturation of by biotin for the unfixed antigen. The elution by denaturation also released the streptactin from the beads leading to a band at around 10 kDa. The nanobodies are expected to be seen between 35 and 15 kDa however we could see just really faint smear or no bands at all (Fig. 3.2 C). This might be due to the low amount of target-specific nanobodies present. We cut this particular region and sent it to collaborators to be analyzed by MS, and matched the obtained peptides to the nanobody database previously created. To ensure the correct matching we established a matching score take took the following elements into account:

1) The number of peptides identified by MS which lead to the identification of a nanobody sequence.

2) The coverage of those peptides to the full nanobody sequence; giving a higher score if the peptides covered complementary determining regions (CDRs) of the nanobody.

3) The uniqueness and the selectivity of the peptide i.e. was the peptide found in the negative control or just in the experimental conditions?

After scoring, manual analysis was performed to narrow down the number of best candidates. This was done taking in consideration the similarity of the nanobodies with best scores and their amino acids compositions (higher solubility and low amount of cysteine, which would ensure proper expression in bacteria). The DNA sequences of the best ten nanobodies candidates for each antigen were then synthetized by a company and cloned into a bacterial expression vector containing a 3xFLAG tag for further validation. A high-throughput validation workflow was established: low scale bacterial expression of the nanobody candidate and use of the bacteria

lysate to stain mammalian cells transfected with the target antigen fused to GFP. The presence of a binding nanobody to the cell was then revealed by an antibody targeting the 3xFLAG tag. A Pearson correlation analysis between the GFP and the 3xFLAG signal was performed. As a positive control, an already validated GFP nanobody was expressed in the same vector cassette as the nanobody candidates. One of the PIK3C2a Nb candidates, clone 68 gave positive results in the established immunostaining workflow validation (Fig. 3.2 D) while VAMP2 did not (data not shown). The clone 68 was therefore analyzed deeply by cloning into a vector containing an ectopic cysteine at the carboxyl terminal of the nanobody, by higher scale expression and site targeted maleimide labeling to a Cy5 dye. However, in this case the GFP signal and the Cy5 did not correlate (Fig. 3.2 E). We then tested the efficiency of the PIK3C2a nanobodies candidates to recognize their target in a native conformation by Nb pull down of the target. A Western Blot was also performed identifying the bound nanobody through its 3xFLAG tag (Fig. 3.2 F). Interestingly clones that did not work in immunostaining, recognized successfully the target in this experimental setting. Suggesting that the epitope of these nanobodies might be modified by the use of chemical fixatives, which impairs the nanobody binding to the aldehyde fix target protein, but not if the protein is in a native condition.

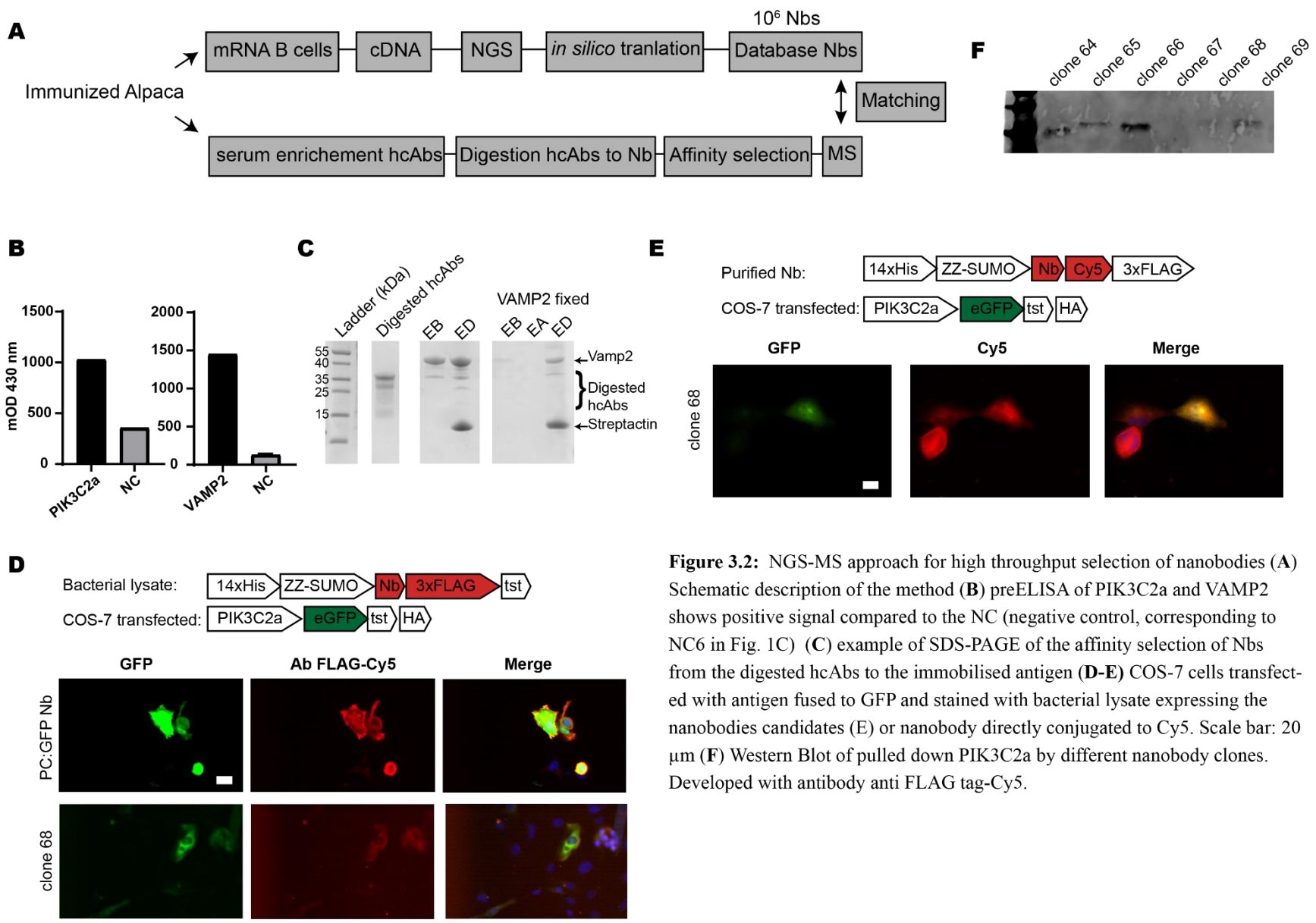

Figure 3.2: NGS-MS approach for high throughput selection of nanobodies (**A**) Schematic description of the method (**B**) preELISA of PIK3C2a and VAMP2 shows positive signal compared to the NC (negative control, corresponding to NC6 in Fig. 1C) (**C**) example of SDS-PAGE of the affinity selection of Nbs from the digested hcAbs to the immobilised antigen (**D-E**) COS-7 cells transfected with antigen fused to GFP and stained with bacterial lysate expressing the nanobodies candidates (E) or nanobody directly conjugated to Cy5. Scale bar: 20 µm (**F**) Western Blot of pulled down PIK3C2a by different nanobody clones. Developed with antibody anti FLAG tag-Cy5.

3.3.3 Synaptosome library generation in minimal phagemid enables higher transformation efficiency

Due to the relatively high cost and poor results with the NGS-MS approach, we turned to the phage display method to select nanobodies against synaptic targets. We used a nested PCR approach to retro transcribe and amplify the nanobody sequences from the total mRNA of the peripheral blood mononuclear cells (PBMCs) of the immunized animals (Fig. 3.3 A). Animal´s blood was drawn several times after the last boost immunization and the mRNA samples were processed to perform the nested PCRs. The PCR product obtained was at the expected base pair size of an average nanobody (around 800 bp) (Fig. 3.3 B). Those PCR were pooled and cloned into a modified version of phagemid that contains a truncated version of the pIII coat protein of the M13 bacteriophage. The reduced size should allow a more efficient transformation efficiency in TG1 bacteria leading to library with high diversity. The phagemid elements are: a Lac operon, a signal peptide to lead the assembly of the phage particles to the periplasm of the bacteria (pelB), a 3xFLAG tag to facilitate the validation process and a TEV protease site to permit removal of the 3xFLAG tag and pIII if necessary (Fig. 3.3 C). The phagemid has an antibiotic resistance against Trimethoprim (Tmp) which has a shorter sequence than the commonly used Ampicillin (Amp) and Kanamycin (Kan) reducing further the plasmid size. The minimal phagemid has a mCherry at the site in which the nanobodies should be inserted by cloning, enabling the analysis by eye if the proper transformation of the nanobody. By looking at the lack of red color of the plated bacterial colonies could estimate that 99% of the transformant have lost the mCherry. It is convention to estimate the diversity of the nanobody library created by plating dilution of the transformation and counting the number of colonies grown on a selective agar plate. For each transformation we obtained around $3x10^6$ clones. We repeated this transformation 20 times and pooled the obtained transformant together to create a highly diverse library with a theroretical diversity of $6x10^7$ clones.

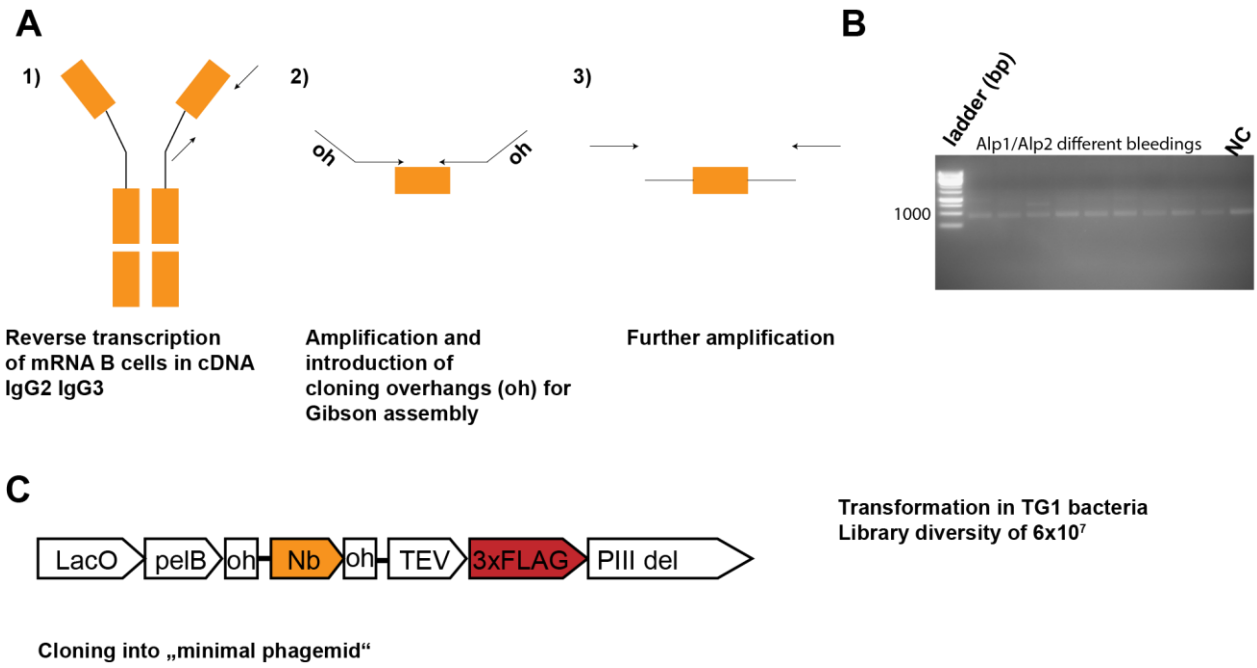

Figure 3.3: (**A**) Schematic of three step PCR retrotranscribes mRNA, amplify the variable domain of the heavy chain antibodies and prepare for cloning in the phagemid. Arrows represent the primers. (**B**) 1.5 % Agarose gel displaying 75 µg DNA. The negative controls (NC) is no starting RNA, shows positive signal displaying probable bench contamination. (**C**) Schematic representation of main components of the minimal phagemid

3.3.4 Phage display allowed selection of synaptic nanobodies

The proteins tested in preELisa that showed an absorption value at least two-fold higher than the negative control was considered antigens with potential possibilities to find specific nanobodies (positive preELISA). For those proteins, we performed between two and three panning rounds of phage display. We then picked around 90 colonies to confirm the binding ability of those cloned by phage ELISA, an ELISA assay detecting the presence of bound phages with an HRP-coupled antibody anti M13 phage major coat protein. The positive clones in phage ELISA were then sequenced and translated to protein sequences. We manually inspected their sequence, focusing mainly on the CDR3 region, the highly diverse region of nanobodies thought to be the most contributing to the recognition of the epitope. We chose nanobodies to represent diverse CDR3,

with a high content of hydrophilic amino acids and a low number of cysteines to ensure high solubility and proper cytosolic bacterial expression. We then validated those nanobodies candidates by a first indirect immunostaining using the bacterial lysate and detecting the 3xFLAG tag of the phagemid and comparing the localization of this signal to the target of interest fused to GFP expressed in a mammalian cell line. If positive, the nanobody candidates were then cloned in an optimized vector for nanobody expression in bacteria and transformed in SHuffle competent cell, an *E. coli* strain optimized for promoting the proper disulfide formation on proteins expressed in the cytoplasm of the bacterium. The vector also contains an extra cysteine at the carboxy-terminal of the nanobody to enable site-directed dye conjugation which was performed with maleimide-functionalized fluorophores. The nanobodies were then tested on antigen transfected mammalian cell lines to confirm their specificity on cells and later in primary neuronal cultures. If the nanobody candidates did not perform well in immunostaining after aldehyde fixation of the sample they were tested with antigens in native conformation on biochemical assays.

VAMP2

VAMP2 is one of the SNAREs involved in the vesicle recycling and neurotransmitter release and has been shown to modulate the gating of potassium voltage gated channels (Lvov et al., 2009). This protein displayed a promising result in the preELISA (Fig. 3.4 A), but lead to no functional nanobody candidates by the NGS-MS approach is VAMP2. We decided therefore to select nanobodies for this target by phage display. After two pannings of phage display, we performed a phage ELISA in which the 17 Nb candidates resulted positive in the phage ELISA (Fig. 3.4 B). Alignment of their CDR3 showed different amino acids composition and distribution, showing good diversity representation in our results. These nanobody candidates were tested in immunofluorescence. To do so in a fast and effective way we used the bacterial lysate of the bacteria expressing each nanobody directly as staining material. We verified that the nanobodies were expressed in the bacterial lysate by WB revealing the 3xFLAG tag fused to the C terminus of the Nb (Fig.4C). We incubated the bacterial lysate on cells transfected with VAMP2 fused to GFP. Out of the 17 Nb candidates, 15 did not show specific staining (example clone C3 Fig. 4C), while two candidates (clone E2 and G3) showed specific staining to the transfected cells and no staining to untransfected cells seen by DAPI nuclear staining (Fig. 3.4 C). We noticed that the

nanobodies stained specifically the membrane of the cells which is the location where VAMP2 is expected to be located, while the GFP signal was also visible in the nucleus. This confirmed us that the two candidates E2 and G3 seems to recognize specifically VAMP2. We, therefore, cloned these candidates into a bacterial expression vector and coupled it to a Cy5 dye. However, the signal from the directly labelled nanobodies (E3 & G3) failed to correlate to the VAMP-GFP signal on transfect HEK293 cells (data not shown).

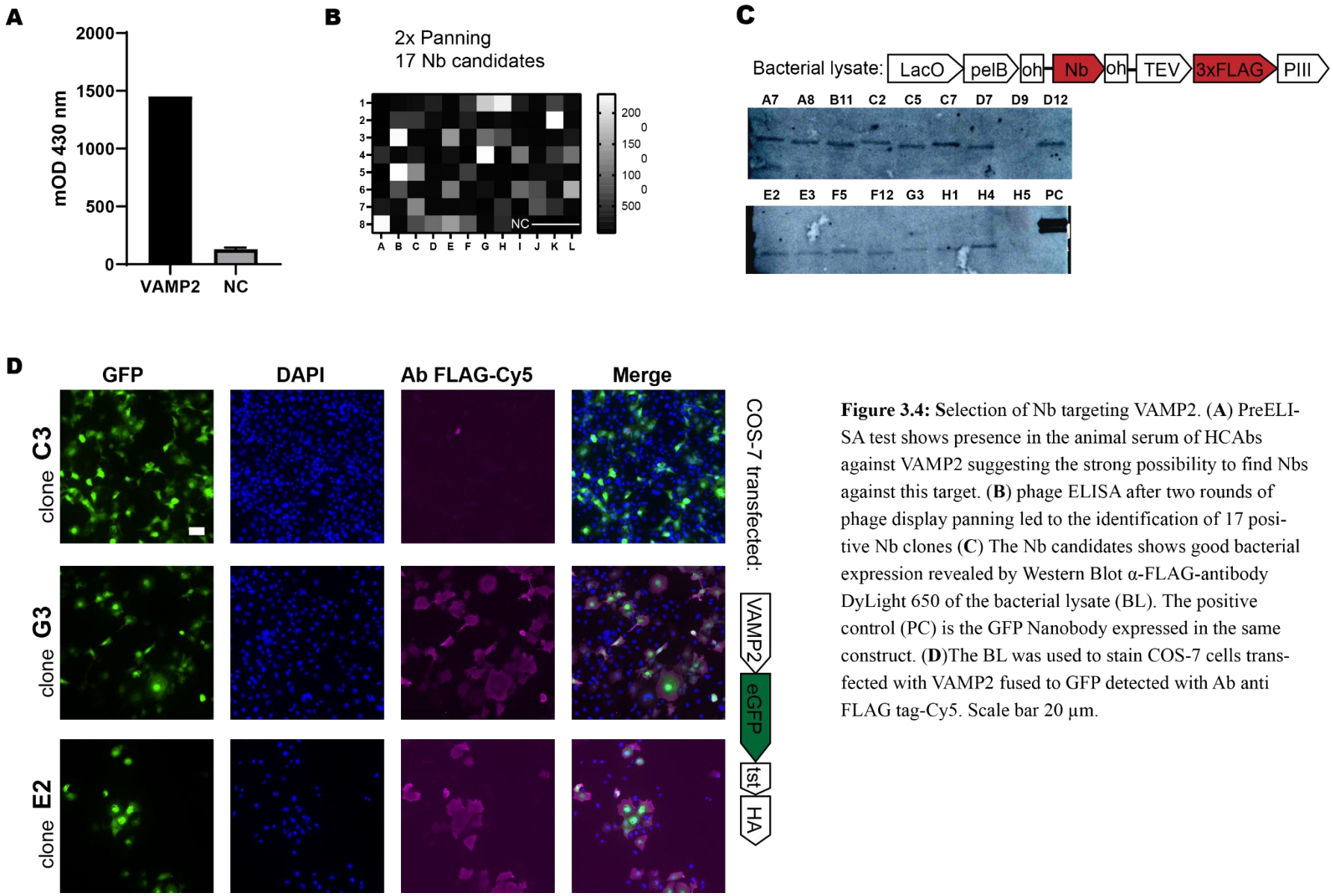

Figure 3.4: Selection of Nb targeting VAMP2. (**A**) PreELISA test shows presence in the animal serum of HCAbs against VAMP2 suggesting the strong possibility to find Nbs against this target. (**B**) phage ELISA after two rounds of phage display panning led to the identification of 17 positive Nb clones (**C**) The Nb candidates shows good bacterial expression revealed by Western Blot α-FLAG-antibody DyLight 650 of the bacterial lysate (BL). The positive control (PC) is the GFP Nanobody expressed in the same construct. (**D**)The BL was used to stain COS-7 cells transfected with VAMP2 fused to GFP detected with Ab anti FLAG tag-Cy5. Scale bar 20 µm.

Bassoon and Homer1

Bassoon is a scaffold protein located in the presynaptic active zone and has been shown to be involved in processes such as autophagy and protein ubiquitination (Ivanova et al., 2015; Terry-Lorenzo et al., 2016). Homer1 is a scaffold protein present at the postsynaptic density of the post synapse involved in intracellular calcium release (Hayashi et al., 2009). Those two proteins have been commonly used as pre and postsynaptic markers. In the preELISA they showed positive signal with two-fold higher than the negative control (Fig. 3.5 A). We performed 3 panning rounds of phage display for each of the two antigens. We obtained 40 positive clones in the phage ELISA. After manual inspection of their sequences, we noticed that most of the sequent obtained were redundant or with minor amino acids substitution. Highly represented sequences might indicate proper expression of the nanobody and high binding capacities; we selected therefore 16 nanobody candidates for Homer1 and 6 for Bassoon. Those nanobody candidates did not show specific signal in indirect immunostaining (data not shown). Therefore, we tested their binding abilities by performing an ELISA with different concentration of antigen (between 0 and 100 ng) coated on the well of an immunosorbent plate (Fig. 3.4 C). We termed this approach “ramp ELISA” due to the increasing amounts of coated antigen on different wells. The Bassoon candidates showed binding to the antigen when at least 10 to 100 ng of antigen was coated. Homer1 candidates seemed to have higher binding abilities with A1 homer candidate detecting as few as 0.1 ng, showing good affinity toward their target in a biochemical assay.

CNPase

We also screen for nanobodies against two isoforms of CNPase (human and mouse), a myelin-associated enzymes (Sakamoto, Tanaka, Ichimiya, Kurihara, & Nakamura, 2005). Three panning rounds of phage display were performed for each. The phage ELISA performed on coated human CNPase gave rise to 10 positive colonies, while the one performed on coated mouse CNPase showed all picked colonies positive. Colonies from phage ELISA were sent for sequencing and the sequences represented in both phage ELISA were chosen as nanobodies candidates. Their

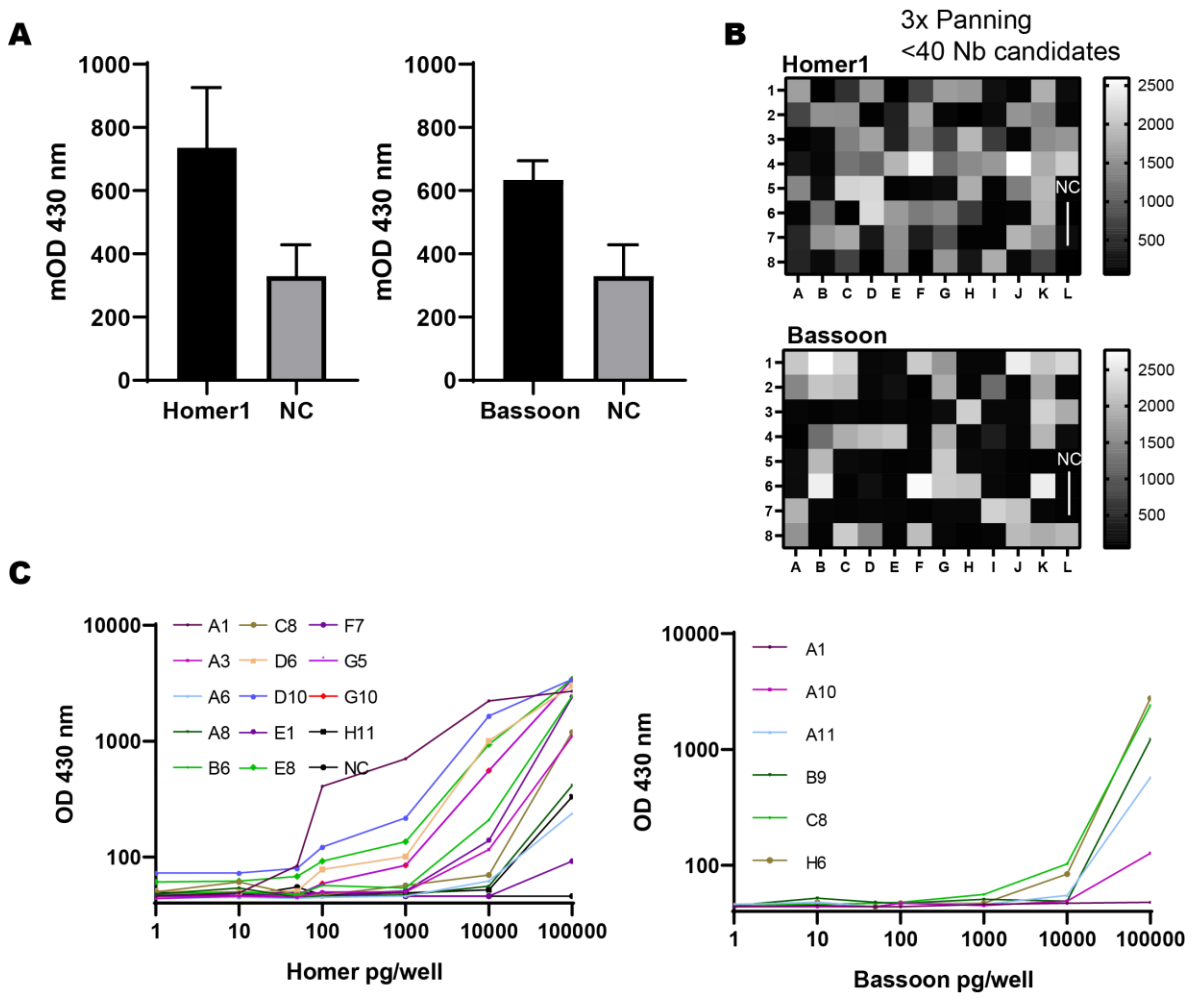

Figure 3.5: Nanobodies recognizes ng amounts of pre and postsynaptic markers. (**A**) PreELISA test shows presence in the animal serum of hcAbs against Homer and Bassoon. (**B**) More than 40 Nb candidates were positive in phage ELISA after 3 panning rounds of phage display (**C**) The Nb candidates were able to detect low amount of protein coated on an ELISA. x axis displayed in log10 scale for better visibility.

binding ability was tested with a ramp ELISA, coating between 0 and 10 pg of human CNPase or mouse CNPase on the well of the immunosorbent plate. The affinity of the nanobodies towards their target seemed high, with candidates detecting as few as 0.1 pg. The specificity of the 4 nanobodies displaying best affinity in the ramp ELISA was then tested in immunofluorescence. We coupled these nanobodies to Aberrior Star 635p and stained a sciatic nerve of mouse obtained from our collaborator (Dr. Hauke Werner; Max Plank Institute for Experimental Medicine). We performed in parallel a commercial antibody-based staining of Myelin-associated glycoprotein

(MAG) as reference. We could see that the signal of the nanobody was overlapping with the signal coming from MAG, showing colocalisation to myelin and therefore specificity to the Schwann cells expressing CNPase. We could also observe accumulations of nanobody signal that might depict the borders of the nodes of Ranvier (Fig. 3.5 D). We also obtained from our collaborator a sciatic nerve preparation of CNPase knock out (KO) mouse (Fig. 3.5 D). The lack of observed staining in the KO sample confirms the specificity of the nanobody.

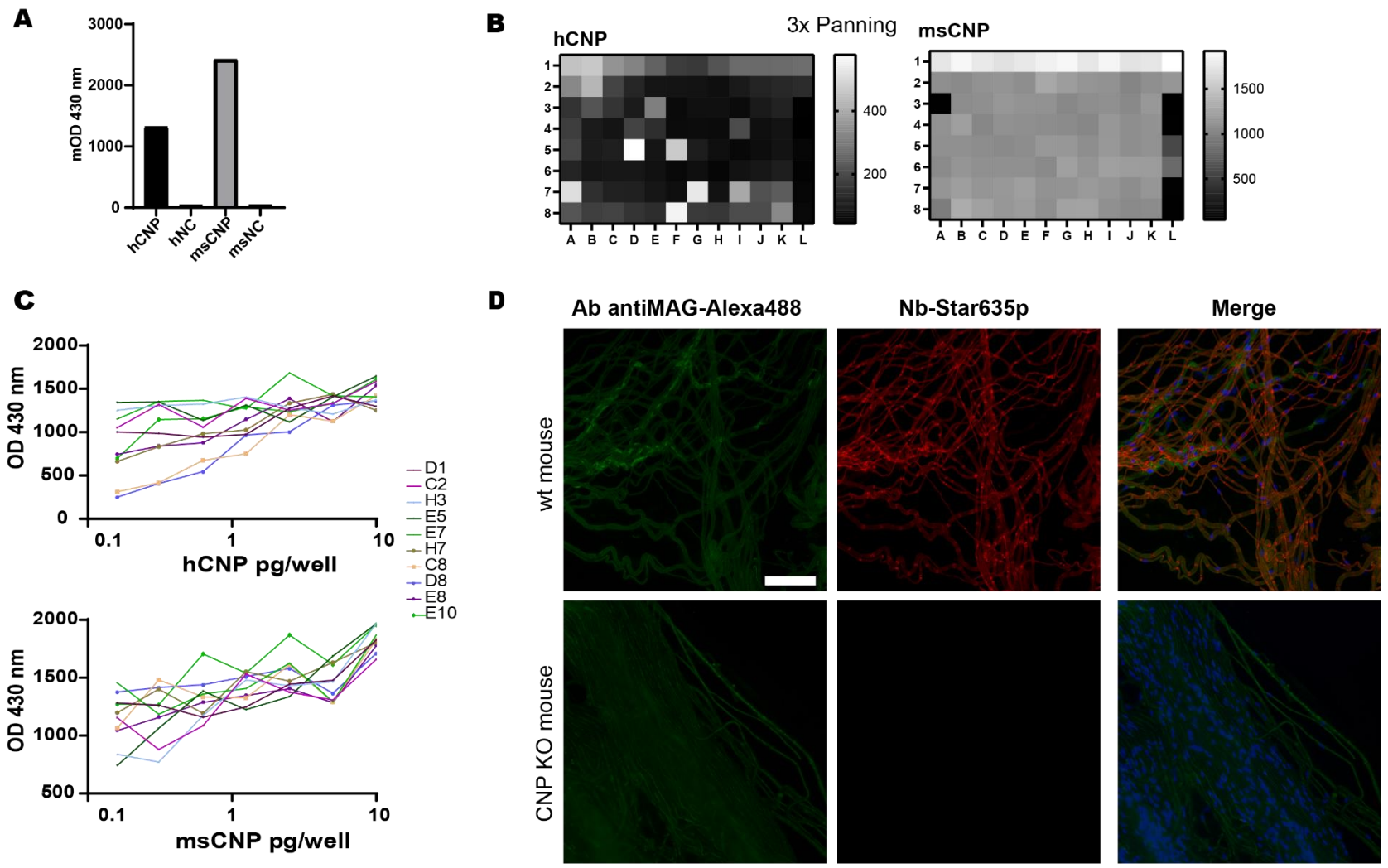

Figure 3.6: Nanobodies against CNPase (CNP) shows specificity and high affinity to its target (**A**) PreELISA test shows presence in the animal serum of hcAbs against CNPase in human (h) and mouse (ms) isoform. (**B**) More than 40 Nb candidates were positive in phage ELISA after 3 panning rounds of phage display (**C**) The Nb candidates were able to detect low amount of protein coated on an ELISA. x axis displayed in log10 scale for better visibility. (**D**) Sciatic nerve from wildtype (wt) mouse or CNP knock out (KO) stained with Nb clone E5- Star635p and costained with antibody myelin associated glycoprotein (MAG)+ secondary antibody Alexa 488. Scale bar: 50 µm

Synaptotagmin 1

Synaptotagmin 1 (Stg1) is another antigen that showed a positive signal in the preELISA (Fig. 3.6 A). It has a calcium sensing ability that plays a regulatory activity in neurotransmitter release at the synapse (Fukuda et al., 2000). After three panning rounds of phage display (Fig. 3.6 B) and manual inspection of the sequence of the picked colonies, the nanobodies candidates against Stg1 were narrowed down to six. We expressed them in SHuffle bacteria, purified and conjugated to Aberrior Star 635p. When tested on COS-7 cells transfected with Stg1-GFP, the signal of the 3 nanobody clones (A9, A5, H1) colocalised with the GFP signal showing specificity (Fig. 3.6 C). We therefore stained endogenous Stg1 in neurons. We co-stained with Synaptophysin antibody, a protein enriched in synapses, and we observed colocalisation of the two targets and bright signal for the clone A5, confirming the specificity of the nanobody (Fig. 3.6 D). Next, we measured the affinity of this nanobody to its target with microscale thermophoresis and determined its kD to 0.7 nM (Fig. 3.6 E).

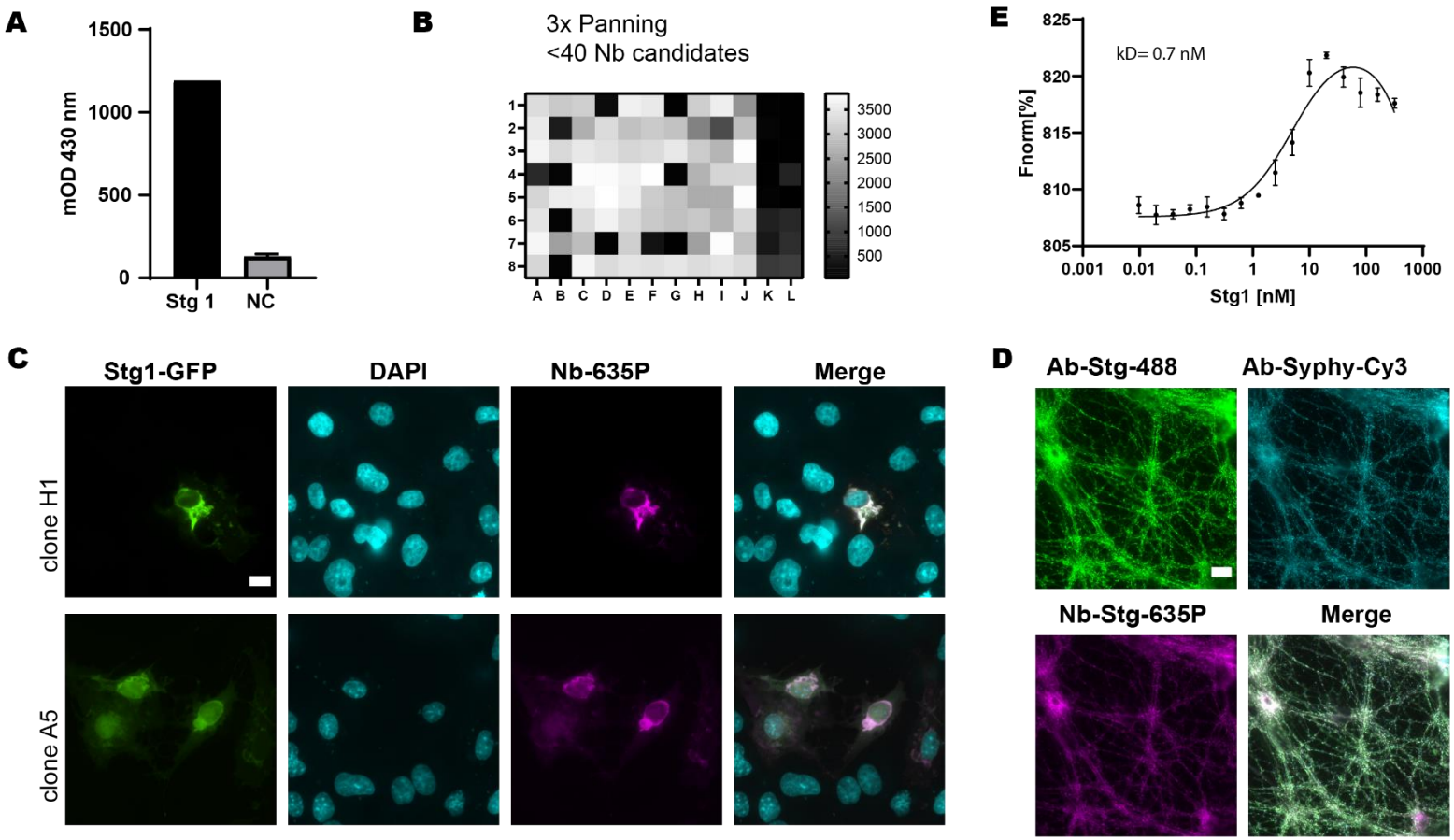

Figure 3.7: Nanobodies against Stg1 shows specificity and high affinity to its target (**A**) PreELISA test shows presence in the animal serum of hcAbs against Stg1 (**B**) Around 40 Nb candidates were positive in phage ELISA after 3 panning rounds of phage display (**C**) Three selected purified nanobody candidates conjugated to Aberrior 635p staining COS-7 cells transfected with Stg1 fused to GFP (**D**)Neurons triple stained with antibody anti synaptotagmin, antibody anti synaptophysin and the nanobody clone A5. Scale bar C and D 20 µm (**E**) Microscale thermophoresis of binding affinity of the nanobody A5 anti Stg1 to its target.

3.4 Discussion

Our approach establishes a pipeline to simplify and fasten the selection of nanobodies against different targets at the same time. The immunization of the alpacas with a full synaptosome preparation, containing several synaptic proteins (Fornasiero et al., 2018) might lead to the generation of hcAbs against many different targets at the same time. Single immunizations would have required cloning, expression, production, and purification of high amounts of every single synaptic protein. In addition, the immunization and boost before drawing the blood of the animals can take up to 4-6 months. In our case, we combined these steps by using a synaptosome preparation as a complex antigen. This allowed us to overcome the time, cost and effort necessary for single immunization of antigen. However, the complexity of the antigen preparation we used for injection cannot guarantee the immunogenicity of every single protein present in the synaptosome. In addition, for the production of nanobodies, the immune response needs to be hcAbs based. In fact, new world camelid contains ~50 % of hcAbs (IgG2 and IgG3 isoforms) and ~50 % of conventional IgGs (IgG1) (Hamers-Casterman et al., 1993), which we confirmed by the amounts obtained during the serum enrichment in IgG2 and IgG3 (Fig. 3.1 B). This implies that the synaptic protein of interest even if immunogenic, might have not triggered the generation of hcAbs and it will therefore not be possible to select nanobodies against such target.

Therefore, we established an assay named preELISA that assesses the presence of hcAbs against a specific target of interest in the animal serum. The preELISA uses a minimal amount of serum extracted from the animal and a minimal amount of protein to be investigated. It allows us to give an estimate on the success of the *in-vitro* selection process performed via phage-display (Fig. 3.1).

We selected nanobodies from these animals following two different approaches. The first consisted of the creation of a database of the nanobody sequences obtained from the B cells of immunized animals, followed by the antigen-specific identification of nanobodies from the animal serum by MS (Fig. 3.2 A). However, we found that this approach was not successful for us for multiple reasons. First, it is a method that requires two complicated and costly techniques, MS and NGS, which expertise are usually not found in the same laboratory. Therefore, those needs to be outsourced either to collaborators, which might become time lengthy, or to professional facilities, which becomes costly. Secondly, the identification of the nanobodies is related to the efficiency of their peptides to be detected by the MS machine. Therefore, there is no guarantee that the

detected nanobodies in MS have a sufficient affinity for our final desired application. On the same line, the expression feasibility in bacteria cannot be predicted (NGS from cells, MS from circulating hcAbs; the nanobodies never passed through any bacteria expression). These last two points increase the probability of selecting nanobodies, which might not fit future purposes: to be expressed in bacteria and to have high affinity towards their targets necessary for immunostainings protocols. Finally, the already high costs of MS and NGS are further increased in this approach since selected nanobodies need to be ordered as synthetic genes to proceed with their subsequent validation steps.

Phage display was a faster, cheaper and amore successful nanobody selection method in our hands. The use of a minimal phagemid (Fig. 3.2 C) with a smaller size compared to commonly used phagemid, enables theoretically a good transfection efficiency and the creation of a highly diverse nanobody library. This diversity was further confirmed by the selection of nanobodies with highly diverse CDR sequences. Testing nanobodies in immunofluorescence is laborious since it requires cloning the nanobodies in a new expression vector, purifying them and coupling them to a dye. For this reason, we established a quick immunostaining by using the bacteria lysate containing the nanobody clone and detect its presence by detecting the 3xFLAG Tag fused to the nanobody with a fluorescently-labeled monoclonal anti FLAG tag. This strategy saved us time and narrowed down the number of nanobodies to be tested in a “cleaner” immunostaining manner. Nanobodies candidates against VAMP2 selected by phage display (Fig. 3.4) however worked in bacterial lysate-based staining but not when the nanobody was purified and directly conjugated to a dye. This problem might come from two different factors: 1) the solubility introduced by the pIII protein that is still fused to the nanobody while doing this approach 2) the presence of the pelB signal leading the expression of the nanobody in the periplasm, instead of the cytoplasm.

ELISA is a method of choice for handling of multiple conditions/candidates at the same time. Therefore, establishing a “rampELISA” allowed us to observe if the nanobody binding to the antigen is dose-dependent, and also to have a draft estimation of the binding strength of the nanobody candidate to their targets. For Bassoon and Homer1, the majority of the nanobodies candidates did not show good results in the rampELISA and indeed they did not work in final immunostainings. (Fig. 3.5). On the other hand, Stg1 nanobodies candidates showed good results in the rampELISA and the high estimated affinity of the nanobodies was confirmed by specific

staining in COS-7 cells and neurons and by binding affinity measurement that resulted in sub-nM range (Fig. 3.6 C-E).

Combination of preELISA, phageELISA and rampELISA and staining method represents an optimized pipeline for the selection of nanobodies after a complex immunization of a camelid such as the synaptosome preparation. This pipeline will in the future enable a major production of nanobodies against different targets in future nanobody discovery projects.

3.5 Material and methods

Cell culture

COS-7 cells and Rat primary hippocampal neurons were prepared and maintained as described in Chapter 5. *HEK293FT* cells (Invitrogen) were cultured in DMEM high glucose (Lonza), supplemented with: 10% fetal bovine serum (FBS), 0.1 mM MEM Non-Essential Amino Acids, 4 mM L-glutamine, 1 mM MEM Sodium Pyruvate, 0.6% Pen-Strep and 500 µg/ml Geneticin. The cells were maintained at 37°C with 5% CO2 and splitted every 2-3 days.

Immunization of alpacas

The synaptosome preparation was performed as described by Fornasiero et al. (Fornasiero et al., 2018). Briefly, rat brains were homogenized using a glass-Teflon homogenizer in precooled sucrose buffer (320 mM Sucrose, 5mM HEPES, pH 7.4). Centrifugation at 1000 xg for 2 min was performed, and the supernatant was further centrifuged at 15’000 xg for 12 min. Next, a discontinuous Ficoll density gradient was applied. The fractions at the interface of the 9% Ficoll were pooled and washed in sucrose buffer. Two alpacas (named Alp1 and Alp2) were immunized with this preparation. The procedure was performed by *Preclinics* (Postdam, Germany).

Six injection were performed weakly with 500 µg of rat synaptosomes (total protein determined by BCA assay). Two weeks after the last immunization a single boost with 500 mg synaptosomes was performed and 100 ml of blood was taken 3 and 5 days after the boost immunization. PBMCs were isolated using Ficoll gradient and Serum was stored at -80°C. Total RNA was extracted using Qiagen kit.

Enrichment of hcAbs from complete serum

Serum from the animal was enriched in IgG2 and IgG3 following the protocol described by Hamers-Casterman et al. (Hamers-Casterman et al., 1993) with some modifications. The affinity selection steps were done using an Äkta-Prime FPLC system (GE Healthcare). Between 5 and 10 mL of serum was diluted in PBS in a one to one ratio and filtered through a .45 µm pore size Syringe Filters (Stedim Minisart®, Sartorius). The serum was then injected in HiTrap protein G HP (GE Healthcare), the flowthrough was collected and injected in HiTrap protein A (GE Healthcare). The bound IgGs were eluted from the HiTrap protein G column with first 0.15 M NaCl, 0.58% Acetic acid, pH 3.5 to collect mainly IgG3 and then : 0.1 M glycine–HCl, pH 2.7 to collect mainly IgG1. The IgG bound to the HiTrap protein A column were eluted with 0.15 M NaCl, 0.58% Acetic, pH 4.0 to collect the IgG2. To neutralize the pH of the collected fractions, 1 M Tris-HCl pH 9.0 was added and the buffer was exchanged to PBS by injection in HiTrap Desalting Columns (GE Healthcare). A sample of the collected and desalted fractions were analyzed by denaturing (SDS) discontinuous Polyacrylamide Gel Electrophoresis (PAGE) as described by Gallagher (Gallagher, 2012). IgG2 and IgG3 fractions were pooled together, and residual IgG1 were further removed by incubating the pooled sample with beads conjugated with anti-llama light chain (Capralogics).

Nb library generation for phage display

The mRNA was extracted from the B cells of Alp1 and Alp2 using standard total RNA extraction kit (Qiagen). 28 µg of total mRNA diluted in RNAse free water was retrotranscribed to cDNA by using Supercript IV (Invitrogen) and the Cal 0002 primer designed originally by Pardon et al. (Pardon et al., 2014). Then a first PCR was performed using Cal0001 and Cal0002 (Pardon et al., 2014) which anneal in conserved regions of the nanobodies, the leader signal sequence and the CH2 domain respectively. PCRs were done using KAPA PCR mix high fidelity (KAPA Biosystems) and after each PCR, Sera-Mag Select (GE Healthcare) was used to remove primers and small fragments. Next, a second PCR was performed to introduce the cloning overhangs for further insertion in the phagemid using a variety of degenerated primers described by Pardon et al. A final PCR was performed using primers annealing to the cloning overhangs to increase the efficiency of cloning. The final PCR product were diluted to 5 ng/µL and 75ng were loaded on a 1.5 % Agarose gel. After confirming the right size of the PCR product on the Agarose gel, they

were cloned in the phagemid by using Gibson assembly (D. G. Gibson et al., 2009). The phagemid used is a modified and smaller version of the pHen2. It contains a pelB leader sequence, an mCherry at the position in which the nanobodies should be inserted, truncated version of PIII surrounded by cloning overhangs, a TEV cleavage site, a 3x FLAG tag and a gene for Trimethoprim (Tmp) resistance. After Gibson cloning, the obtained construct was purified by PCR purification kit (Quiagen) and the concentration was measured by Nanodrop (PeqLab). The construct was then electroporated in TG1 bacteria (Biocat). For the transformation, 65 ng of DNA were added to 50 L of TG1 and this process was repeated 20 times. The reactions were left 1 hour at 37°C 300 rmp for initial growth and then pooled together in 400 mL of 2YT medium (ThermoFisher) supplemented with 20 µg/mL and let grow overnight at 37°C. The next day when OD600 reached 10, the bacteria were pelleted for 15 min at 4000 xg and resuspended in 25 mL LB medium (ThermoFisher) and 25 % Glycerol. The library was aliquoted, snap freezed and stored at -80 °C.

ELISA as PRE test

In order to detect the presence of hcAbs prior the affinity selection process of nanobodies, an ELISA was performed in the following way. Purified antigen was immobilized on a 96 well immunosorbent plate. All the following steps were done by gentle shaking on a platform shaker. The immobilization of the antigen was done either by direct adsorption to the plastic or by using streptaviding-biotin interaction. For the first approach, 300 nmol of purified protein diluted in 200 µL 100 mM Tris, 150 mM NaCl (pH 8) were coated overnight at 4°C on an immunosorbent plate (Iba). For the second approach, the cell lysate of transfected cells expressing protein fused to twin-Strep-Tag was incubated on Strep-Tactin® coated microplate (Iba). The plate was then washed with PBS and blocked with 5% (w/v) Milk in PBS either overnight or for 3 hours at RT. After rinsing the wells with PBS, the enriched serum prepared as described above, was added to the wells in a concentration of 0.5 mg/mL. The serum was let incubated on the wells for 2 hours at RT. A series of three washes with PBS for 10 min each was performed to remove the unbound IgGs. The presence of bound IgG2 and IgG3 was then revealed with the addition of monoclonal mouse anti-Camelid antibody coupled to HRP (Preclinics, clone: P17Ig12) diluted 1:2000 in PBS. The antibody was let incubated for 2 hours at RT, then washed 3 times with PBS for 10 min. The ELISA was revealed by addition of 100 µL of TMB substrate (Thermoscientific) until the blue

color was stable (around 5 to 10 min). The reaction was quenched by addition of 100 µL of 1 M sulfuric acid. The plate was then imaged at 430 nm with a plate (BioTek Cytation).

Phage Display

Phage display was performed to select nanobodies against specific target. The procedure was done as described in Maidorn PhD Thesis 2017 with some modifications. All steps described below were performed under a fume hood to avoid contamination of other bacterial cultures used in the lab. To start the process, a 1 mL aliquot of the previously generated nanobody library was diluted in 500 mL of 2YT supplemented with 20 µg/mL of Tmp and 4% Glucose and let grow at 37°C 120 rpm until OD600 reached 0.5. Next, M13KO7 Helper Phages (NEB) were added to the culture. The bacteria were let being infected for 45 minutes at 37°C with gentle shaking. Bacteria were then pelleted for 10 min at 4000 xg and the pellet was resuspended in 500 mL 2YT medium supplemented with 20 µg/mL of Tmp and 50 µg/mL of Kanamycin (Kan) which resistance is carried by the helper phage. The infected bacteria were then incubated overnight at 30° C 120 rpm to produce the phages. The next day the culture was centrifuged 10 min 4000 xg and the supernatant containing the secreted phages was incubated with 4 % (w/v) PEG-8000 to be precipitated. The phages were let precipitated on ice for <2 hours. The phages were further pelleted by centrifugation at 4°C 4000 xg for 30 minutes. The pellet was resuspended in precooled PBS, and 4% PEG was further added to the phages and let on ice for 1 hour to precipitate. The phages were again centrifuged 4°C 4000 xg for 30 minutes and the supernatant was collected. Next to remove residual bacterial debris, the solution was centrifuged 5 min at 4000 xg and filtered with a 0.45 µm syringe filter (Sartorius).

To proceed with the affinity selection of the nanobody targeting specific protein, a phage display panning round was performed. The antigens fused to twin Step Tag were immobilized on MagStrep XT beads (Iba). Between 3 and 10 nmol of antigen was incubated with 200 µL of beads previously equilibrated to PBS. The other antigens not containg the twin Strep Tag were first desthiobioninilated by addition of 10-20 molar excess of Desthiobiotin-N-Hydrosuccimide Ester (Beryy and Associates) in carbonate buffer for 1 hour at 4°C. The reaction was arrested by addition of 0.1 M Tris-HCl. Between 1 and 3 nmol of antigen was bound to 250, 500 or 750 µL of pre-equilibrated DynabeadsTM MyOne Streptavidin C1 (ThermoFisher) for 1 hour at RT. After binding of the antigen to the beads, the beads were washed 3 times 5 min with PBS supplemented

with 0.01 % (v/v) Tween (PBS-T). Next, the previously produced phages were added to the beads and incubated 2 hours at RT with slow shaking. To ensure the high affinity of the selected nanobodies, the beads were washed from unbound or loosely bound phages by at least three washes 10 min with PBS-T and one wash overnight with PBS-T at 4°C. The bound phages were then eluted with buffer BXT (Iba) containing 50 mM Biotin. The eluted phages were then used to reinfect TG1 cells. To ensure that the TG1 cells express the F'-pilus necessary for infection of phages, they were grown on M9 minimal medium (90 mM Na_2HPO_4, 22 mM KH_2PO_4, 18 mM NH_4Cl, 9 mM NaCl, 0.2 & w/v glucose, 1 mM $MgSO_4$, 0.1 mM $CaCl_2$ in 1 L H_2O containing 15 g agar and 1 µg thiamine) for 3 days before infection. From this minimal plate, one colony was picked and grow in 50 mL 2YT medium at 37°C. The eluted phages were added to this TG1 culture and let infect for 1 hour at 37°C 30 rpm. The bacteria were then pelleted and resuspended in selective media to continue with phage production, phage precipitation and panning as described above. For each antigen two to three panning rounds were performed. After the panning rounds, the infected TG1 culture was pelleted by centrifugation 4000 xg for 20 min and resuspended in 5 mL 2YT. This concentrated liquate culture was plated on LB agar supplemented with 20 µg/mL of Tmp in different dilutions and let grow overnight at 37°C. The next day around 90 colonies were picked to be analysed. The picked colonies were dipped in the wells of a 96-well round-bottom plate containing 200 µl 2-YT medium supplemented with 20 µg/ml Tmp and let grown overnight at 37°C 120 rpm to be used for Phage ELISA. The next day, 5 µL of bacteria were transferred to fresh 200 µL 2YT+ 20 µg/mL Tmp and grown at 37°C 120 rpm for 3 hours. The rest of the culture was supplemented with 25 % (v/v) glycerol and stored at -80 °C.

Phage ELISA

In order to screen for the correct binding of the selected nanobodies to their target, an ELISA was performed (the phage ELISA). The bacteria grown in the 96 well plate, were infected with MK13KO7 Helper Phages 37°C 30 rpm for 1 hour. The bacteria were then pelleted 4000 xg 15 min, the pellet was then resuspended in fresh 200 µL 2YT supplemented with 20 µg/mL Tmp and 50 µg/mL Kan. The culture was incubated overnight at 30°C 120 rpm for phage production. The next day, bacteria were pelleted and the supernatant containing the phages was transferred to a new plate and stored at 4°C until being used for the Phage ELISA. The antigen was immobilized on MaxiSorp® flat-bottom 96-well plates (Thermo Fisher Scientific) by adsorbtion to the well

overnight at 4°C with slow shaking. The next day, the wells were washed 3 times 10 min with PBS and the wells were blocked using 5% Milk in PBS-T for 3 hours at RT. Next, 25 µL of phages produced by the picked colonies were incubated on the well with 75 µL 5% Milk in PBS for 2 hours at RT. The unbound phages were then washed with PBS-T for 3 times 10 min, and the bound phages were detected with anti major coat protein M13-HRP (Santa Cruz) diluted 1:1000 in 100 µL PBS. The antibody was let for 1 hour at RT and washed away with PBS 3 times 10 min. The signal was detected with 100 µL TMB substrate until no drastic change in color could be detected. The reaction was stopped by addition of 100 µL of 2M sulfuric acid. The plate was images as described before at 430 nm. The "ramp ELISA" used for determining the binding affinity of the nanobody candidates toward different amounts of target was performed in the same way as a phage ELISA with the difference that logarithmic dilutions of the antigens were coated in different wells.

Protein expression and purification

Protein expressed in bacteria:

The DNA constructs were electroporated in different *E. coli* according to the protein to be expressed: SHuffle T7 (Biolabs) for nanobodies and NEB Express (Biolabs) for other type of proteins. To express the proteins, bacteria were scraped from a previously made glycerol stock and inoculated to 5 mL of Terrific Broth (TB) (Thermofisher) supplemented with appropriate antibiotics. The bacteria were let grown overnight at 37°C. The next day the 1 mL of this pre-culture was diluted in 100 mL of fresh TB with antibiotic. After 3 to 6 hours of incubation at 37°C, 120 rpm, the expression of the protein was induced by addition of 1 mM Isopropyl-β-D-thiogalactopyranosid (IPTG) and let overnight at 37°C 120 rpm. The next day 5 mM Ethylenediaminetetraacetic acid (EDTA) was added to the culture and the bacteria were harvested by centrifugation at 4°C for 30 min 3600 xg. The supernatant was discarded and the pellet was resuspended in precooled Buffer 1 (50 mM HEPES, 0.5 M NaCl, 25 mM imidazole, 5 mM $MgCl_2$, pH 8) supplemented with 1 mM PMSF, 1 mM DTT, 500 µg/ml lysozyme and 100 µg/ml DNaseI (Sigma-Aldrich). The bacteria were then lysed by sonication using three times 10 pulses at 95 % in a cell disruptor (Branson Digital) and the cell debris were removed by centrifugation at 4°C for 1 hour 16000 xg. The supernatant was then added to Ni+-resin beads (Roche) pre-equilibrated in Buffer 1. The protein was let to bound to the beads by incubation at RT for 1h with gentle shaking. The beads were then washed three times with Buffer 1 and the protein was then eluted with Buffer

1 supplemented with 500 mM imidazole and adjusted pH 7.5. The eluted protein was then analyzed by SDS-PAGE as described above.

Protein expressed in mammalian system.

Plasmid coding for the antigen was transfected in *HEK293FT* cells (Invitrogen) using polyethylenimine (PEI, Sigma-Aldrich) as transfection method following the protocol by Longo et al.(Longo et al., 2013). In brief, 40µg of DNA was diluted in reduced serum medium Opti-MEM (Gibco), while PEI was diluted in PEI. The two solution were mixed and incubated for 15 min at RT. The mixture was then added dropwise to the cells previously seeded on a 14 cm petri Dish. The cells were let expressing the protein for two days at 37°C with 5% CO2. Two days after transfection, the cell media was removed and the cells were washed briefly with prewarmed PBS which was then removed. The lysis was then carried on ice by adding 50 mM Tris/HCl, pH 7.5, 150 mM NaCl, 2 mM EDTA, 0.5% IgePAL, 0.5 % Sodium deoxycholate and freshly added 1:1000 DNAse 1:1000 Protease inhibitors Aprotinin, Leupeptin, Pepstain A, 1 mM PMSF 1:1000 protease inhibitor cocktail. The cells were with cell scraper and the lysate was collected into a tube and let on ice for 40 min with occasional vortexing. The cells were then sonicated using a cell disruptor using one pulse of 45 seconds 70%. The cells debris were then removed by centrifugation for 45 min at maximum speed on a table top at 4°C centrifuge. The supernatant then used as a cell lysate.

Nanobody coupling to fluorophore

In order to label the nanobodies, they were expressed with an additional Cysteine at their C terminus. This allow site targeted maleimide coupling without interfering with the nanobody conformation and binding capabilities (Pleiner et al., 2015). To reduce the intermolecular disulfide bonds, tris(2-carboxyethyl)phosphine TCEP was added in 50 molar excess to the nanobody and let for 2 hours on ice. The excess of TCEP was removed by NAP5 columns (GE Healthcare) previously equilibrated with PBS. The dye with a maleimide function was added to the nanobody in 3-5-fold molar excess and incubated at RT for 2 hours in the dark. The excess of dye was removed by using Superdex™ 75 increase 10/300 GL column (GE Healthcare) on Äkta-Prime FPLC system.

KD measurement

The affinity of the nanobodies were measure by microscale thermophoresis using the device NT.115 Pico (Monolith). Nanobody labelled with Aberrior635p was diluted in MST buffer (Nanotemper) supplemented with 0.05 % Tween and incubated with different dilutions of the target protein. Measurement were done using the Premium Capillaries (Monolith). For operation of the instrument and evaluation of affinity data, the MO.Control and MO.Affinity Analysis software (NanoTemper) were used.

Microscopy Setups

The microscopy setups used in this chapter are the same described in Chapter 5.

Author contributions

S.SI. designed and performed experiments, analyzed data, and wrote the manuscript, K.VR designed and performed experiments, analyzed data. N.B. performed experiments, M.M. designed experiments, performed experiments and analyzed data F.O. designed and conceived the project, designed and performed experiments.

Acknowledgements:

We would like to thank Petri Kursula for providing the CNPase protein. We would like to thank Hauke Werner for providing nerve tissue of wildtype and knockout animal. We would like to thank Eugenio Fornasiero for the synaptosome preparation, Sunit Mandad for the mass spectrometry measurement and the group of Stefan Bonn for the next generation sequencing.

3.6 References

1. Wilhelm, B. G. *et al.* Composition of isolated synaptic boutons reveals the amounts of vesicle trafficking proteins. *Science* **344**, 1023–8 (2014).

2. Hamers-Casterman, C. *et al.* Naturally occurring antibodies devoid of light chains. *Nature* **363**, 446–8 (1993).

3. Maidorn, M., Olichon, A., Rizzoli, S. O. & Opazo, F. Nanobodies reveal an extra-synaptic population of SNAP-25 and Syntaxin 1A in hippocampal neurons. *MAbs* **11**, 305–321 (2019).

4. Schenck, S. *et al.* Generation and Characterization of Anti-VGLUT Nanobodies Acting as Inhibitors of Transport. *Biochemistry* **56**, 3962–3971 (2017).

5. Modi, S., Higgs, N. F., Sheehan, D., Griffin, L. D. & Kittler, J. T. Quantum dot conjugated nanobodies for multiplex imaging of protein dynamics at synapses. *Nanoscale* **10**, 10241–10249 (2018).

6. Seitz, K. J. & Rizzoli, S. O. GFP nanobodies reveal recently-exocytosed pHluorin molecules. *Sci. Rep.* **9**, 7773 (2019).

7. Gomes de Castro, M. A. *et al.* Differential organization of tonic and chronic B cell antigen receptors in the plasma membrane. *Nat. Commun.* **10**, 820 (2019).

8. Breda, C. *et al.* Tryptophan-2,3-dioxygenase (TDO) inhibition ameliorates neurodegeneration by modulation of kynurenine pathway metabolites. *Proc. Natl. Acad. Sci. U. S. A.* **113**, 5435–40 (2016).

9. Sograte-Idrissi, S. *et al.* Nanobody Detection of Standard Fluorescent Proteins Enables Multi-Target DNA-PAINT with High Resolution and Minimal Displacement Errors. *Cells* **8**, 48 (2019).

4 Nanobody Detection of Standard Fluorescent Proteins Enables Multi-Target DNA-PAINT with High Resolution and Minimal Displacement Errors

Shama Sograte-Idrissi*, Nazar Oleksiievets*, Sebastian Isbaner, Mariana Eggert-Martinez, Jörg Enderlein, Roman Tsukanov, Felipe Opazo.

*These authors contributed equally to the work

Published in Cells **2019,** 8**(1), 48**;

Detailed author contribution of Shama Sograte-Idrissi:

- Experimental work and analysis:
    - Establishment and optimization of the protocol for Nanobody coupling to docking strands (Fig.4.2, A-B)
    - Coupling of the Nanobodies to the docking strands and purification (Fig.4.2, C-D)
    - Optimization of cell seeding and triple plasmid transfection for imaging chamber
    - Sample preparation (seeding, transfection, staining in imaging chamber) (Fig.4.4)
- Preparation of the manuscript (together with N.O, R.T, F.O with contributions from S.I and J.E)

The paper here was formatted to fit the editing format of the thesis.

Nanobody Detection of Standard Fluorescent Proteins Enables Multi-Target DNA-PAINT with High Resolution and Minimal Displacement Errors

Authors: Shama Sograte-Idrissi[1,2,4,*] , Nazar Oleksiievets[3,*], Sebastian Isbaner[3], Mariana Eggert-Martinez[1,2,4], Jörg Enderlein[3], Roman Tsukanov[3,#], Felipe Opazo[1,2,#]

[1]Institute of Neuro- and Sensory Physiology, University Medical Center Göttingen, 37073 Göttingen, Germany

[2]Center for Biostructural Imaging of Neurodegeneration (BIN), University of Göttingen Medical Center, 37075 Göttingen, Germany

[3]Third Institute of Physics − Biophysics, Georg August University, 37077 Göttingen, Germany

[4] International Max Planck Research School for Molecular Biology, Göttingen, Germany

* These authors contributed equally to the work

#Correspondence: fopazo@gwdg.de, roman.tsukanov@phys.uni-goettingen.de; Tel.:+49 (0) 55139 61155/ +49-(0)55139 22297

4.1 Abstract:

DNA-PAINT is a rapidly developing fluorescence super-resolution technique which allows for reaching spatial resolutions below 10 nm. It also enables the imaging of multiple targets in the same sample. However, using DNA-PAINT to observe cellular structures at such resolution remains challenging. Antibodies, which are commonly used for this purpose, lead to a displacement between the target protein and the reporting fluorophore of 20-25 nm, thus limiting the resolving power. Here, we used nanobodies to minimize this linkage error to ~4 nm. We demonstrate multiplexed imaging by using 3 nanobodies, each able to bind to a different family of fluorescent proteins. We couple the nanobodies with single DNA strands via a straight forward and stoichiometric chemical conjugation. Additionally, we built a versatile computer-controlled microfluidic setup to enable multiplexed DNA-PAINT in an efficient manner. As a proof of principle, we labeled and imaged proteins on mitochondria, the Golgi apparatus, and chromatin. We obtained super-resolved images of the 3 targets with 20 nm resolution, and within only 35 minutes acquisition time.

Keywords: Nanobodies, Super-resolution microscopy, multi-color imaging, fluorescent proteins, microfluidics, DNA-PAINT, molecular localization, single domain antibodies (sdAb), multiplexing, linkage error.

4.2. Introduction

Super-resolution light microscopy is developing rapidly, and a growing number of cell biologists are embracing this technology to study proteins of interest (POI) at the nanoscale. Single molecule localization techniques like PALM[1], (d)STORM[2], [3], and others[4] achieve resolutions that allows for distinguishing molecules that are separated by only a few nanometers. Among these localization techniques, **DNA P**oint **A**ccumulation for **I**maging in **N**anoscale **T**opography (DNA-PAINT)[5] has demonstrated to achieve a resolution below 5 nm on DNA origami structures[6], [7] and offers the possibility to detect multiple POIs within the same sample[8]. A special feature of DNA-PAINT is that it is not limited by photobleaching of the fluorophore, due to the constant replenishment of fluorophores from solution. In fact, a target site carries one or more single stranded DNA oligonucleotides (commonly referred to as the docking strand or handle) instead of a single fluorophore, while a second single stranded DNA molecule with a complementary sequence to the docking strand bears a fluorophore (referred to as the imager strand). In a DNA-PAINT experiment, the imager strands continuously bind to the docking strands and unbind due to thermal fluctuations. The continuous transient binding of the imager strands results in sparse “blinking-like” fluorescence detection events. Similar to PALM or STORM, these events are then precisely localized to reconstruct a super-resolved image. The localization precision depends on the number of photons collected in a single event, whereas the total number of events recorded affects the quality of the final super-resolved image. Importantly, DNA-PAINT benefits from the orthogonality of DNA hybridization (with different sequences). DNA docking strands with different nucleotide sequences can be associated with different targets, thus making it easy to obtain multi-target super-resolution images using a single fluorophore. Thereby, chromatic aberrations are avoided, resulting in a comparable resolution for all the POIs under investigation[9]. For such multiplexed imaging (known as Exchange PAINT[8],[9]), the sequential introduction of different imager strands is required.

However, this methodology imposes several challenges to cell biologists who want to optimally image POIs with DNA-PAINT. Usually, primary antibodies that bind to a POI are labeled with secondary antibodies which carry the docking strand[10]. But such an approach introduces a spatial displacement of up to 25 nm between the target site and the fluorophore[11]–[13] which seriously limits the resolving power of all single molecule localization super-resolution techniques which use conventional antibody-based immunofluorescence labeling. The first

attempt to minimize this “linkage-error”[14] was to use primary antibodies that are directly coupled to docking strands[15]. Typically, this has been performed by using undirected coupling chemistry via maleimide-peG2-succinimidyl ester or via DBCO-sulfo-NHS-ester cross linkers[10]. These non-targeted coupling methods can interfere with the binding ability of the primary antibody to the POI by reacting at the paratope of the antibody. Additionally, they result in a mixture of antibodies containing a broad distribution of the number of docking strands (even including antibodies with none), which results in an inhomogeneous labeling density of the POIs and makes single molecule detection non-quantitative.

To further tackle the “linkage error” of the reporter fluorophores, several small monovalent affinity probes are continuously emerging[16]. For instance, small DNA or RNA molecules, known as aptamers[17]–[19] or single-domain antibodies (sdAb, or nanobodies)[20] have recently gained popularity in the field of super-resolution imaging[21]–[23]. Nanobodies are obtained from a special type of immunoglobulins known as heavy chain antibodies (hcAb) and which are found in camelids. The recombinant production of the variable domain of these hcAbs result in a functional nanobody with only 2-3 nm size[24]. Recently, a significant improvement in spatial resolution, as compared to conventional antibody immunofluorescence, was demonstrated by using nanobodies for labeling[12], [25]. In addition to their small size, high specificity, and monovalent binding affinities, which make them an ideal tool for microscopy, the recombinant nature of nanobodies endows them with great flexibility and allows introducing all types of modifications in a precise manner. This last feature permits to rationally design and control the number and location of desired functional elements on them (e.g. the number and locations of fluorophores or docking strands)[22].

Unfortunately, only few nanobodies able to recognize endogenous mammalian proteins are currently available. However, several new nanobodies against different fluorescent protein families like GFPs (from *Aequorea Victoria*), RFPs (from *Dicosoma* sp.) or mTagBFPs (from *Entacmaea quadricolor*) are now easily accessible. This opens the opportunity to obtain super-resolution images with a minimal linkage-error on a wide range of biological samples. Fluorescent proteins like EGFP[26], mCherry[27] and mTagBFP[28] are widely used in the life-sciences, fused to POIs within simple cell lines, large yeast libraries[29], and countless other genetically modified organisms (e.g. *Arabidopsis thaliana*[30], *Caenorhabditis elegans*[31], *Drosophila melanogaster*,[32] or mice[33]).

Here, we used a custom-built multi-channel Total Internal Reflection Fluorescence (TIRF) microscope and three nanobodies targeting mTagBFP, EGFP and mCherry to perform Exchange PAINT experiments on three different targets inside the same cell. For efficient buffer solution exchange, a versatile custom-built microfluidics system was developed and implemented. Exchange PAINT was performed by sequential introduction of three different imager strands and washing in between. Recorded single-molecule localization detection events were subsequently analyzed for reconstructing super-resolved images for each of the three targets. We achieved a resolution of 20 nm with a localization precision of 14 nm within 35 minutes of acquisition time (per target). We envision that nanobody-based DNA-PAINT will provide an efficient solution for the protein-DNA linkage problem and will help to exploit the full power of DNA-PAINT for cellular imaging, considering the broad availability of many fluorescent proteins.

4.3. Materials and Methods

Nanobody coupling to docking oligo

The unconjugated nanobodies FluoTag®-Q anti-GFP, FluoTag®-Q anti-RFP, and the FluoTag®-Q anti-TagBFP (NanoTag Biotechnologies GmbH, Cat. No: N0301, N0401, and N0501, respectively) carry one ectopic cysteine at the N-terminus then allowing for chemical couplings via a thiol reactive compound. The DNA docking strands (Biomers GmbH, Ulm, Germany) were functionalized with an azide group at 5´-end and, in some cases, Atto488 fluorophore at 3`-end. The coupling of the docking strands to the nanobodies were performed following procedure from Schlichthärle and colleagues [34], with minor modifications. In brief, 15 to 20 nmol of nanobodies in phosphate buffer saline (PBS, 127 mM NaCl ,10 mM Na_2HPO_4, 2.7 mM KCl, 0.2 mM KH_2PO_4, pH7.4) were incubated with a final concentration of 5 mM TCEP (Sigma-Aldrich) for 2 h at 4°C to reduce the ectopic cysteine. Afterwards, the excess of TCEP was removed by exchanging the buffer to PBS pH 6.5 using spin Amicon filters with a MWCO of 10 kDa (Merck/EMD Millipore, Cat. No. UFC501096). The reduced TCEP-free nanobodies were immediately mixed with 50 molar excess of DBCO-maleimide crosslinker (Sigma-Aldrich, Cat. No. 760668) and incubated overnight at 4°C with mild stirring. The excess of DBCO crosslinker in the buffer was exchanged to PBS pH 7.4 using Amicon Filters (MWCO 10 kDa) as described previously. Functionalized docking strands were added (10 molar excess) to the crosslinker-coupled nanobody, and incubated at room temperature for ~2 hours with slow head-to-tail shaking. The excess of docking strands

was then removed from the conjugated nanobodies using size exclusion chromatography (Superdex 75 Increase 10/300 column, Cat. No: 29148721) and ÄKTA pure 25 system (GE life science). The correct fractions of labeled nanobodies were then identified by the SDS-PAGE followed by SYBR GOLD staining (Thermo Fisher, Cat No: S11494). The docking strands sequences used for the assay were taken from Agasti et al[8]. FluoTag®-Q anti-GFP was coupled to P1* sequence (5`-CTAGATGTAT-Atto488-3`), FluoTag®-Q anti-RFP was coupled to P2* (5`-TATGTAGATC-3`), and the FluoTag®-Q anti-TagBFP was coupled to P3* (5`-GTAATGAAGA-3`). Imager strands were labeled with Atto655 fluorophore at 3` end.

Immunostaining

COS-7 cells were cultured in DMEM medium with 4 mM l-glutamine and 10% fetal calf serum (Thermo Fisher Scientific), supplemented with 60 U/ml of penicillin and 0.06 mg/ml streptomycin (Sigma-Aldrich) at 37°C and 5% CO_2. Prior immunostaining and imaging, ca. 20,000 cells/well, were plated in 8-well chamber (155411PK, ThermoFisher Scientific). In the next day, the cells were transfected using 2.5% lipofectamine 2000® and 300 ng of plasmid in Optimem medium (Thermo Fisher Scientific). After incubation of ca. 16 h, the cells were fixed using 4% paraformaldehyde (PFA) for 30 minutes at room temperature. The remaining aldehydes were quenched with 0.1 M glycine in PBS for 30 minutes. Afterwards, cells were permeabilized and blocked using 3% bovine serum albumin (BSA) and 0.1% Triton X-100 in PBS for 30 minutes at room temperature. Buffer solution containing nanobodies coupled to the docking strand (50 nM) was used to stain the cells. For this purpose, we proceeded with incubation of 1 h at room temperature, with slow orbital shaking. Finally, the cells were rinsed with PBS and then post-fixed with 4% PFA for 30 minutes at the room temperature. As described previously, remaining aldehydes were quenched with 0.1 M glycine in PBS. Cells were stored in PBS buffer at 4°C.

Exchange PAINT Experiment

The imager strands P1 5`-CTAGATGTAT-3`-Atto655, P2 5`-TATGTAGATC-3`-Atto655, and P3 5`-GTAATGAAGA-3`-Atto655 (Eurofins Genomics) were aliquoted in TE buffer (Tris 10 mM, EDTA 1 mM, pH 8.0) at a concentration of 100 µM and stored at -20°C. Prior to the experiment, the strands were diluted to the final concentration of 2 nM in PBS buffer, containing

500 mM NaCl. A chamber with 8 wells (155411PK, Thermo Fisher Scientific) was fixed on the microscope stage with clips. A PDMS layer was used as a chamber cover and supported the inlet tubes and a tube for suction. The slide was held on the microscope stage for 0.5 h before the acquisition to equilibrate to the room temperature and achieve mechanical stability. Injection of fluids and its removal was done using our custom-built microfluidic setup, designed and constructed particularly for Exchange PAINT experiment. First, the well was rinsed twice with 500 µL PBS buffer (pH 8.0, NaCl 500 mM). Then, suitable cells for imaging were selected based on the presence of signal from the expressed fluorescent proteins: mTagBFP, mCherry, and EGFP. The cells were located by exposing them to the following laser excitation wavelengths and detecting the fluorescence in the corresponding emission channel: mTagBFP - 405 nm laser, EGFP - 488 nm laser, and mCherry - 561 nm laser. A HILO-illumination scheme was used to excite the cells. Laser power was adjusted according to the sample brightness (respectively 0.5 mW, 1 mW and 2 mW at the output of optical fiber). Each selection movie of the fluorescent proteins included between 200-250 frames (Figure 4.4, A1-A3). Afterwards, we proceeded with Exchange PAINT on the selected cell. All the solutions were injected into the cell by applying air pressure in the corresponding pressurized tube. First, imager strand P1 (2 nM) in PBS buffer (500 µL) was injected into the well and incubated for 10 minutes before the acquisition. Typical DNA-PAINT movie included 21,000 frames (corresponds to 35 minutes). The following acquisition settings for emCCD camera were used: exposure time 100 ms, pre-amplifier gain 3.0, EM gain 10. The laser 638 nm was set to 10-15 mW (corresponds to an excitation illumination power density of 0.4-0.6 kW/cm^2). After PAINT movie acquisition, an extensive wash of the well was performed (4-6 times volume exchange, in total about 3 mL buffer within 5 minutes), in order to remove the imager solution from the well completely. Suction was performed by the micro peristaltic pump (Makeblock) After the extensive wash, the next imager solution was introduced. We proceeded with the same solution exchange procedure also for the imagers P2 and P3 (see comprehensive chart in Figure 4.3B). All the experiments were carried out at a constant temperature of 22±1 °C, which was crucial for the mechanical stability of the sample (remaining mechanical drifts were corrected for during the analysis).

DNA-PAINT movies analysis

Raw DNA-PAINT movies were analyzed using the Picasso software package[10]. In the end, drift-corrected super-resolution images were reconstructed and the average localization accuracy was estimated. For further analysis of the achieved image resolution, the Fourier Ring Correlation (FRC)[35] technique was employed. First, localization events were detected using Picasso: Localize. For the specific binding-events recognition, the signal box size length was set to 7 pixels and the minimum net gradient was limited to the range of 1,700 to 3,500 (depends on the protein expression level in a particular cell). Then, the localized bright spots were fitted with the LQ Gaussian method to obtain precise fluorophore coordinates. The total number of localization events varied from 150,000 to 2,500,000 for the whole movie. The output file with the localization coordinates was then loaded into Picasso: Render. Using the Undrift RCC feature (segmentation 500 frames), movies were corrected for mechanical drift. The final reconstructed super-resolved images were exported in PNG format. Finally, all three reconstructed images of different organelles were merged together for each imaged cell using ImageJ[36], see Figure 4.4 C1,C2, D1-D3. The average localization precision (NeNa[37]) was estimated for each reconstructed super-resolved image. For image resolution quantification, Fourier Ring Correlation (FRC)[35] was applied using the FIRE ImageJ plugin [38], for detailed numbers see Supplementary Information, Table S1. Further image resolution analysis was performed by creating a resolution map using SQUIRREL[39] (super-resolution quantitative image rating and reporting of error locations), see Figure S4.4 in the Supplementary Information.

4.4. Results

Optimization of cells transfection and nanobody staining for Exchange DNA-PAINT imaging

First, we optimized the transfection of mammalian cells (COS-7) with plasmids encoding for proteins present in different organelles fused to various fluorescent proteins. We used TOM70 fused to EGFP to reveal mitochondria, GalNacT was fused to mCherry to detect the Golgi apparatus and histone H2B was fused to mTagBFP to detect the cellular chromatin (nucleus). Additionally, we used currently available nanobodies, which bind strongly and specifically to the three fluorescent proteins mentioned above. Each type of nanobodies was labelled with a unique docking strand, enabling the acquisition of multiple targets using Exchange PAINT, in single cells (see scheme in Figure 4.1).

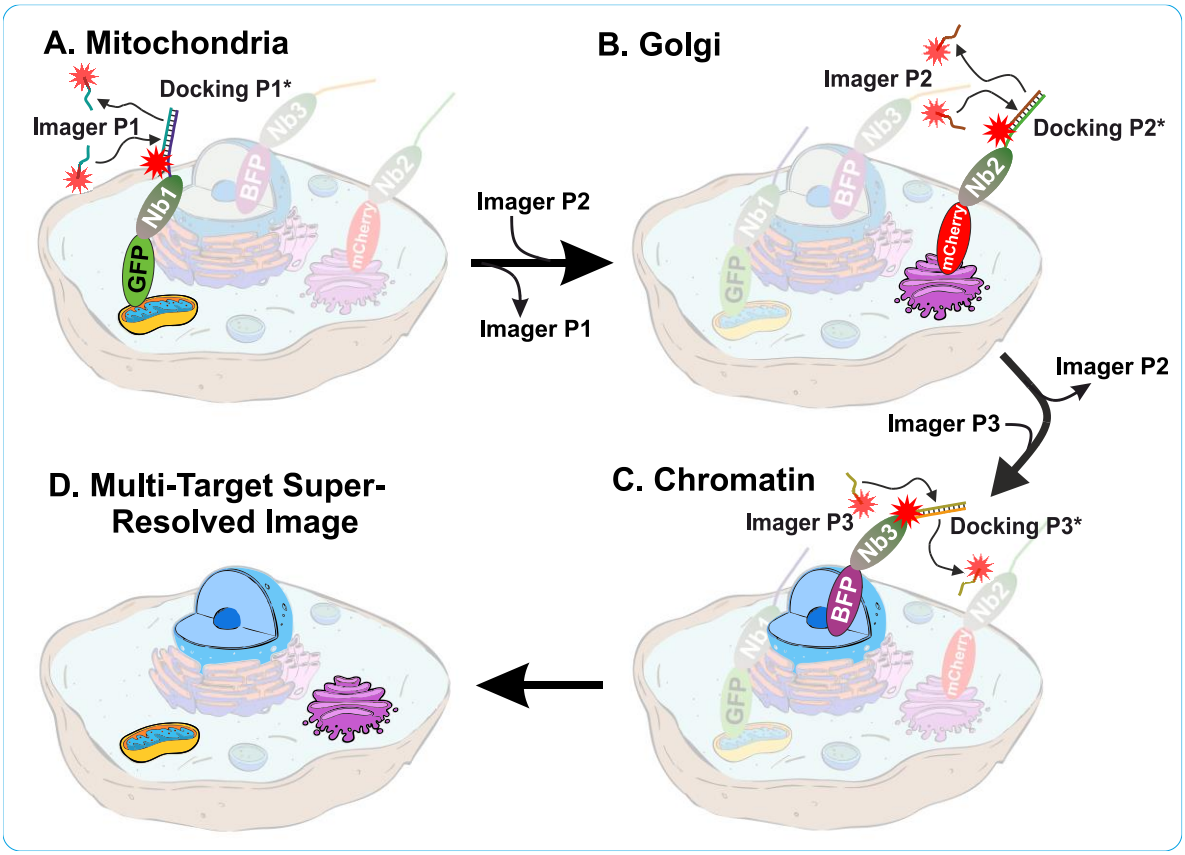

Figure 4.1: Schematic representation of multi-target Exchange PAINT in COS-7 cells. Sequential introduction of Imager strands with different sequences reveal multiple targets and result in multi-color super-resolution image. (**A**) DNA-PAINT imaging of mitochondria with Imager P1. (**B**) DNA-PAINT imaging of the Golgi apparatus with Imager P2. (**C**) DNA-PAINT imaging of nucleus/chromatin. (**D**) The resulting super-resolved image of a single cell with 3 colors overlaid. The cells were stained with (1) nanobody anti-GFP (Nb1) coupled to the DNA strand P1, (2) nanobody anti-mCherry (Nb2) coupled to the docking P2, and (3) nanobody anti-mTagBFP (Nb3) coupled to the docking strand P3.

All nanobodies had an extra ectopic cysteine at their C-terminus that allowed the conjugation of molecules via maleimide chemistry. We used a maleimide-DBCO as a cross-linker to attach the single stranded DNA oligo bearing an azide group on its 5´ end (Figure 4. 2A, B). The coupling of the docking strand was thus performed in two sequential steps. First, the nanobody was incubated with a 50 molar excess of the maleimide-DBCO cross-linker, inducing a thiol-maleimide conjugation with the previously reduced single ectopic cysteine at the C-terminus of the nanobody[22]. After removing the excess of cross linker, the complex was incubated with a 10 molar excess of azide functionalized DNA oligo to induce a strain-promoted azide–alkyne cycloaddition (copper-free click chemistry[40]). The separation of the excess of DNA oligo from the mixture was performed using a size exclusion chromatography (SEC), resulting typically in two obviously separated elution fractions (Figure 4.2C). This is an essential step to avoid unspecific signal from the free DNA oligo. As a first routine quality control after SEC, different elution fractions were passed through a polyacrylamide gel electrophoresis (PAGE), stained with SYBR gold, to report for the presence of the oligonucleotides (Figure 4.2D). Only the fractions containing a clean band at the right molecular weight were used subsequently for the immunoassays of the transfected COS-7 cells. Due to the large excess of cross-linker and docking strands used for each coupling step (see Methods section), we are confident that a major proportion of the nanobodies were labelled with the docking oligo.

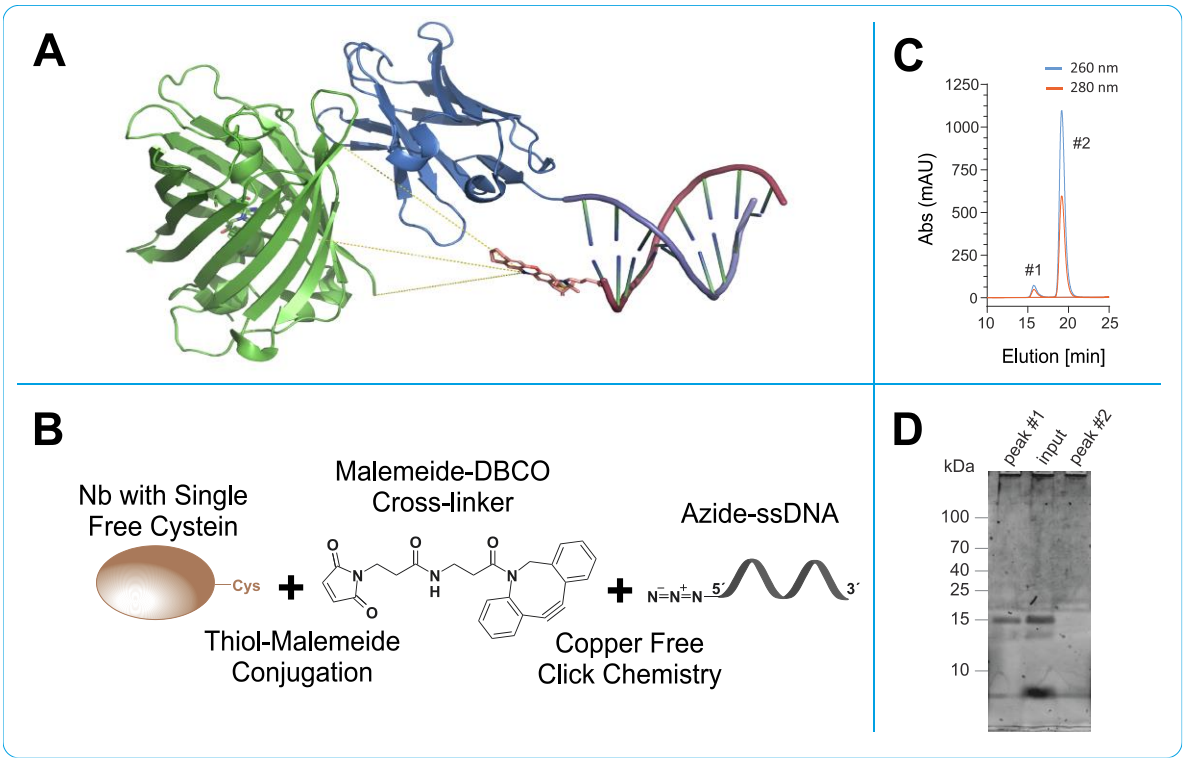

Figure 4.2: Click- and thiol-based strategy to conjugate nanobodies to a docking DNA strand for DNA-PAINT. (A) Anti-GFP nanobody (blue) bound to EGFP (green). The nanobody is modified with a docking stand with a complementary Atto655-labelled Imager strand attached (EGFP: nanobody complex extracted from (PDB: 3K1K), DNA strand and Atto655 were generated using ChemDraw (CambridgeSoft) and The PyMOL Molecular Graphics System (Schrödinger, LLC). Yellow lines represent 3 possible distances (3.1 nm, 3.3 nm and 3.4 nm) of the fluorophore to the POI. (B) Scheme representing the orthogonal coupling strategy of docking DNA strand to the nanobody. (C) Example of the size-exclusion chromatography (SEC) for the separation of DNA-coupled nanobody (#1) from the excess of docking strand (#2). (D) Example of the SDS-PAGE of fraction collected from the SEC run, post stained with SYBR gold, which reports DNA. Peak #1 collected from SEC shows a prominent band matching the expected molecular weight (~15 kDa). Peak #2 lacks the band at the nanobody molecular weight, suggesting that the peak contains the un-reacted excess of docking oligonucleotide.

Microfluidic setup for Exchange DNA-PAINT experiment

Solution exchange inside the sample chamber was done using a custom-built microfluidics setup, designed and constructed in particular for the Exchange PAINT experiments. The setup allows operation of up to 24 independent inlet channels and is capable of fluid injection/removal with an adjustable flow speed in/out of the experimental chamber.

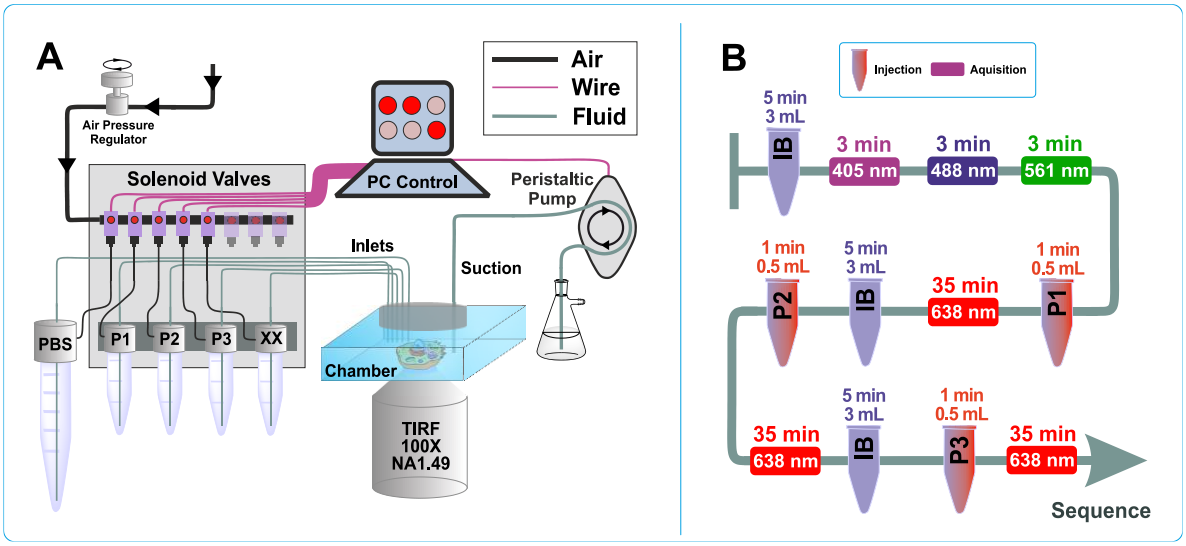

Figure 4.3: Scheme of custom-built microfluidics setup and Exchange PAINT experiment. (A) Microfluidics setup: the setup is controlled by a computer software, which includes both manual and automated operation modes. Maximum number of the input channels is 24 (only 5 channels are shown). The peristaltic pump used to remove the solutions from the chamber is also computer-controlled. (B) Typical sequence of actions for the Exchange PAINT experiment. The tube-shape sketches depict the injection of solutions (P1, P2 or P3) or the imaging buffer (IB) (solution volume and injection duration are indicated on top of the objects). Rectangles represent movie acquisition with certain laser excitation (laser wavelength and total acquisition time are indicated inside the rectangle and on top of the rectangle, respectively).

Magnetic solenoid valves (MH1, Festo) were used to turn on and off the air pressure in the channels, which were connected in turn to pressurized tubes. When air pressure is applied to such a tube, a liquid flowis created. Flow speed can be adjusted by changing air pressure using a pressure regulator (MS6, Festo). We used air pressure values in the range of 3-5 psi to generate a

gentle flow of solutions. The pressurized air was purified with an air filter (PTA013, Thorlabs). Tygon tubing (VERNAAD04103, VWR) was used to guide the solutions from pressurized tubes to the experimental chamber. Suction was performed by a micro peristaltic pump DC12.0V (Makeblock). For washing, buffer solution for was loaded into a 15 mL test tube (Greiner Bio-One™ 188271, Fisher Scientific). The tube was equipped with a cap for pressurization (FLUIWELL 1C-15, Fluigent). The solutions of imager strands P1, P2 and P3 (concentration 2 nM, volume 1 mL) were loaded into 2.0 mL tubes (Micrewtube T341-6T, Simport), which were then mounted into a holder for four pressurized tubes (FLUIWELL-4C, Fluigent). Both magnetic solenoid valves and peristaltic pumps were operated by a custom-written LabView (National Instruments) routine, which included both manual and automatic operation modes. A custom-built electronic controller served as an interface between the magnetic valves and the computer.

Super-resolution multiplexed DNA-PAINT images of COS-7 cells

We performed Exchange PAINT imaging of COS-7 cells stained with nanobodies, each functionalized with a single docking strand. For this purpose, aversatile custom-built optical setup was designed and constructed (see Figure S 4.1). Initially, we checked that all cells to be imaged were triple transfected with the plasmids encoding for the TOM70, GalNacT and H2B fused to EGFP, mCherry and mTagBFP, respectively. The signal from each fluorescent protein was first imaged with a wide-field HILO illumination (see Figure 4.4, A1-A3). Afterwards, we sequentially introduced and removed imager strands P1, P2, and P3 as shown in Figure 4.3B. Each DNA PAINT movie was acquired during 35 minutes and then analyzed with the Picasso software[10] to obtain the super-resolved images (Figure 4.4, B1-B3). The experiment was designed to monitor three different proteins that are located in very distinct organelles, in order to simplify the evaluation of our Exchange DNA-PAINT images. Clearly, the reconstructed super-resolved DNA-PAINT images (one for each of the imagers P1, P2, and P3) showed the “patterns” expected for the respective organelle, thereby providing additional confirmation of our imaging strategy. For a more informative representation, and to further confirm the specificity of each imager strand, the

three super-resolved images (from each P-imager movie) were merged together (Figure 4.4, C1). The result suggests that every "channel" remains clean, without significant unspecific binding events between the different docking-imager partners. The whole imaging cycle for the three target molecules, including imager strand injections, incubations, the removal of solutions and the acquisition of more than 60,000 frames took in total 2-3 h to be completed. The whole procedure worked robustly, and provided high quality super-resolved DNA-PAINT images for nearly every imaged cell (selected at the initial wide-field HILO checkup).

In order to evaluate the image quality in a more quantitative manner, we performed a detailed analysis for the average localization accuracy and the actual resolution of the images. For the images presented in Figure 4.4, the average localization accuracy estimated by NeNa[37] was 19±2 nm (the lowest value was 14 nm, Table S1) and the average resolution, as estimated by Fourier Ring Correlation (FRC)[35], was 27±5 nm (the lowest value was 20 nm, Table S1). The full list of localization accuracies and FRC resolutions obtained for each organelle in each cell in Figure 4.4 can be found in Table S1 in the Supplementary Information.

Finally, we performed image quality analysis using FRC resolution maps using the SQUIRREL software[39]. The resolution values for different images varied between 26-34 nm. Moreover, we also compared the super-resolved images as obtained by Picasso and by RapidStorm[41]. Interestingly, both tools produce super-resolved images of similar quality (Figure S4.2).

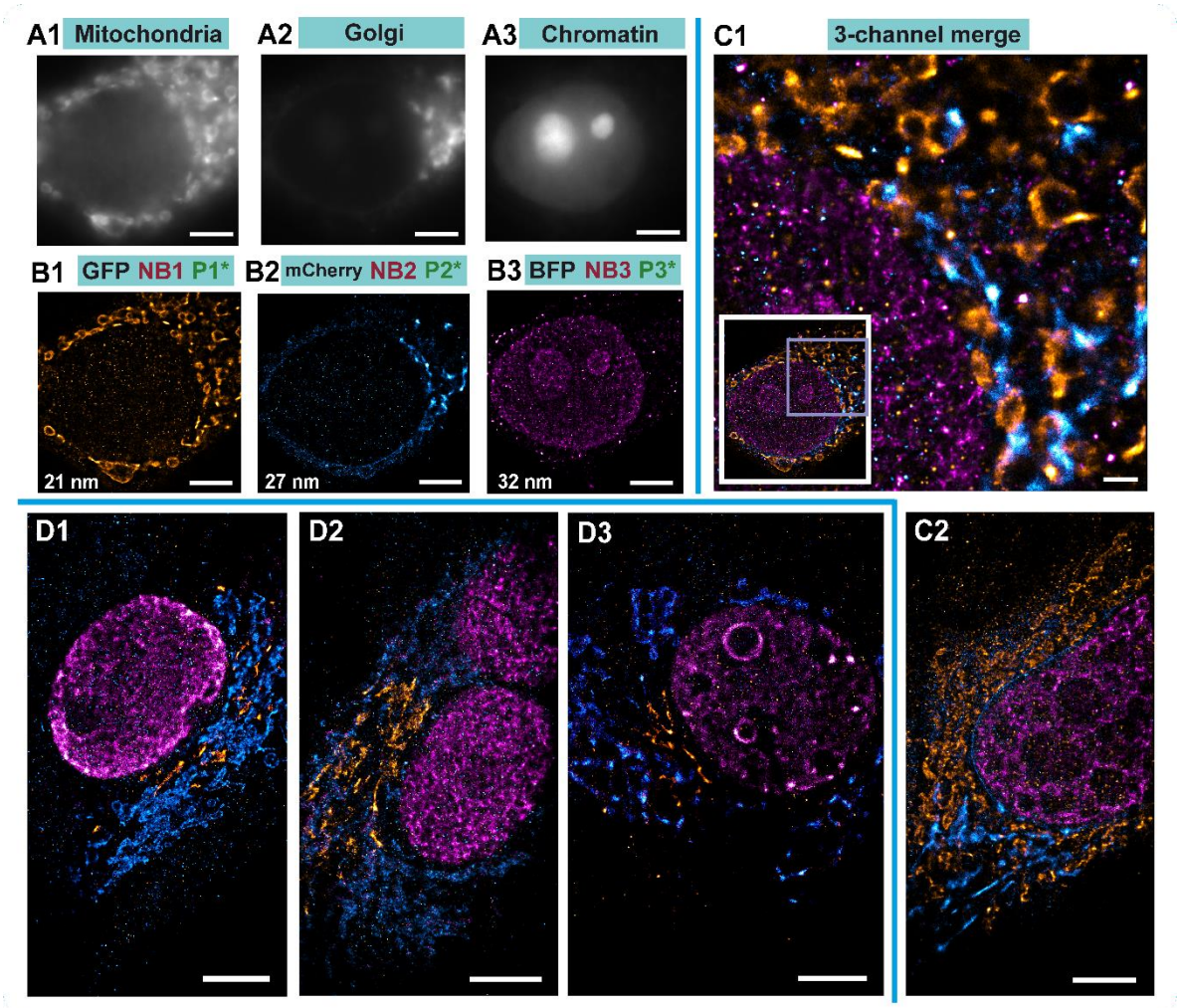

Figure 4.4: Exchange PAINT imaging. A1-A3 Diffraction-limited wide-field images of individual target fluorophores: Mitochondria with TOM70-EGFP (A1), Golgi with GalNacT-mCherry (A2), Chromatin with H2B-mTagBFP (A3). (B1-B3) Single-channel super-resolution DNA-PAINT images of respective organelles. The number represents FRC number for resolution for the respective image. (C1) Left bottom inset is the full view of the cell imaged in B with all 3-target Exchange PAINT images merged. Right, zoom of the boxed area I the inset. (C2) One more example of Exchange PAINT imaging with the same set of staining as in B and C. (D1-D3) Specificity controls were performed by swapping the fluorescent proteins and changing the Golgi marker. Now cells were expressing TOM70-mCherry and GM130-EGFP (a different Golgi marker). All scale bars correspond to 5 µm, except in C1 where the scale bar represents 1 µm.

To assess the effectiveness of our method, we performed several controls. First, the targeted protein GalNacT that we used to detect the Golgi, was changed to GM130 to ensure that the reconstructed organelle is labeled specifically regardless of the target protein used for reporting the Golgi apparatus (Figure 4.4, D1-D3). Additionally, we exchanged the fluorescent proteins we used for targeting the Golgi and the mitochondria by transfecting cells with plasmids encoding for TOM70 fused to mCherry and GM130 fused to EGFP. The same coupled nanobodies were used to reveal those targets. Nb1 (nanobody anti GFP) coupled to P1 docking strand, Nb2 (nanobody anti-mCherry) coupled to P2, and Nb3 (nanobody anti-mTagBFP) coupled to P3. Therefore, in this experiment, the imager P1 revealed the structure of the Golgi apparatus and the imager P2 revealed the mitochondria. Detailed comparison of NeNa and FRC for both cases can be found in Table S1. These control experiments confirmed the efficiency of our system, the specificity of the coupled nanobody, and the interchangeability of the targets. Finally, cells transfected with a single plasmid coding for TOM70-EGFP were immunostained with anti-GFP nanobodies bearing the P1-docking DNA and were imaged with imager P3 under the same conditions as before. We observed very few binding events (i.e. P3 imager binding P1 docking) without showing any recognizable pattern (Figure S 4.3). This extra control suggests a high specificity of the imager to its docking strand. Additionally, unspecific binding (e.g. stickiness of the imager to the glass coverslip or cellular elements) were negligible (Figure S 4.3).

4.5 Discussion

Conventional antibodies (150 kDa and 12-15 nm in length) are often used for labelling cellular targets in DNA-PAINT imaging[5]. This approach has demonstrated to achieve an impressive spatial resolution[6], [7], to a level where the size of the primary and secondary antibody sandwich (with ~25 nm linkage-error) limits its imaging resolution. It has been demonstrated that small camelid single domain antibodies or nanobodies (15 kDa and ~3 nm in length) have the capacity to increase the accuracy of super-resolution microscopy for mapping POIs in a cellular context[15], [42]. Recently, nanobodies have been coupled to docking oligos to perform DNA-PAINT [25]. Unfortunately, only few nanobodies are currently available that work efficiently in immunoassay applications. Some of them have a strong affinity and high specificity towards

specific fluorescent proteins. In this work, we exploited this property, which makes our method highly versatile since many bio-medical researchers typically have their favorite proteins already fused to fluorescent proteins[43]. Here, we showcase the use of three specific nanobodies against the EGFP family (this nanobody also binds to EYFP, Citrine, mVenus, Cerrulean, Emerald EGFP, and more GFP derivatives), mCherry and similar variants (it also binds to mOrange2, tdTomato, dsRed1 & 2, mScarlet-I, and other mRFP derivatives), and finally to mTagBFP (it also recognizes mTagRFP, mTagRFP657, mKate, and mKate2) for DNA-PAINT super-resolution microscopy. As a proof of principle, we used cells expressing three different fluorescent proteins in different organelles. The cells were immunostained with anti EGFP, mCherry, and mTagBFP specific nanobodies, each coupled to a unique and single DNA-docking strand for performing Exchange PAINT on them (Figure 4.4). We achieved an overall resolution of 20 nm, and an average localization precision of ~14 nm (in the best case, see Table S1), within only 35 minutes of acquisition time per target. We anticipate that, by further experimental and protocol optimizations, it will be possible to improve the resolution and acquisition time even further. The set of nanobodies presented in this work makes it already possible to investigate three proteins of interest within the same cell, all at diffraction-unlimited resolution, with the enhanced precision provided by the nanobody monovalency (no clustering of target protein) and small size (minimal linkage-error) [13], [16]. We hope that our study will motivate other scientists who have their POIs already fused to fluorescent proteins to benefit from this technique.

Author Contributions: S.SI and N.O performed experiments, analyzed data, wrote the manuscript; S.I analyzed data and corrected the manuscript; M.EM performed experiments; J.E conceptualized the project and acquired funding; R.T conceptualized the project, performed experiments, analyzed data, wrote the manuscript F.O conceptualized the project, analyzed data, wrote the manuscript and acquired funding.

Funding: FO and SSI were supported by the *Deutsche Forschungsgemeinschaft* (DFG) through the Cluster of Excellence Nanoscale Microscopy and Molecular Physiology of the Brain (CNMPB). NO is grateful to the DFG for financial support via project A10 of the SFB 803. JE is grateful to the Deutsche Forschungsgemeinschaft (DFG) for financial support via the Cluster of Excellence and DFG Research Center “Nanoscale Microscopy and Molecular Physiology of the Brain.”

Acknowledgments: The authors are grateful to Dr. Anna Chizhik for advising during the experiment, Dr. Oleksii Nevskyi and Arindam Ghosh for the fruitful discussions, Dr. Alexey Chizhik for advices in with graphics design and Dr. Ingo Gregor for the advices during the construction of the optical setup. We thank Dieter Hille and his team from the precision engineering workshop of the Third Institute of Physics, Georg August University. We also thank Markus Schönekeß and his team, in particular Simon Hoelscher, from the electronics workshop Third Institute of Physics, Georg August University. We thank Thomas Schlichthärle and his supervisor Prof. Dr. Ralf Jungmann for sharing their initial protocol and guidance for conjugation of the nanobody with the docking strand. We thank Dr. Selda Kabatas for helping with the molecular models in Figure 4.2. Finally, we would like to thank Prof. Dr. Silvio Rizzoli for his support.

Conflicts of Interest: FO is a shareholder of NanoTag Biotechnologies GmbH. All other authors declare no conflict of interest.

4.6 References

[1] E.Betzig, G. H. Patterson, R.Sougrat, O. W. Lindwasser, S. Olenych,, H. F. Hess, J. S. Bonifacino, M. W. Davidson, J.Lippincott-Schwartz and H. F. Hess "Imaging Intracellular Fluorescent Proteins at Nanometer Resolution," *Annu. Rev. Biochem*, vol. 75, p. 12352, 2006.

[2] M. Heilemann, S. van de Linde, M. Schüttpelz, R. Kasper, B. Seefeldt, A. Mukherjee, P. Tinnefeld, and M. Sauer, "Subdiffraction-Resolution Fluorescence Imaging with Conventional Fluorescent Probes," *Angew. Chemie Int. Ed.*, vol. 47, no. 33, pp. 6172–6176, Aug. 2008.

[3] M. J. Rust, M. Bates, and X. Zhuang, "Sub-diffraction-limit imaging by stochastic optical reconstruction microscopy (STORM)," *Nat. Methods*, vol. 3, no. 10, pp. 793–796, Oct. 2006.

[4] P. R. Selvin, T. Lougheed, M. Tonks Hoffman, H. Park, H. Balci, B. H. Blehm, and E. Toprak, "Fluorescence Imaging with One-Nanometer Accuracy (FIONA).," *CSH Protoc.*, vol. 2007, p. pdb.top27, Oct. 2007.

[5] R. Jungmann, C. Steinhauer, M. Scheible, A. Kuzyk, P. Tinnefeld, and F. C. Simmel, "Single-Molecule Kinetics and Super-Resolution Microscopy by Fluorescence Imaging of Transient Binding on DNA Origami," vol. 10, p. 43, 2010.

[6] M. Raab, J. J. Schmied, I. Jusuk, C. Forthmann, and P. Tinnefeld, "Fluorescence Microscopy with 6 nm Resolution on DNA Origami," *ChemPhysChem*, vol. 15, no. 12, pp. 2431–2435, Aug. 2014.

[7] M. Dai, R. Jungmann, and P. Yin, "Optical imaging of individual biomolecules in densely packed clusters," *Nat. Nanotechnol.*, vol. 11, no. 9, pp. 798–807, Sep. 2016.

[8] S. S. Agasti, Y. Wang, F. Schueder, A. Sukumar, R. Jungmann, and P. Yin, "DNA-barcoded labeling probes for highly multiplexed Exchange-PAINT imaging."

[9] R. Jungmann, M. S. Avendaño, J. B. Woehrstein, M. Dai, W. M. Shih, and P. Yin, "Multiplexed 3D cellular super-resolution imaging with DNA-PAINT and Exchange-PAINT," *Nat. Methods*, 2014.

[10] J. Schnitzbauer, M. T. Strauss, T. Schlichthaerle, F. Schueder, and R. Jungmann, "Super-resolution microscopy with DNA-PAINT," 2017.

[11] J. Ries, C. Kaplan, E. Platonova, H. Eghlidi, and H. Ewers, "A simple, versatile method for GFP-based super-resolution microscopy via nanobodies," *Nat. Methods*, vol. 9, no. 6, pp. 582–584, 2012.

[12] M. Mikhaylova, B. M. C. Cloin, K. Finan, R. van den Berg, J. Teeuw, M. M. Kijanka, M. Sokolowski, E. A. Katrukha, M. Maidorn, F. Opazo, S. Moutel, M. Vantard, F. Perez, P. M. P. van Bergen en Henegouwen, C. C. Hoogenraad, H. Ewers, and L. C. Kapitein, "Resolving bundled microtubules using anti-tubulin nanobodies.," *Nat. Commun.*, vol. 6, p. 7933, Aug. 2015.

[13] M. Maidorn, S. O. Rizzoli, and F. Opazo, "Tools and limitations to study the molecular composition of synapses by fluorescence microscopy.," *Biochem. J.*, vol. 473, no. 20, pp. 3385–3399, Oct. 2016.

[14] F. G. Wouterlood, *Cellular imaging techniques for neuroscience and beyond*. Elsevier/Academic Press, 2012.

[15] S. S. Agasti, Y. Wang, F. Schueder, A. Sukumar, R. Jungmann, and P. Yin, "DNA-barcoded labeling probes for highly multiplexed Exchange-PAINT imaging," *Chem. Sci.*, vol. 8, no. 4, pp. 3080–3091, 2017.

[16] E. F. Fornasiero and F. Opazo, "Super-resolution imaging for cell biologists: concepts, applications, current challenges and developments.," *Bioessays*, vol. 37, no. 4, pp. 436–51, Apr. 2015.

[17] A. D. Ellington and J. W. Szostak, "In vitro selection of RNA molecules that bind specific ligands.," *Nature*, vol. 346, no. 6287, pp. 818–22, Aug. 1990.

[18] A. D. Ellington and J. W. Szostak, "Selection in vitro of single-stranded DNA molecules that fold into specific ligand-binding structures," *Nature*, vol. 355, no. 6363, pp. 850–852, Feb. 1992.

[19] C. Tuerk and L. Gold, "Systematic evolution of ligands by exponential enrichment: RNA ligands to bacteriophage T4 DNA polymerase.," *Science*, vol. 249, no. 4968, pp. 505–10, Aug. 1990.

[20] C. Hamers-Casterman, T. Atarhouch, S. Muyldermans, G. Robinson, C. Hamers, E. B. Songa, N. Bendahman, and R. Hamers, "Naturally occurring antibodies devoid of light chains.," *Nature*, vol. 363, no. 6428, pp. 446–8, 1993.

[21] F. Opazo, M. Levy, M. Byrom, C. Schäfer, C. Geisler, T. W. Groemer, A. D. Ellington, and S. O. Rizzoli, "Aptamers as potential tools for super-resolution microscopy.," *Nat. Methods*, vol. 9, no. 10, pp. 938–9, Oct. 2012.

[22] T. Pleiner, M. Bates, S. Trakhanov, C.-T. Lee, J. E. Schliep, H. Chug, M. Böhning, H. Stark, H. Urlaub, and D. Görlich, "Nanobodies: site-specific labeling for super-resolution imaging, rapid epitope-mapping and native protein complex isolation.," *Elife*, vol. 4, p. e11349, Dec. 2015.

[23] S. Strauss, P. C. Nickels, M. T. Strauss, V. Jimenez Sabinina, J. Ellenberg, J. D. Carter, S. Gupta, N. Janjic, and R. Jungmann, "Modified aptamers enable quantitative sub-10-nm cellular DNA-PAINT imaging," *Nat. Methods*, vol. 15, no. 9, pp. 685–688, Sep. 2018.

[24] A. Kirchhofer, J. Helma, K. Schmidthals, C. Frauer, S. Cui, A. Karcher, M. Pellis, S. Muyldermans, C. S. Casas-Delucchi, M. C. Cardoso, H. Leonhardt, K.-P. Hopfner, and U. Rothbauer, "Modulation of protein properties in living cells using nanobodies," *Nat. Struct. Mol. Biol.*, vol. 17, no. 1, pp. 133–8, 2010.

[25] V. Fabricius, J. Lefèbre, H. Geertsema, S. F. Marino, and H. Ewers, "C-terminal labeling of nanobodies for DNA-PAINT dual-color imaging."

[26] B. P. Cormack, R. H. Valdivia, and S. Falkow, "FACS-optimized mutants of the green fluorescent protein (GFP)," *Gene*, vol. 173, no. 1, pp. 33–38, Jan. 1996.

[27] N. C. Shaner, R. E. Campbell, P. A. Steinbach, B. N. G. Giepmans, A. E. Palmer, and R. Y. Tsien, "Improved monomeric red, orange and yellow fluorescent proteins derived from Discosoma sp. red fluorescent protein," *Nat. Biotechnol.*, vol. 22, no. 12, pp. 1567–1572, Dec. 2004.

[28] O. M. Subach, I. S. Gundorov, M. Yoshimura, F. V. Subach, J. Zhang, D. Grüenwald, E. A. Souslova, D. M. Chudakov, and V. V. Verkhusha, "Conversion of Red Fluorescent Protein into a Bright Blue Probe," *Chem. Biol.*, vol. 15, no. 10, pp. 1116–1124, Oct. 2008.

[29] I. Yofe, U. Weill, M. Meurer, S. Chuartzman, E. Zalckvar, O. Goldman, S. Ben-Dor, C. Schütze, N. Wiedemann, M. Knop, A. Khmelinskii, and M. Schuldiner, "One library to make them all: streamlining the creation of yeast libraries via a SWAp-Tag strategy," *Nat. Methods*, vol. 13, no. 4, pp. 371–378, Apr. 2016.

[30] Y.-L. Xiao, J. C. Redman, E. L. Monaghan, J. Zhuang, B. A. Underwood, W. A. Moskal, W. Wang, H. C. Wu, and C. D. Town, "High throughput generation of promoter reporter (GFP) transgenic lines of low expressing genes in Arabidopsis and analysis of their expression patterns," *Plant Methods*, vol. 6, no. 1, p. 18, Aug. 2010.

[31] A. S. Gonzalez-Serricchio and P. W. Sternberg, "Visualization of C. elegans transgenic arrays by GFP.," *BMC Genet.*, vol. 7, no. 1, p. 36, Jun. 2006.

[32] R. Fatima, "Drosophila Dynein Intermediate Chain Gene, Dic61B, Is Required for

Spermatogenesis," *PLoS One*, vol. 6, no. 12, p. e27822, Dec. 2011.

[33] S. Kawamoto, H. Niwa, F. Tashiro, S. Sano, G. Kondoh, J. Takeda, K. Tabayashi, and J. Miyazaki, "A novel reporter mouse strain that expresses enhanced green fluorescent protein upon Cre-mediated recombination," *FEBS Lett.*, vol. 470, no. 3, pp. 263–268, Mar. 2000.

[34] T. Schlichthaerle, A. S. Eklund, F. Schueder, M. T. Strauss, C. Tiede, A. Curd, J. Ries, M. Peckham, D. C. Tomlinson, and R. Jungmann, "Site-Specific Labeling of Affimers for DNA-PAINT Microscopy," *Angew. Chemie Int. Ed.*, vol. 57, no. 34, pp. 11060–11063, Aug. 2018.

[35] R. P. J. Nieuwenhuizen, K. A. Lidke, M. Bates, D. L. Puig, D. Grünwald, S. Stallinga, and B. Rieger, "Measuring image resolution in optical nanoscopy," *Nat. Methods*, vol. 10, no. 6, pp. 557–562, Jun. 2013.

[36] J. Schindelin, I. Arganda-Carreras, E. Frise, V. Kaynig, M. Longair, T. Pietzsch, S. Preibisch, C. Rueden, S. Saalfeld, B. Schmid, J.-Y. Tinevez, D. J. White, V. Hartenstein, K. Eliceiri, P. Tomancak, and A. Cardona, "Fiji: an open-source platform for biological-image analysis," *Nat. Methods*, vol. 9, no. 7, pp. 676–682, Jul. 2012.

[37] U. Endesfelder, S. Malkusch, F. Fricke, and M. Heilemann, "A simple method to estimate the average localization precision of a single-molecule localization microscopy experiment," *Histochem. Cell Biol.*, vol. 141, no. 6, pp. 629–638, Jun. 2014.

[39] S. Culley, D. Albrecht, C. Jacobs, P. M. Pereira, C. Leterrier, J. Mercer, and R. Henriques, "Quantitative mapping and minimization of super-resolution optical imaging artifacts," *Nat. Methods*, vol. 15, no. 4, pp. 263–266, Feb. 2018.

[40] Nicholas J. Agard, and Jennifer A. Prescher, and C. R. Bertozzi*, "A Strain-Promoted [3 + 2] Azide−Alkyne Cycloaddition for Covalent Modification of Biomolecules in Living Systems," 2004.

[41] S. Wolter, A. Löschberger, T. Holm, S. Aufmkolk, M.-C. Dabauvalle, S. van de Linde, and M. Sauer, "rapidSTORM: accurate, fast open-source software for localization microscopy," *Nat. Methods*, vol. 9, no. 11, pp. 1040–1041, Nov. 2012.

[42] M. Mikhaylova, B. M. C. Cloin, K. Finan, R. van den Berg, J. Teeuw, M. M. Kijanka, M. Sokolowski, E. A. Katrukha, M. Maidorn, F. Opazo, S. Moutel, M. Vantard, F. Perez, P. M. P. van Bergen en Henegouwen, C. C. Hoogenraad, H. Ewers, and L. C. Kapitein, "Resolving bundled

microtubules using anti-tubulin nanobodies," *Nat. Commun.*, vol. 6, p. 7933, Aug. 2015.

[43] R. N. Day and M. W. Davidson, "The fluorescent protein palette: tools for cellular imaging.," *Chem. Soc. Rev.*, vol. 38, no. 10, pp. 2887–921, Oct. 2009.

4.7 Supplementary Information for

Nanobody Detection of Standard Fluorescent Proteins Enables Multi-Target DNA-PAINT with High Resolution and Minimal Displacement Errors

Custom-built optical setup description

Measurements were performed on an in-house-built optical setup. In brief, the excitation part included four lasers: 405 nm (CUBE 405-100C, Coherent), 488 nm (PhoxX+ 488-100, Omicron), 561 nm (MGL-FN-561-100, *Changchun*), and 638 nm (PhoxX+ 638-150, Omicron). Manual shutters were used to easily switch between excitation lasers. The lasers were combined into the same optical path using dichroic mirrors DM1 (BrightLine DiO2-R561, Semrock), DM2 (BrightLine FF495-Di03, Semrock), and DM3 (zt405 RDC, Chroma). Then, the laser beams were coupled into a single-mode fiber (P1-460B-FC-2, Thorlabs) with typical coupling efficiency of 40-50%. After exiting the fiber, the beam was collimated and expanded by a factor of 3.6X using telescopic lenses. In order to achieve wide-field illumination, lens L1 (AC508-200-A-ML, Thorlabs) focused collimated laser beam on the back focal plane of the high-NA objective (UAPON 100x oil, 1.49 NA, Olympus). In order to switch between Epi-, HILO-, or TIRF-illumination schemes, the translation stage TS (LNR50M, Thorlabs) was used to mechanically shift the corresponding optical elements. The translation XY stage (M-406, Newport) ensured smooth and stable sample movement during the scan.

A separate translation stage with a differential micrometer screw (DRV3, Thorlabs) was holding the objective and was used for focusing. The emitted fluorescence was separated from the excitation laser using the multi-band dichroic mirror DM4 (Di03 R405/488/532/635, Semrock). Lens L2 (AC254-200-A-ML, Thorlabs) was used as a tube lens. An adjustable slit (SP60, OWIS) was positioned in the image plane and was used to limit the field of view. The multi-band filter BP1 (ZET488/561/635m, Chroma) was used to filter out laser remains in the detection path. Lenses L3 (AC254-100-A, Thorlabs) and L4 (AC508-150-A-ML, Thorlabs) were used to transfer the image plane from the slit to the EMCCD camera (iXon Ultra 897, Andor), thereby providing rectangular space for wavelength-based splitting of the emission light into two or three emission

channels according to the experimental requirements. For this purpose, the dichroic mirrors DM5 (Chroma 550 LPXR) and DM6 (FF648-Di01, Semrock) were positioned on magnetic bases MB (KB50/M, Thorlabs). For each channel, additional band-pass filters were used: BP2 (BrightLine FF 445/20, Semrock) for the blue channel, BP3 (BrightLine FF 536/40, Semrock) for the green channel, and BP4 (BrightLine HC 692/40, Semrock) for the red channel. The overall magnification factor of the optical setup was 166.6X, the pixel size was 103.5 nm x 103.5 nm and the full field of view was 53 µm X 53 µm. Focus stability was achieved by robust construction of the custom microscope body, tightly fixing the 8-well chamber (155411PK, THERMOFISHER SCIENTIFIC) to the sample holder and keeping the temperature in the room stable.

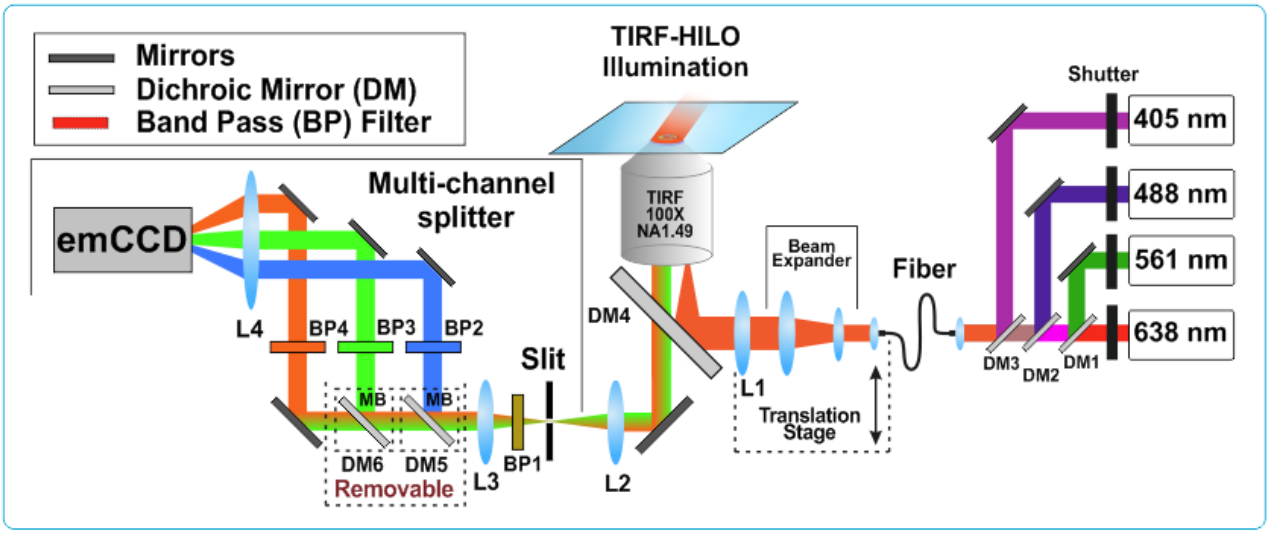

Figure S4.1: Schematic drawing of custom wide-field TIRF optical setup. The excitation is equipped with four lasers and allows excitation of fluorophores on broad spectral range. Multi-channel detection enables simultaneous imaging of fluorophores with different emission spectrum on the same CCD camera. Number of emission channels can be easily switched between one, two and three channels by removing the dichroic mirrors DM5 or/and DM6. The size of region of interest is controlled by a slit.

Localization accuracy and resolution estimations

Detailed numbers as for each reconstructed image resolution are listed in the Table S 4.1.

Cell name	Organelle, protein, docking	NeNa, nm	FRC, nm
Fig.4.4, C1	Mito GFP P1*	20	21
	Golgi RFP P2*	18	27
	Nucleus BFP P3*	22	32
Fig. 4.4, C2	Mito GFP P1*	22	34
	Golgi RFP P2*	16	23
	Nucleus BFP P3*	23	34
Fig. 4.4, C3	Mito GFP P1*	19	38
	Golgi RFP P2*	16	28
	Nucleus BFP P3*	22	31

Cell name	Organelle, protein, docking	NeNa, nm	FRC, nm
Fig 4.4, D1	Mito RFP P2*	19	22
	Golgi GFP P1*	18	24
	Nucleus BFP P3*	23	38
Fig 4.4, D2	Mito RFP P2*	20	28
	Golgi GFP P1*	19	20
	Nucleus BFP P3*	19	24
Fig 4.4, D3	Mito RFP P2*	14	24
	Golgi GFP P1*	18	27
	Nucleus BFP P3*	17	26

Table S1. Average localization precision (NeNa) and resolution estimation using FRC technique for each of the reconstructed images presented in Figure 4. Cell names appear according to the order in Figure 4.

DNA-PAINT analysis toolkits comparison: Picasso vs. Rapidstorm

Verification of Picasso analysis was done by analysing same image with RapidStorm.[1] Recorded DNA-PAINT movie was loaded into RapidStorm. Blinking event were identified by setting the intensity threshold to 60 % of a total brightness. Resolution (both X and Y direction) was set to 10 nm/pixel. The comparison between reconstructed images shown on Figure S 4.2. The achieved resolution was estimating by exporting the localization file output and then running it into SQUIRREL ImageJ plugin[2]. Resulting numbers and comparison to Picasso output shown on Table S1. We saw good agreement between Picasso and RapidStorm results.

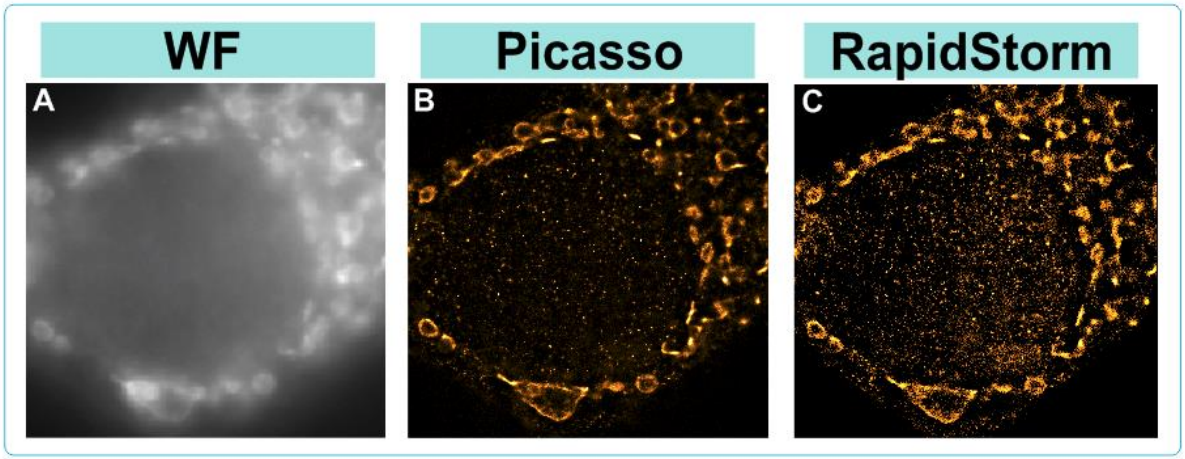

Figure S 4.2: Comparison between Picasso and RapidStorm software packages. (**A**) Wide-field (WF) diffraction-limited image of GFP protein. (**B**) Reconstructed super-resolution image obtained with Picasso software. (**C**) Reconstructed super-resolution image obtained with Picasso software.

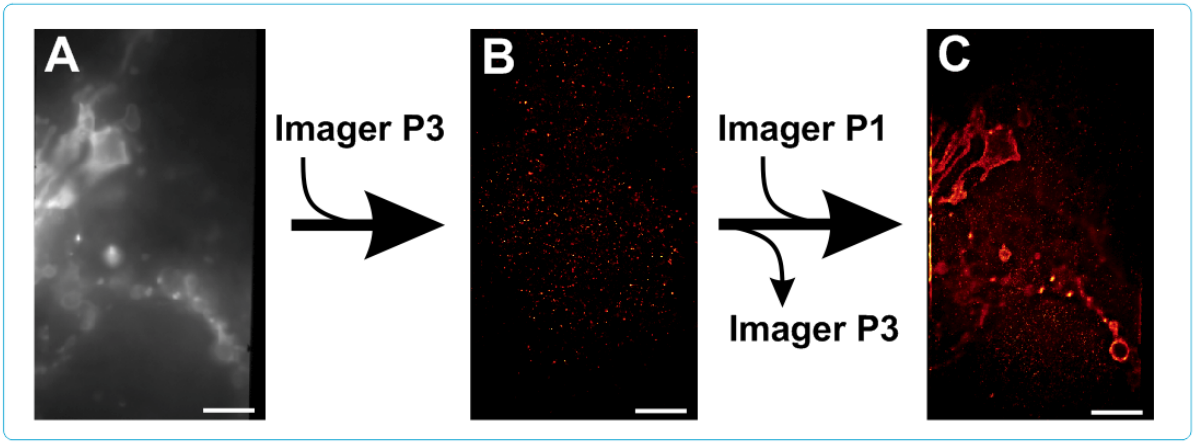

Figure S 4.3: Control experiment for the nanobody specificity and the stickiness of the imager strand inside fixed COS-7 cell transfected with TOM70-GFP-P1*. (**A**) wide-field image of TOM70 GFP. (**B**) Super-resolution image from a DNA-PAINT movie taken in presence of P3 imager. Only few random localization events detected in presence of the imager P3 (**C**) Super-resolution image of the same region of interest, taken in presence of P1 imager (after washing/removing the imager P3).

DNA-PAINT Fourier Ring Correlation resolution maps

For NanoJ-SQUIRREL analysis stack of two statistically independent super-resolution images of the same structure were reconstructed using Picasso and RapidStorm software. Then using 'Calculate FRC Map' feature (block per pixel value 25 and pixel size 10 nm) the FRC map was made and overlaid with respective super-resolution image. Average FRC resolution value was obtained by finding the mean value from the area with high localization density. For this purpose, obtained super-resolution image was cropped and whole procedure was repeated for this area. The average resolutions obtained are 26 nm for Picasso and 30 nm for RapidStorm.

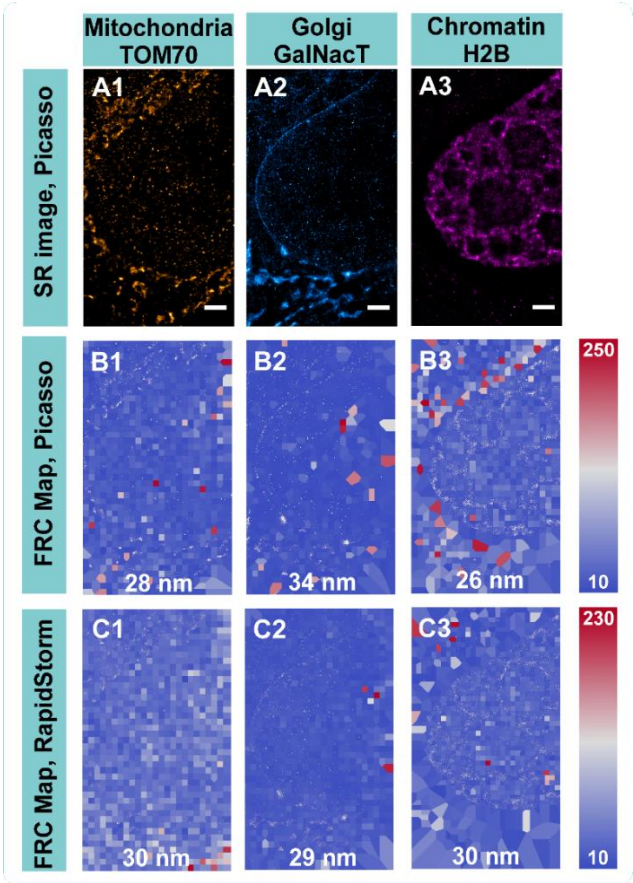

Figure S4.4. Resolution estimation using Fourier Ring Correlation maps realized by SQUIRREL ImageJ plugin[2]. Comparison between Picasso and RapidStorm analysis tools. (A1-3) Super-resolution DNA-PAINT images of COS-7 cell organelles reconstructed by Picasso. (B1-3) FRC map overlaid with the corresponding super-resolution images, as reconstructed by Picasso toolkit. (C1-3) FRC map overlaid with the corresponding super-resolution images, as reconstructed by RapidStorm toolkit. The numbers on the images represent the resolution averaged over the

object region. The colors on B and C indicated resolution, according to scale shown on the right-hand side.

References

1. Wolter, S. *et al*. rapidSTORM: accurate, fast open-source software for localization microscopy. *Nat. Methods* **9,** 1040–1041 (2012).

2. Culley, S. *et al*. Quantitative mapping and minimization of super-resolution optical imaging artifacts. *Nat. Methods* **15,** 263–266 (2018).

5 Circumvention of common labelling artefacts using secondary nanobodies

Shama Sograte-Idrissi, Thomas Schlichthaerle, Carlos J. Duque-Afonso, Mihai Alevra, Sebastian Strauss, Tobias Moser, Ralf Jungmann, Silvio Rizzoli, Felipe Opazo.

Published in Nanoscale **2020, 12**, 10226-10239

Detailed author contribution of Shama Sograte-Idrissi:

- Experimental work and analysis:
  - Performed staining experiments (Fig.5.1, Fig.5.5, Fig 5.6, Supp. Fig 5.1, Supp Fig.5.5, Supp. Fig. 5.6, Supp. 5.7)
  - Analysed data using code by M.A (Fig.5.5 and Fig.5.6, Supp. Fig 5.6, Supp. Fig.5.7)
  - Coupling of the Nanobodies to the docking strands and purification (Fig.5.2, Fig. 5.3)
  - Prepared sample for DNA PAINT and collaborated on the imaging (Fig. 5.2 and Fig.5.3C)
- Wrote the manuscript with the help of F.O and contributions from all the other authors

The paper here was formatted to fit the editing format of the thesis.

Circumvention of common labelling artefacts using secondary nanobodies

Shama Sograte-Idrissi[1,2,3], Thomas Schlichthaerle[4,5], Carlos J. Duque-Afonso[6,7,8,9], Mihai Alevra[1], Sebastian Strauss[4,5], Tobias Moser[6,7,8,9], Ralf Jungmann[4,5], Silvio Rizzoli[1,2,8], Felipe Opazo[1,2,10 *]

[1]Institute of Neuro- and Sensory Physiology, University Medical Center Göttingen, 37073 Göttingen, Germany

[2]Center for Biostructural Imaging of Neurodegeneration (BIN), University of Göttingen Medical Center, 37075 Göttingen, Germany

[3] International Max Planck Research School for Molecular Biology, Göttingen, Germany

[4] Faculty of Physics and Center for Nanoscience, LMU Munich, 80539, Munich, Germany

[5] Max Planck Institute of Biochemistry, 82152, Martinsried, Germany

[6] Institute for Auditory Neuroscience and InnerEarLab, University Medical Center Göttingen, 37075 Göttingen, Germany.

[7] Max Planck Institute for Experimental Medicine, 37075 Göttingen, Germany

[8] Multiscale Bioimaging Cluster of Excellence (MBExC), Göttingen, Germany

[9]University of Göttingen, 37075 Göttingen, Germany

[10] NanoTag Biotechnologies GmbH, 37079, Göttingen, Germany

Key words: DNA-PAINT, STED, light sheet, immunostaining, artifacts, linkage error, nanobodies.

[*] Corresponding Author: fopazo@gwdg.de

5.1 Abstract

A standard procedure to study cellular elements is via immunostaining followed by optical imaging. This methodology typically requires target-specific primary antibodies (1.Abs), which are revealed by secondary antibodies (2.Abs). Unfortunately, the antibody bivalency, polyclonality, and large size can result in a series of artefacts. Alternatively, small, monovalent probes, such as single-domain antibodies (nanobodies) have been suggested to minimize these limitations. The discovery and validation of nanobodies against specific targets are challenging, thus only a minimal amount of them are currently available. Here, we used STED, DNA-PAINT, and light-sheet microscopy, to demonstrate that secondary nanobodies 1) increase localization accuracy compared to 2.Abs; 2) allow direct pre-mixing with 1.Abs before staining, reducing experimental time, and enabling the use of multiple 1.Abs from the same species; 3) penetrate thick tissues more efficiently; and 4) avoid probe-induced clustering of target molecules observed with conventional 2.Abs in living or poorly fixed samples. Altogether, we show how secondary nanobodies are a valuable alternative to 2.Abs.

Graphical abstract

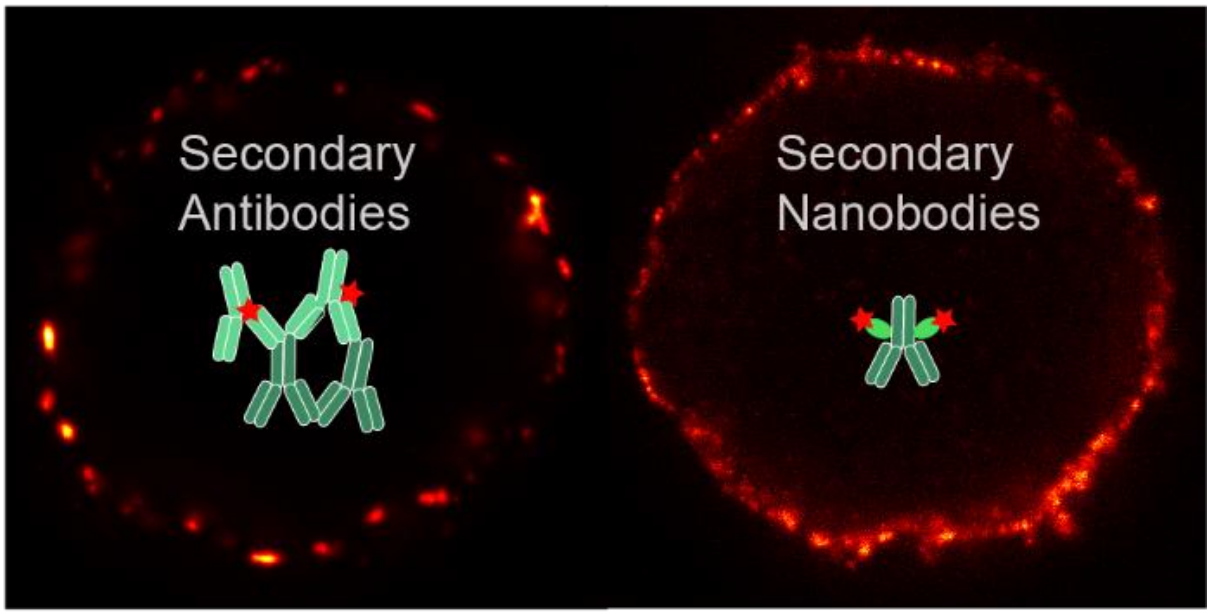

5.2 Introduction

Standard immunodetection approaches use typically a primary antibody (1.Ab) which binds the protein of interest (POI) and a secondary antibody (2.Ab) that binds to the 1.Ab and carries a detection element. In fluorescent microscopy techniques, the detection element is a fluorophore[1,2] or a single strand of DNA. The latter is used in DNA Point Accumulation for Imaging in Nanoscale Topography (DNA-PAINT), a single molecule localization microscopy technique reaching <5 nm resolution by transiently binding of single stranded DNA bearing a fluorophore to their complementary strand on the target of interest[3]. The complex formed by the primary antibody and the secondary antibody (1.Ab-2.Ab) is widely used because it is a cost effective and flexible approach since only the 2.Abs need to be coupled to the detection element. However, the use of this complex carries some relevant limitations. First, the 1.Ab-2.Ab can measure up to 30 nm, leading to a large distance between the targeted molecule and the detection element, causing the so called "linkage" or "displacement" error[4]. While this might not influence the results in some applications (e.g. epifluorescence, ELISA or FACS), it is of major relevance for super-resolution microscopy techniques where the localization precision can be as high as 1 nm[5]. The linkage error can be reduced by using directly labelled small affinity probes like camelid single domain antibodies (sdAbs) also known as nanobodies (Nbs)[4,6], affibodies[7], aptamers[8,9] or affimers[10], which all have sizes below 3 nm. Unfortunately, such small probes exist only for a handful of targets[11] due to their rather laborious selection and validation process, while conventional 1.Abs are readily available for a large number of POIs. An alternative to the standard 2.Abs was recently developed: monovalent recombinant secondary nanobodies (2.Nbs)[12]. Secondly, the large size of the 1.Ab-2.Ab complex makes them to perform poorly in crowded cellular environments or when the epitopes are abundant and densely arranged. In this respect, smaller probes such as aptamers or nanobodies are more efficient in the detection of the POI[8,13,14]. Moreover, sample penetration of full antibodies is a problem when staining thick biological specimen such as tissues, biopsies or whole organisms[13,15]. For the optimal labelling of these thick samples, protocols have been established, but they are often laborious and require time-consuming incubations of weeks[16] or need artefact-prone epitope retrieval protocols[17]. Smaller probes are expected to shorten some of these long incubations. Third, in a multiplex immunostaining, i.e. when multiple targets are stained in the same sample, scientists are typically constrained to use 1.Abs coming from different species. This is because, standard immunostaining needs to be done in a sequential manner: first 1.Abs are

incubated on the sample, washed off and only then 2.Abs are incubated. Therefore, 1.Abs should be raised in different species and 2.Abs should recognize one species specifically, limiting the choice of antibodies for a multiplexing staining. It has been shown that by pre-mixing 1.Abs with 2.Nbs in a tube prior staining, one could circumvent this species limitation and use on a sample 1.Abs from the same species[12]. Finally, conventional antibodies used commonly for immunodetections are bivalent binders, i.e. each antibody molecule can bind two POIs/epitopes simultaneously. In the case of polyclonal antibodies, they are not only bivalent binders, but they also contain an unknown number of different antibodies able to bind the POI. This is the case of the vast majority of 2.Abs used for detection of 1.Ab in immunofluorescence applications. The bivalency and polyclonality of 2.Abs combined have been proposed as characteristics that induce clustering of the POI and their interactors, which can have a strong impact in the conclusions obtained from such experiments[18,19]. The use of monovalent secondary probes should minimize the potential of secondary probe induced clustering effects.

In this work, we tested and thoroughly validated the use of 2.Nbs for several microscopy applications. We first confirmed that the usage of 2.Nbs decreases linkage error by using them in STED microscopy and DNA-PAINT. We then exploited the ability of these probes to allow the simultaneous use of several 1.Abs from the same species by using them in Exchange-PAINT multiplexed super-resolution microscopy. This technique enables to image a virtually infinite number of targets in high resolution in the same sample[20,21]. Additionally, we observed that pre-mixing 1.Ab and 2.Nb can save time in staining thick biological samples imaged under light-sheet microscopy, ensuring also a better sample penetration and homogenous staining. Finally, we systematically compared the probe-induced clustering of the target protein either using directly-labelled monovalent probes, like affibodies and single Fab' fragments, and conventional 1.Abs detected by polyclonal and bivalent 2.Abs or by monovalent 2.Nbs. We observed that 2.Nbs drastically reduced the clustering of the target in both live and fixed sample. This makes 2.Nbs a real alternative to conventional 2.Abs by minimizing experimental time, expanding the multiplexing ability of immunostainings, improving the tagging precision and signal linearity, and finally avoiding the probe-induced clustering artefacts.

5.3 Results

Secondary nanobodies provide higher staining accuracy than secondary antibodies

First, we investigated the accuracy of 2.Abs or 2.Nbs in revealing their 1.Ab target. To do so, we imaged (using a two-color STED microscopy setup) COS-7 cells fixed with cold methanol to ensure a strong immobilisation of the POI[22], then stained with a monoclonal 1.Ab anti-alpha tubulin directly conjugated to the fluorAbberiorStar635P. The primary antibody was subsequently recognized by either a polyclonal 2.Ab or a monovalent 2.Nb, both carrying the fluorophore AbberiorStar580. An autocorrelation analysis was performed on these images to evaluate the staining accuracy of the secondary probes by comparing them with the directly labelled primaries. Initially, the autocorrelation of the images with the fluorescent 1.Ab provided an idea of the distribution or density of the 1.Ab on microtubule filaments. The autocorrelation curve obtained from the signal of the 2.Nb followed the tendency of the autocorrelation obtained for the anti-alpha tubulin primary antibody, which proposes that the 2.Nb signal accurately follows the fluorescent signal from the 1.Ab. In contrast, when performing the same analysis on the staining performed with the polyclonal 2.Abs, the correlation curve was shifted to the right. This suggests that the 2.Ab inaccurately reveals the location of the 1.Ab anti-alpha tubulin (Fig. 5.1A). To confirm this, we decided to analyse paraformaldehyde (PFA) fixed peroxisomes within primary hippocampal neurons. We compared the diameter of these small organelles when imaged with STED microscopy after using a 1.Ab anti-pmp70 (a peroxisomal membrane protein) revealed by a 2.Ab or a 2.Nb. We observed a significant shift to smaller diameters of 1.Ab-2.Nb labelled organelles after comparing 3020 peroxisomes stained with 1.Ab-2.Ab and 3109 peroxisomes stained with 1.Ab-2.Nb (Fig. 5.1B). To evaluate more precisely if the 2.Nbs decrease the linkage error, we needed a technique providing higher spatial resolution. For this purpose, we used DNA-PAINT that has achieved sub-10-nm resolution[3]. As DNA-PAINT uses affinity reagents attached to short DNA oligonucleotides, we coupled the 2.Nbs site-specifically to a single stranded DNA oligo (termed docking strand) as described previously[23]. We performed an assay which has been used as gold standard in the field to assess linkage error[24]. We immunostained the microtubule network of fibroblast cells with a monoclonal 1.Ab against alpha tubulin, and detected it by either a 2.Ab or a 2.Nb coupled to docking strands (Fig. 5.2). After analysing the diameter of ~80 microtubules for each condition, we obtained an average diameter of 61.3±13.2 nm (mean±SD) when using the

2.Ab and 38.3±9.34 nm when using a 2.Nb (Fig. 5.2 G, I). A similar gain in precision was observed previously using dSTORM[12]. Additionally, we performed an autocorrelation analysis on single microtubules to corroborate their difference in size, and we observed a significantly faster loss in autocorrelation for microtubules stained with 2.Nb (Fig. 5.2H).

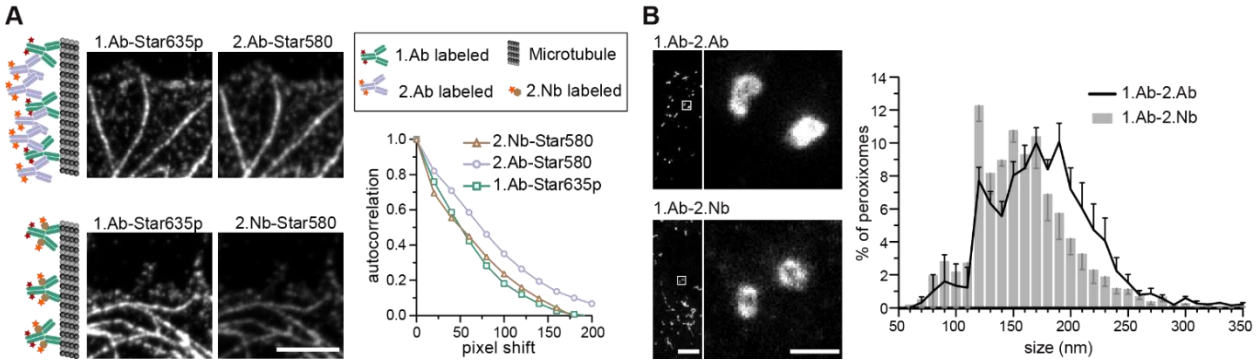

Figure 5.1. 2.Nbs minimize the linkage error caused by 2.Abs and increase detection accuracy. (**A**) Two-color STED imaging of microtubules stained with 1.Ab directly labelled with AbberiorStar635P dye and secondary reagents (either 2.Ab or 2.Nb) labelled with AbberiorStar580. Fixation conditions were the same for both conditions (methanol fixation, see Methods). Example images and schematic representation of the experimental procedure. Scale bar 2.5 µm. Autocorrelation analysis on signal obtained from either the 1.Ab or the secondary probe microtubules. N=51 line profiles for 2.Nb, N= 70 for 2.Ab and N=121 for 1.Ab. One-way ANOVA p=1.061x10-6 F=14.58 followed by post hoc Bonferroni tests indicates that the 2.Ab is different with p<0.01 from the 1.Ab and 2.Nb which themselves are indistinguishable. **(B)** Primary hippocampal neurons were fixed for 30 minutes with 4% PFA, and stained against the peroxisome protein (pmp70) with 1.Ab-2.Ab or 1.Ab-2.Nb. Exemplary STED images. Scale bars 10 µm (overview) and 100 nm (zoom). Size distribution analysis of peroxisomes. N=3109 peroxisomes were analysed when stained with 2.Nb and N= 3020 stained with 2.Ab. Error bars correspond to the standard error of the mean from 4 independent experiments. Paired t-test shows that the apparent size of peroxisomes stained with 2.Nb is on average smaller with p<0.01 compared to the one stained with 2.Ab.

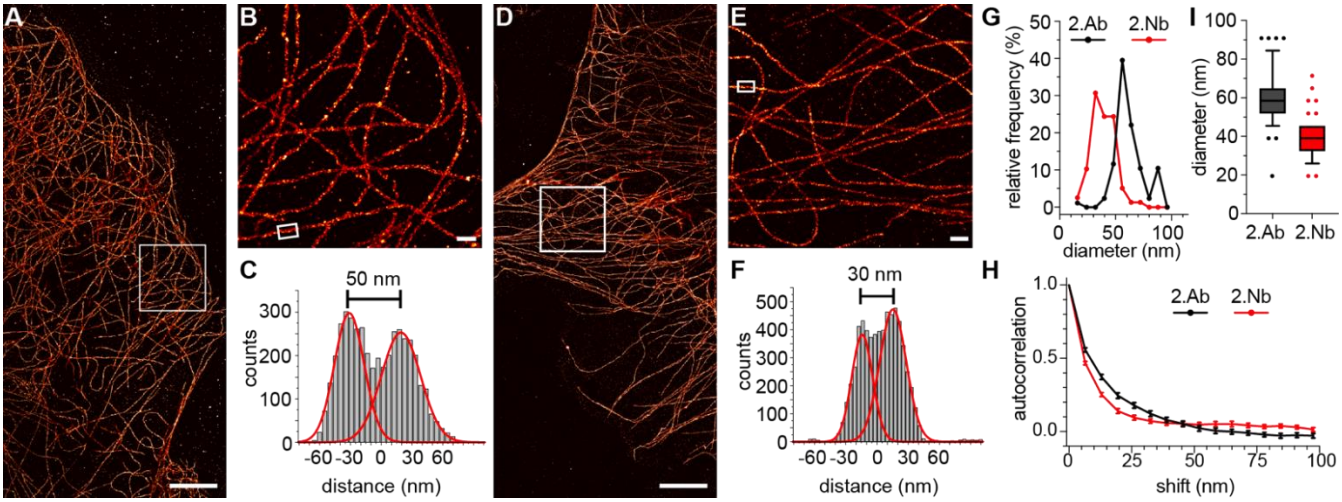

Figure 5.2: DNA-PAINT imaging using secondary antibodies or secondary nanobodies shows differences in microtubule´s diameter size. (**A**) Overview DNA-PAINT image of COS-7 cells fixed with cold methanol and stained with 1.Ab targeting alpha tubulin and 2.Ab coupled to a DNA-PAINT docking strand. (**B**) Zoom-in image of the region highlighted in A. (**C**) Cross-sectional histogram example of the region highlighted in B, showing a microtubule filament diameter of ~50 nm. (**D**) Overview DNA-PAINT image of alpha tubulin stained with 1.Ab and 2.Nb (**E**) Zoom-in image of the region highlighted in D. (**F**) Cross-sectional histogram example of the region highlighted in E, showing a microtubule filament diameter of ~30 nm. Scalebars: 5 □m (A, D), 500 nm (B, E). (**G**) Histogram analysis for the microtubules diameter distribution (86 cross-sections for 2.Ab and 78 for 2.Nb). (**I**) Box & Whiskers graph of G. Whiskers represent 10 & 90 percentiles. Two-tailed unpaired t-test results in $p < 0.0001$ (****). (**H**) Autocorrelation analyses with N=57 line profiles for each condition; 2.Nb display a significantly faster loss of autocorrelation than 2.Abs (Mann Whitney test $p<0.0001$).

Premixing secondary nanobodies bypasses the primary antibody animal-species limitations

In standard immunoassays, 1.Abs are first incubated with the sample followed by washes to remove unbound excess of primary antibodies. Only at this point, labelled-2.Abs are incubated for a period of time with the sample followed by washes to eliminate the non-bound excess of 2.Abs before imaging the specimen. Pre-mixing the 1.Ab with the 2.Ab before adding them to the sample would shorten protocols and save considerable amount of time and costs (e.g. in clinical pathology laboratories). However, this is not possible due to the polyclonality and bivalency of 2.Abs that result in agglutination or aggregation of the 1.Abs-2.Abs complexes and thus in a failure to stain the intended target in the sample (Supp. Fig. 5.1). If the secondary probe binds to the 1.Ab in a monovalent fashion, pre-mixing primary and secondary probes would be possible. The pre-mixing of 2.Nbs with a

mouse monoclonal 1.Ab anti-alpha tubulin for 15 minutes resulted in properly stained filaments (Supp. Fig. 5.1) and single bands detected in a fluorescent Western blot assay (Supp. Fig. 5.2 A). Bypassing this limitation by pre-mixing with monovalent secondary probes open a new possibility in immunoassays, i.e. it allows to use several 1.Abs against different targets raised in the same species. To detect two or more POIs it was typically required that each 1.Ab comes from a different animal (e.g. mouse, rabbit and chicken for the detection of 3 POIs on the same specimen). This strict requisite is necessary to ensure the indirect detection of the POIs with species-specific 2.Abs. This restriction provides a limitation for the choice of 1.Ab and it can reduce the multiplexing capability of immunoassays. Here we chose three different monoclonal 1.Abs raised all in mouse directed against alpha-tubulin, GM130 (Golgi), and FXFG repeats in nucleoporins (nuclear pore complex; NPC). Each was pre-mixed with anti-mouse kappa-light chain 2.Nbs carrying different fluorophores (Fig. 5.3A, B). COS-7 cells were imaged under scanning confocal microscopy, and they clearly displayed the three stained structures (microtubules, Golgi and NPC) with minimal background and negligible cross-talk between the channels. This multiplexing assay requires that the 2.Nb stays bound to its primary antibody without swapping to another primary during the staining incubation, which would result in the cross-contamination of signals. To asses this potential problem, we performed a control experiment where mouse 1.Ab anti-GM130 was pre-mixed with excess of fluorescently labelled 2.Nb anti mouse antibody (2.Nb-Star635p). In parallel, mouse 1.Ab anti-alpha tubulin was premixed with excess of non-fluorescent 2.Nb anti mouse antibody. Finally, these individual pre-mixtures were added simultaneously to methanol-fixed cells and were incubated for 1 hour, 3 hours or overnight. We were not able to observe the distinctive microtubule pattern in any of the conditions, which demonstrates that no cross-contamination from the fluorescent 2.Nbs pre-mixed with the 1.Ab anti-GM130 onto the 1.Ab anti-tubulin occurred (Fig. 5.3 C-G; Supp. Fig 5.3). Similarly, this pre-mixing capability could be applied for the detection of 2 different POIs in fluorescent Western blots assays (Supp. Fig. 5.2 B). The option of pre-mixing primary antibodies with secondary nanobody is ideal for techniques that allow the detection of multiple targets (multiplexing). Therefore, we turned once again to DNA-PAINT, this time we used an extension termed Exchange-PAINT that can, in theory, image an unlimited number of POIs on the same

sample with a few nanometer precision[20,23]. We stained primary hippocampal neurons with two mouse monoclonal 1.Abs and each was pre-mixed with 2.Nbs conjugated to DNA docking strands with orthogonal sequences. We performed Exchange-PAINT on synapses stained against bassoon, a protein highly enriched at the pre-synaptic active zone[25], and the scaffold protein homer that is concentrated at the post-synaptic density[26] (Fig. 5.3 H, I). Notably, we obtained a super-resolved view of single neuronal synapses using two primary antibodies from the same species. We measured a distance of 129.5±10.9 nm (Fig. 5.3 J-K) between bassoon (pre-synaptic) and homer (post-synaptic), reproducing previous results obtained with other advanced microscopy techniques such as dSTORM[27] and X10 expansion microscopy[28]. The presence of localisations of homer in the pre-synaptic area is most likely due to unspecific background staining caused by the respective 1.Ab (Supp. Fig. 5.4).

Secondary nanobodies enhance sample penetration in shorter incubation time

We used the time advantage of pre-mixing 1.Abs with the 2.Nbs to stain a complex thick sample that requires long incubation with the probes to ensure proper sample staining. We used cochleae extracted from three weeks old mice and stained parvalbumin-α, a calcium buffering protein present in inner hair cells and type I spiral ganglion neurons (Fig. 5.4). We compared how long the 1.Ab-2.Nb and 1.Ab-2.Ab needed to be incubated to result in a homogenous staining throughout the sample. In order to image the entire volume, we used light-sheet microscopy after decalcification and clearing. Two cochleae obtained from the same animal were stained either with 1.Abs and sequentially with 2.Abs or with 1.Abs pre-mixed with 2.Nbs for comparable amount of time. The cochleae stained with 1.Ab-2.Ab for a total of 6 days (3 days 1.Ab, 3 days 2.Ab) showed insufficient penetration of the staining, with signals accumulated in the outer bone surface and in the edges exposed to the solution (Fig. 5.4 A). The cochlea stained with the same antibody for 14 days (7 days 1.Ab, 7 days 2.Ab) showed a better staining performance, revealing hair cells and neurons. However, the ganglion displayed a staining gradient with stronger signals on the edges, indicating insufficient detection of target molecules deep in the tissue (Fig. 5.4 A, area depicted with white discontinuous lines). On the other hand, the cochleae stained with pre-mixed 1.Ab-2.Nb for 6 and 14 days revealed a homogenous staining of neurons in an analogue area. No apparent difference in term of signal homogeneity between the two incubation times was observed (Fig. 5.4 B, area depicted with white discontinuous lines).

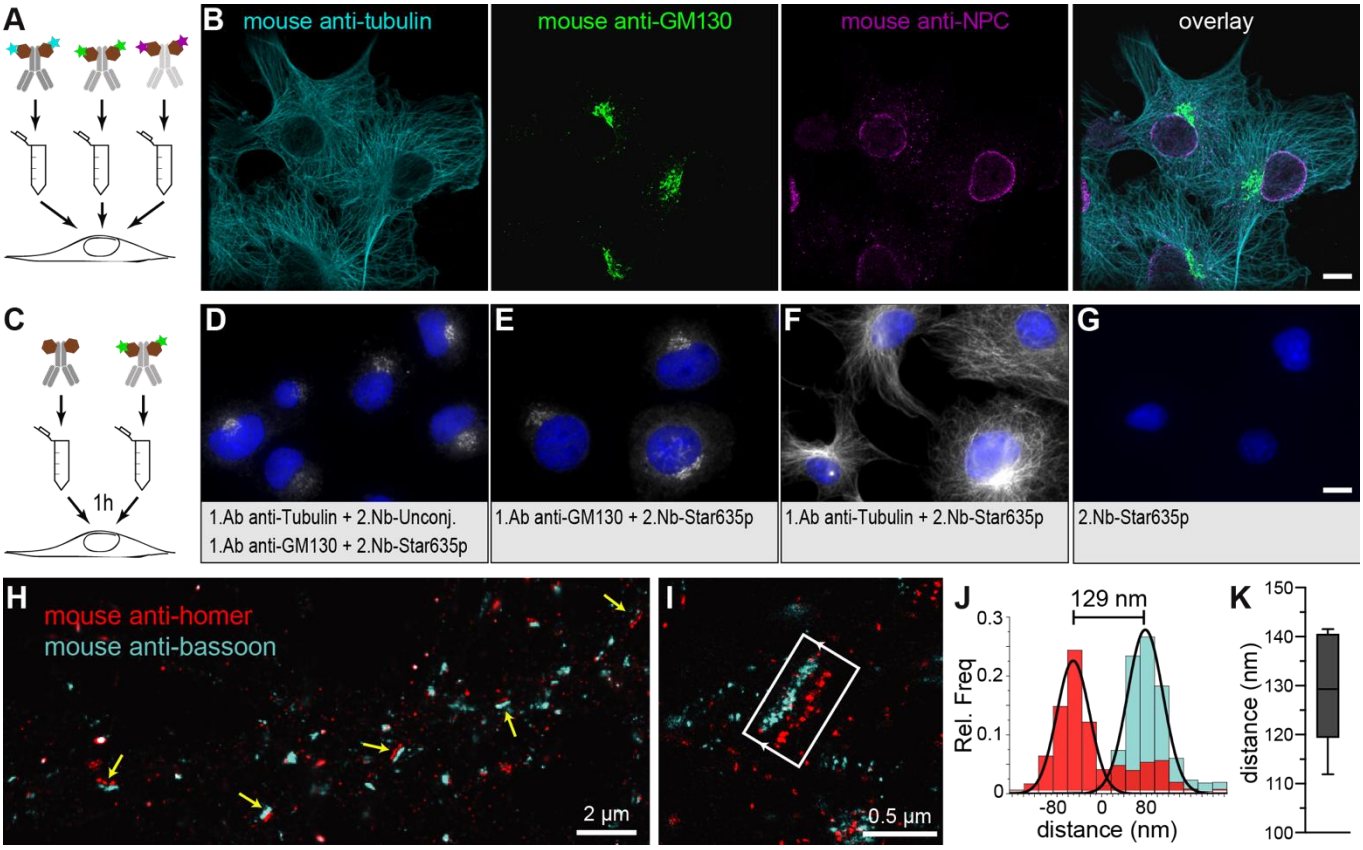

Figure 5.3. Pre-mixing 1.Abs with 2.Nbs allows to use same animal-species 1.Ab for several target proteins on the same sample. (**A**) Scheme of pre-mixing: different 1.Abs were pre-mixed with 2.Nbs each carrying different fluorophores and subsequently incubated on cells. (**B**) Example of confocal images performed on COS-7 cells stained with the pre-mixing methods. Cyan: mouse anti-tubulin 1.Ab pre-mixed with 2.Nb-CF633. Green: mouse anti-GM130 1.Ab pre-mixed with 2.Nb-Alexa488. Magenta: mouse anti-NPC 1.Ab pre-mixed with 2.Nb-Alexa 546. Scale bar represents 10 µm. (**C**) Scheme of the experimental procedure: a mouse monoclonal anti-tubulin antibody was pre-mixed with unconjugated 2.Nbs. A monoclonal anti-GM130 antibody was pre-mixed with 2.Nb conjugated to Star635p. (**D**) Epifluorescence example image of cells co-incubated with both mixtures simultaneously for 1h. (**E**) Control where only the anti-GM130 premixed with 2.Nb-Star635p was used. (**F**) Control sample stained only with anti -Tubulin premixed with 2.Nb-Star635p. (**G**) Control where 2.Nb conjugated to Star635p was used without 1.Ab. All images displayed in D-G are equally scaled, for direct comparison. Scalebar represents 10 µm (**H**) Exchange-PAINT overview image of primary rat hippocampal neurons. Yellow arrows indicate evident mature synapses where the pre-synaptic active zone (mouse 1.Ab anti-bassoon) and post-synaptic density (mouse 1.Ab anti-homer) are in front of each other. (**I**) Higher magnification of a selected synapse where a synaptic cleft is recognized. (**J**) Exemplary histogram analysis of the selected synapses displaying the length of the synaptic cleft. (**K**) Distance analysis of 8 different synapses averaging a mean of 129.5±10.9 nm (mean±SD). Graph shows the data as Box & Whiskers representing 10 & 90 percentiles.

A custom written analysis quantifying the signal intensity throughout the ganglion of the cochleae (Fig. 5.4 C, Supp. Figs 5.5 and 5.6) showed how the signal coming from cochleae stained with 1.Ab-2.Nb displayed a plateau phase meaning homogenous staining, while the ones stained with 1.Ab-2.Ab displayed a peak showing a gradual staining from the distal to the central portion of the ganglion.

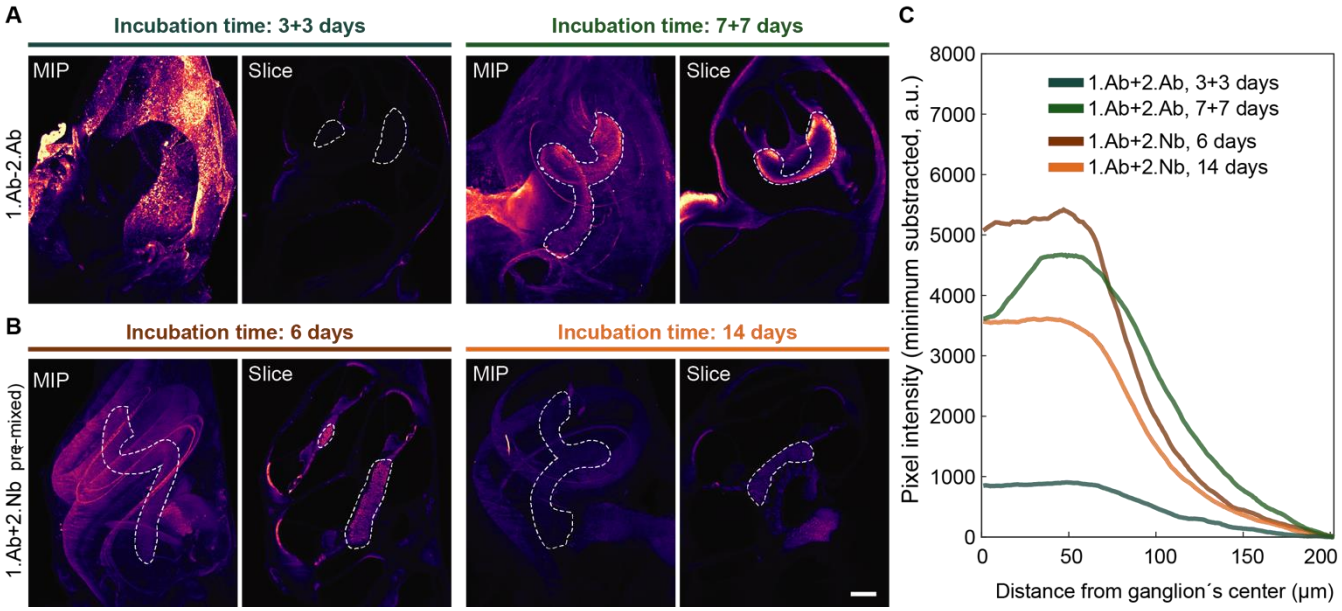

Figure 5.4: Pre-mixing decreases the incubation time necessary to obtain homogenous staining of the cochlea. Mice intact cochleae were stained with a parvalbumin-α antibody, either pre-mixed with 2.Nb (**A**) or sequentially incubated with 2.Ab (**B**) for the time indicated. In each panel, the maximal intensity z-projection (MIP) and an exemplary light-sheet microscopy slice of an intact cochlea (Slice) are depicted. Scale bar: 200 µm. Ganglion outlined by dotted line (**C**) Mean pixel line profile from radii crossing the ganglion distributed along the centerline of the ganglion. See Supp. Fig. 5.5 for schematic analysis explanation and Supp. Fig. 5.6 for raw data. N=2 cochlea per condition. Note: the plateau profile depicted by the samples stained with 2.Nb, as opposed to the relatively pronounced peak profile in the samples stained with 2.Ab for 7 days or to the flat profile in the samples stained for 3+3 days.

Secondary nanobodies reduce probe-induced clusters of target proteins on living cells

To test if the 2.Nbs have an effect in the probe-induced clustering of target molecules, we decided to analyse the surface distribution of IgM containing B cell receptors (IgM-BCRs) on a human B cell line (Ramos cells). This cellular model allows simple visual inspection and numerical analysis because the POIs are evenly distributed in the cellular surface of these resting B cells[29]. Cells were first stained and then chemically fixed with aldehydes to be imaged under stimulation emission depletion (STED) microscopy. Initially, the surface IgM-BCRs on living Ramos cells were stained using fluorescent-monovalent probes: a monoclonal affibody[29] or a polyclonal single Fab fragment (polyFab) (Fig. 5.5). In this case a smooth continuous plasma membrane signal from the surface IgM-BCRs distribution was observed at the optically sliced equator of the cells. However, when cells were stained using a 1.Ab-2.Ab, a sparse clustered signal was clearly identified (Fig. 5.5). Finally, we tested if the 2.Nbs elicit a similar clustering effect observed using 1.Ab-2.Ab detection system. Interestingly, a considerably milder effect was observed when using the same 1.Ab detected by a 2.Nbs, partially rescuing the distribution pattern observed when stained with the monovalent affibody or polyFab that bind directly to the IgM-BCRs (Fig. 5.5). These results suggest that although the bivalency of the monoclonal 1.Ab still deviates slightly from the signal distribution obtained with fluorescent monovalent primary probes, the major cluster-inducing element is contributed by the conventional 2.Abs. A Pearson´s autocorrelation analysis[30] was used to quantify the probe-induced clustering. The custom-written analysis consists of collecting the STED image intensity along the membrane and correlating it to itself for different rotation angles. We then plotted the autocorrelation curves, which start with a perfect correlation ($r = 1$) at zero rotation and decrease at higher rotations (Fig. 5.5 B, with rotation angle converted to corresponding membrane distance). The major empirical effect between the different conditions was observed at membrane distances between 0.7 to 1 µm. Therefore, the correlations measured throughout this interval were then averaged with the value obtained from each cell corresponding to a spot on the scatter plot (Fig. 5.5 C). With this method we determined an average autocorrelation of 0.34±0.19 (mean±SD) for cells stained with the monovalent polyFab and 0.29±0.16 for cells stained with the monovalent affibody, while it was only 0.07±0.12 for the cells stained with monoclonal 1.Ab and polyclonal 2.Ab. Interestingly, this effect was not only evident

using super-resolution microscopy, but it was also observed in diffraction limited scanning confocal microscopy images (Supp. Fig. 5.7). As expected by the more continuous pattern observed, the average autocorrelation of cells stained with 1.Ab-2.Nb was 0.21±0.17 indicating a significant decrease (rescue) of the probe-induced clustering artefact caused by the polyclonal 2.Ab (Fig. 5.5).

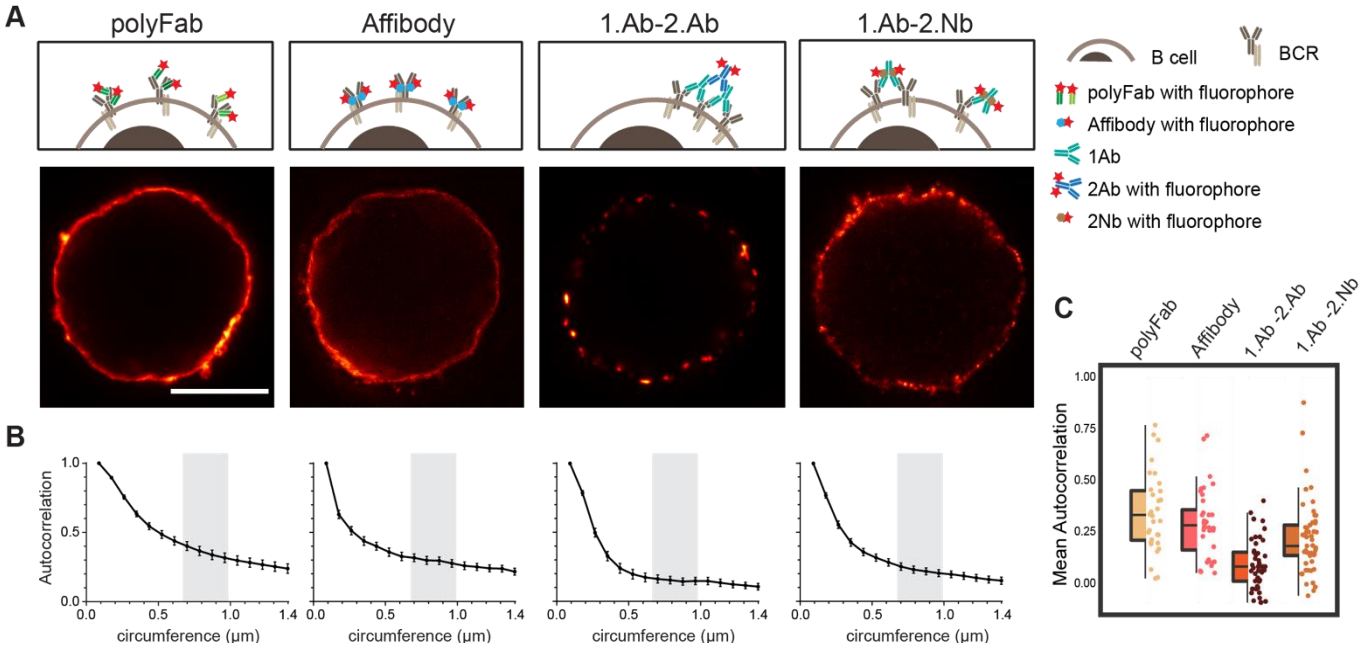

Figure 5.5: Live staining of IgM-BCRs on Ramos cells shows different pattern according to the probe used. (A) STED images of a B cell stained with fluorescent polyclonal single Fab' fragment (polyFab); affibody; primary antibody revealed by a fluorescent secondary antibody (1.Ab-2.Ab); primary antibody revealed by a secondary nanobody (1.Ab-2.Nb). All fluorescent probes were conjugated to AbberiorStar635P fluorophores. Scale bars = 5 µm. (B) Autocorrelation analysis along the circumference of cells. We analysed three independent experiments with N≥ 10 cells for each conditions (C) Box-dot plots show the average autocorrelation from 0.7 µm to 1.0 µm circumference (grey zones shown in the graphs in B). Boxes show the interquartile range (IQR). Lines signify medians, and whiskers extend to 1.5 times the IQR. Lower box represents higher clustering. The autocorrelation observed in 1.Ab-2.Ab differs from the monovalent probes (polyFab and affibody) by $p \leq 0.0001$ and from 1.Ab-2.Nb by $p \leq 0.001$. P values were calculated with one-way ANOVA followed by Tukey Multiple Comparison Test. See Supp. Table 5.5 for full statistics.

Probes induce clusters of target proteins in aldehyde-fixed cells

It has been noticed that conventional fixations times with 4% paraformaldehyde (PFA) does not necessarily prevent protein movement[34]. Also, other variables like blocking reagents and temperature need to be taken into consideration and tested case-by-case depending on the imaged target31. A more efficient fixative such as glutaraldehyde (GLU) could be used, but it generates unwanted autofluorescence and only few affinity molecules bind their target epitopes after GLU crosslinking. A recently described di-aldehyde alternative that seems to alleviate some of these problems caused by PFA and GLU is glyoxal[32]. However, glyoxal implementation is very recent and the vast majority of researchers still use PFA-fixation for conventional immunofluorescence. Therefore, we tested and compared the probe-induced clustering after exposing the Ramos cells for 10 and 30 minutes with 4% PFA or 30 minutes with a combination of 4% PFA and 0.1% GLU (Fig. 5.6 and Supp. Fig. 5.8). We compared these fixative conditions and live staining using the classical 1.Ab-2.Ab complexes or the 1.Ab-2.Nb imaged under STED microscopy. Our observations suggest that applying 4% PFA for 10 minutes is not enough to avoid the artefactual formation of clusters induced by 1.Ab-2.Ab (autocorrelation of 0.14±0.11 not significantly different from the live staining condition 0.07±0.12). However, 4% PFA fixation for 30 minutes seems to be sufficient to rescue to a great degree the clustering artefact caused by the 2.Ab (0.23±0.18 different from the live staining condition with p value $P \leq 0.001$; see also Fig.5.2 A). Using the 2.Nbs had no significant change between live, 10 or 30 minutes of fixation with 4% PFA (0.21±0.17, 0.20±0.17 and 0.21±0.18 respectively; Fig. 5.6 B). As expected, similar non-clustering effects are observed for a primary monovalent probe like the monovalent polyFab directed against human IgM-BCRs (Supp. Fig. 5.8). In addition, when observing the staining pattern created by the combination of 4% PFA and 0.1% GLU for 30 minutes, the stained rim of the cells is not a thin layer as observed by PFA fixation, but it displays a texture-like surface. From studies in electron microscopy, it is expected that GLU fixation results in a better ultrastructure preservation. Due to the uneven texture-like surface when fixing with PFA and GLU, and therefore a reduced homogeneity at the investigated spatial scale, the Pearson´s correlation analysis has the tendency to paradoxically display a slightly lower correlation (Fig. 5.6, boxplot).

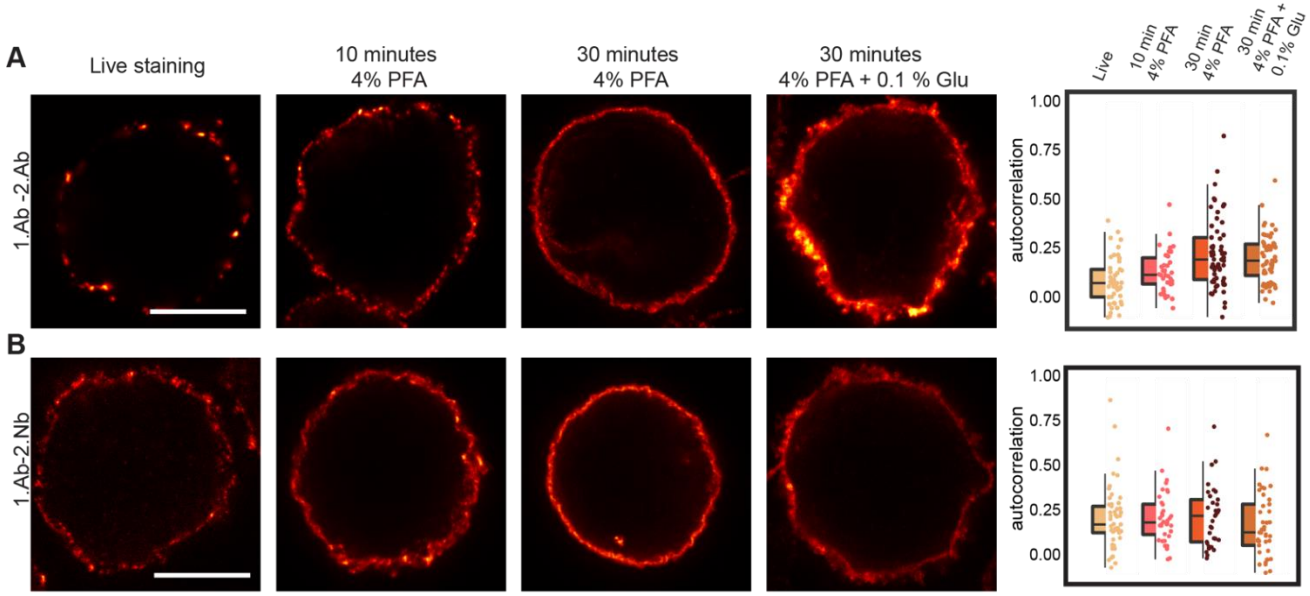

Figure 5.6: Probe-induced clustering on aldehyde fixed B cells. (**A**) and (**B**) STED images showing the effect of fixation on clustering induced by 1.Ab-2.Ab or 1.Ab-2.Nb. Scale bars represent 5 µm. Box-dot plots show the average autocorrelation from 0.7 µm to 1.0 µm circumference (grey zones shown in the Supp. Fig. 9). Boxes show the interquartile range (IQR). Lines signify medians, and whiskers extend to 1.5 times the IQR. Lower box represents higher clustering. Autocorrelation curves are detailed in Supp. Fig. 5.9 and statistics in Supp. Table 5.5.

5.3 Discussion

In this study we have systematically studied how secondary nanobodies detecting primary antibodies can be used to overcome several limitations and artefacts caused by conventional polyclonal secondary antibodies. Additionally, problems with polyclonal secondary antibodies have been repeatedly attributed to the poor reproducibility provided by polyclonal serums, which can be highly heterogeneous[37]. Therefore, we propose that using recombinantly produced monoclonal and monovalent secondary reagents, like the nanobodies characterized here, not only eliminates the ethically controversial use of animals for conventional 2.Abs (e.g. from donkey, goat, sheep, etc.), but importantly also minimizes artefacts, linkage errors and increases the reproducibility of biomedical experiments.

Smaller size of the secondary probe decreases linkage error and increases staining accuracy

Although it has been already demonstrated that small primary affinity probes are able to minimize the linkage error[4,8,12], there was just one indication performed in dSTORM that secondary nanobodies can increase the labelling precision[12]. Here we show, in addition to the resolution improvement by using 2.Nbs on DNA-PAINT and STED microscopy, that bulky secondary antibodies not accurately represent the distribution of the primaries, due to a combination of their polyclonal nature and large size (Fig. 5.1 A). We show that the 1.Abs directly labelled with a fluorophore decorates microtubules with a certain periodicity that can be followed when revealed with a 2.Nb but not with a conventional 2.Ab, suggesting that the 2.Ab blurs the localization of the 1.Ab. This inaccuracy of the polyclonal 2.Abs can have major consequences in one of the main application of fluorescence microscopy, namely co-localization studies.

Pre-mixing overcomes the species limitation for multiplexing microscopy

Mixing the primary and the secondary reagents prior to incubating them with the sample (pre-mixing) is a desired feature as it saves experimental time. This cannot be performed with conventional bivalent polyclonal 2.Abs (Supp. Fig. 5.1), however, pre-mixing has been shown to work when using monovalent binders against 1.Abs[12]. This feature eliminates the animal-species limitation of the primaries when detecting two or more POIs. We first showed that it is possible to use 2 mouse 1.Abs in a simpler Western-blot assay (Supp. Fig. 5.2), and then we tried 3 different mouse 1.Abs in immunofluorescence under conventional scanning confocal microscopy. Nevertheless, pre-mixing needs to be carefully tested and well validated for every application and for each set of 1.Abs, since the 2.Nbs are not covalently bound to the 1.Abs. However, our control experiments (Fig. 5.3 C & Supp. Fig. 5.3), suggest that no significant movement between primaries can be observed if incubation with pre-mixed primary and secondary nanobodies is for 1 and 3 hours, even overnight incubations did not show signs of cross-contamination when using two primaries of the same species. To ensure the permanence of the secondary nanobody on its primary antibody in demanding applications like DNA-PAINT, we decided to perform a short post fixation between the applications of the different pre-mixed pairs. Here we showcased the proof-of-principle of pre-mixing with 2.Nbs and multiplexing using Exchange-PAINT super-resolution microscopy. We determined the distance between the pre- and post-synapses with high accuracy (Fig. 5.3), and we obtained average synaptic cleft distances comparable to values from other

methods[27]. Exchange-PAINT not only provides high spatial resolution, but it also eliminates the limit on the number of POIs that can be imaged in the same sample. This makes the combination of pre-mixing using 2.Nbs with Exchange-PAINT a very powerful approach for multiplexing.

Pre-mixing shortens experimental time and allows a better penetration of probes in thick tissue

Immunostaining protocols of complex thick tissue samples typically require days to weeks[16,17]. This is because it takes time for the antibody to penetrate into the tissue, for thoroughly washing unbound binders, and also because the 1.Abs and 2.Abs have to be performed sequentially. This may be a problem even in cell monolayers, where it has been suggested that primary and conventional secondary antibodies have difficulties penetrating in crowded areas and revealing all epitopes[8,13].

Pre-mixing the primary antibodies and the secondary nanobodies reduces the experimental time of immunostainings and becomes a very important time-saver when used in samples that require long staining protocols. Here we used cleared mouse cochlea imaged with light sheet microscopy to compare the staining pattern of primaries pre-mixed with 2.Nbs or using conventional secondary antibodies. Our observation suggest that pre-mixing shorten the conventional protocol by at least half the time (i.e. 6 days of staining; Fig. 5.4). We did not test shorter times for pre-mixing, but the fact that no clear difference in intensity or signal distribution between pre-mixed stainings for 6 or 14 days were observed, suggests that optimal incubation time might be even shorter.

Antigen clustering on cells rescued by the use of secondary nanobodies

Our results on probe-induced clustering of the POI show strong indications of conventional polyclonal 2.Abs as the major clustering element. We first demonstrated that these probe-induced artefacts can be minimized using monovalent probes as secondary reagents (e.g. 2.Nbs). The staining of living Ramos cells show how the distribution of BCRs at the plasma membrane went from a smooth to a clustered pattern when using 1.Ab-2.Ab, which was rescued by the use of 2.Nb (Fig. 5.6). This result suggests that monoclonal bivalent 1.Ab has some minor effect on probe-induced clustering compared to the major clusters of the POI observed when using polyclonal 2.Ab. Importantly, this probe-induced clustering artefact could also be observed when short

aldehyde fixation was performed. Sample fixation with 4% paraformaldehyde for 10 minutes is a widespread practice in biology laboratories, but seems to be insufficient to fully immobilize cellular elements, in agreement with previous work[22,32]. We complemented the previous observations by demonstrating that polyclonal 2.Abs drastically enhance the clustering of the POIs if samples are poorly fixed (Fig. 5.6). The artificial aggregation of POIs even after chemical fixation can lead to several misleading conclusions when studying for example co-localization of two or more POIs, poly-molecular arrangements or if molecular mechanisms are interpreted after imaging analysis.

Conclusion

Small, monovalent, and monoclonal probes specific to the endogenous targets are clearly the ideal probes to reveal POIs. Unfortunately, their availability is limited to a handful of targets. On the other hand, a large amount of well validated monoclonal antibodies is available. Our data suggests that the localization of primary antibodies with recombinant secondary nanobodies or probably other small monovalent binder such as Protein A[33], can minimize the probe-induced clustering of targets, increase the localization accuracy in super-resolution microscopy, lower steric hindrance for detecting more target molecules, enhance the sample penetration, remove the species-limitation by pre-mixing allowing high multiplexing capabilities, and finally, increase the reproducibility of results with no needs of animals.

5.4 Material and Methods

Cell culture

Cells were cultured at 37°C, 5% CO_2 in a humified incubator. The human Burkitt lymphoma B cell lines DG75 and COS-7 fibroblast were obtained from the Leibniz Institute DSMZ—German Collection of Microorganisms and Cell Culture (DSMZ Braunschweig, Germany). For maintenance, cell lines were kept on petri dishes. For experiments cells were plated on poly-L-lysine (PLL)-coated coverslips. DG75 cells were splitted every 3 days using fresh complete medium (RPMI medium supplemented with 10% Fetal Bovine Serum (FBS), 4 mM L-glutamine and 100 U/ml penicillin and streptomycin). COS-7 fibroblast cells were cultured in complete Dulbecco's MEM with the addition of 10% FBS, 4 mM L-glutamine, 0.6% penicillin and streptomycin. A549 cells (ATCC, Cat. No. CRL-1651) were maintained in DMEM (Thermo Fisher Scientific, Cat. No. 10566016), supplemented with 10% Fetal Bovine Serum (Thermo Fisher Scientific, Cat. No. 10500-064) and 1% Penicilin/Streptomycin (Thermo Fisher Scientific, Cat. No. 15140-122).

Rat primary hippocampal neuron cultures were prepared as described before by Opazo *et al*.[33] In brief, the brains of P1-2 were extracted and placed in cold HBSS (ThermoFisher, Waltham, Massachusetts, USA). The hippocampi were extracted and placed in a solution containing 10 mL DMEM (Thermo Fisher), 1.6 mM cystein, 1 mM $CaCl_2$, 0.5 mM ethylenediaminetetraacetic acid (EDTA), 25 units of papain per mL of solution, with CO_2 bubbling, at 37°C for 1 h. The solution was removed and the hippocampi were incubated in 10% FBS-DMEM, 73 µM albumin for 15 minutes. The hippocampi were triturated using a 10 mL pipette in complete-neurobasal medium [Neurobasal A (Thermo Fisher), containing 2% B27 (Thermo Fisher) and 1% Glutamax-I (Thermo Fisher). Neurons were plated (12-well plate) on poly-L-lysin-hydrochloride (Sigma-Aldrich, St. Louis, Missouri, United States) coated coverslips in plating medium (500 mL MEM, 50 mL horse serum, 5 mL glutamine, 330 mg glucose. After 2 h the plating medium was replaced with 1.25 ml neurobasal-A Medium.

Staining of BCRs

For the staining of BCRs on living cells the staining was performed on ice to avoid the internalization of BCRs. Cells (~200,000 cells/sample) were pelleted by centrifuging at 1000 x g, resuspended in 50 µL of ice-cold complete medium (see above) containing the investigated affinity probe (see Supp.Table 1) and incubated for 10 minutes on ice. Cells were centrifuged at 400 x g at 4°C in a table top centrifuge and the excess of probe was removed. Cells were washed by resuspension in 1 ml of ice-cold Dulbecco's Phosphate Buffered Saline (DPBS) followed by incubation on ice for 3 minutes and centrifugation at 400 x g at 4°C. The washing step was repeated 3 times to remove most of the excess of the fluorescent probes. When a secondary probe was used (see Supp. Table 1), the cells were further incubated with 50 µL ice-cold complete medium containing the secondary reagent and incubated for another 30 minutes on ice (staining controls without secondary probes were left for the same time on DPBS only). Washing was performed as described for the primary probe. After staining, cells were resuspended in 1 ml of cold DPBS and transferred to a 12 well plate (containing PLL coated coverslips). The plate was centrifuged at 500 rpm for 5 minutes at 4°C. The DPBS was carefully discarded and cells were fixed with 1 mL of 4% paraformaldehyde and 0.1% GLU in PBS for 10 minutes on ice followed by 30 minutes at room temperature. The fixative was removed and quenched by adding 1 mL of 0.1 M Glycine in DPBS and incubated at room temperature for additional 20 minutes. Finally, cells were rinsed with 1 mL DPBS and mounted on a glass slide using Mowiol (6 g glycerol, 6 ml deionized water, 12 ml 0.2 M Tris buffer pH 8.5, 2.4 g Mowiol 4–88, Merck Millipore). The staining of BCRs of fixed Ramos cells, around 200,000 cells/sample were pelleted by centrifuging at 1000 x g, resuspended in 1 mL DPBS and transferred to a single well on a 12 well plate containing PLL coated coverslips. The cells were let to sediment on the coverslips at 37°C for 1 h. DPBS was removed and cells were fixed with one of the following conditions: 10 minutes with 4% PFA, 30 minutes with 4% PFA or 30 minutes with 4% PFA and 0.1% GLU. For all fixation conditions the first 5 minutes incubation were performed on ice and the remaining fixation time at room temperature. After fixation, the quenching of reactive aldehydes was performed as described above. Cells were finally rinsed and staining was done in 1 mL DPBS containing the different probes. After staining, cells were washed 3 times with DPBS for 5 minutes at room temperature and coverslips were mounted in Mowiol.

Imaging and Analysis of BCRs

Cells were imaged with multicolor confocal STED microscope (Abberior Instruments, Göttingen, Germany) described below. Imaging was performed using a 640 nm excitation laser and a 775 nm depletion laser. The final raw STED images were obtained after the summation of 3 successive scans. STED images of cells were analyzed using custom written MATLAB scripts (MATLAB Release 2014b, The MathWorks, Inc., Natick, Massachusetts, United States). For each cell center, the radii of two circles were manually adjusted so that the area between the circles contained all of the cell membrane. From this area, pixels were grouped by their angle to the cell center (in 360 bins of 1°) and maximum-projected to obtain the angle-dependent intensity $\hat{y}_i$along the membrane. The self-similarity of this function was then assessed by calculating its normalized autocorrelation

$$a_i = F^{-1}\{F(\hat{y}_i) \cdot conj(F(\hat{y}_i))\} \qquad (1)$$

using the normalized intensity

$$\hat{y}_i = \frac{y_i - \acute{y}}{\sqrt{\Sigma(y_i - \acute{y})^2}} \qquad (2)$$

the mean value $\hat{y}$, the complex conjugate *conj* and the fast Fourier transform F. It gives a measure of how similar the intensity of two points are on the membrane depending on their angular distance. As the effect of different labeling homogeneities was best observed at a range of 8-12°, the autocorrelation from this area was then averaged for each cell (and translated to the perimeter in µm in the figures by approximating the cell diameters to 10 µm).

Peroxisome size

Primary neurons from rat hippocampi were fixed with 4% PFA 30 minutes followed by 30 minutes at room temperature. The neurons were incubated in a blocking and permeabilizing solutions containing 5% bovine serum albumin (BSA) and 0.1% Triton X-100 for 20 minutes at room temperature. The rabbit polyclonal anti Pmp70 antibody (Abcam, Cat No: ab85550) was added on the cells in a 1:300 dilution in PBS containing 2.5% BSA 0.05% for 1 h at room temperature. The cells were washed 3 time for 10 minutes each in PBS and incubated with either secondary goat anti rabbit conjugated to AbberiorStar635P (Abberior GmbH, Cat. No: 2-0012-007-2) or the 2.Nb FluoTag-X2 anti rabbit also conjugated to AbberiorStar635P (NanoTag Biotechnologies, Cat. No: N1002) and diluted to 1:200 and 1:100 respectively in 2.5% BSA, 0.05% Triton X-100 for 1 h at

room temperature. The cells were washed 3 times for 10 minutes in PBS and finally mounted in Mowiol. The peroxisomes on neurons were imaged with the STED setup described above using a 640 nm excitation laser and 775 nm depletion laser.

For determining the peroxisome diameter, the images were filtered using a bandpass filter, in MATLAB, to remove background noise, and peroxisome regions of interest were identified using an empiric threshold. The smallest ellipse diameter that fitted each peroxisome region of interest was then obtained by using the self-written MATLAB routine.

Autocorrelation on Microtubule stainings

COS-7 cells were fixed with -20°C pre-cooled methanol for 20 minutes at -20°C. Methanol was removed and cells were blocked with 3% BSA for 20 minutes at room temperature. The cells were incubated with primary mouse monoclonal antibody anti-tubulin (SySy, Cat No: 302 211) directly coupled to Atto647N fluorophore and diluted at 1:25 in 1.5 % BSA for 1 h at room temperature. The cells were washed 3 times, 5 minutes each with PBS. Cells were then incubated with either secondary nanobody FluoTag-X2 anti mouse conjugated to AbberiorStar580 (NanoTag Biotechnologies, Cat No: N1202) or secondary full antibody anti mouse coupled to AbberiorStar580 (Abberior, Cat. No: 2-0002-005-1) diluted at 1:100 in 1.5% BSA for 1 h at room temperature. Finally, cells were washed as described above and mounted in Mowiol. Images of microtubules were taken using the Abberior Expert line STED system. A 640 nm excitation laser and 775 nm depletion laser were used for imaging the 1.Ab (AbberiorStar635P) while a 561 nm excitation laser and 775 nm depletion laser were used for imaging the fluorophore on the secondary probes (AbberiorStar580). The correlation of the STED signal provided by the secondary probe to the primary probe was analyzed as follows. Lines were drawn following the stained microtubules using a self-written routine in MATLAB. The Pearson´s correlation between the directly labeled 1.Ab and the secondary probes were measured at the drawn lines. The autocorrelation of the signal from the 1.Ab was used as control.

Pre-mixing experiment Immunostaining

COS-7 cells were fixed in -20°C pre-cooled methanol for 20 minutes at -20°C. The cells were blocked by addition of 3% BSA in PBS for 30 minutes at room temperature. In the meantime, the 1.Abs were pre-mixed for 30 minutes with two molar excess of fluorescently-labeled 2.Nbs in PBS containing 1.5% of BSA (see Supp. Table 2). The pre-mixed complexes were then incubated on the fixed cells sequentially. In between each round of pre-mixed complex, the cells were washed 3 times for 5 minute each with PBS and post-fixed with 4% PFA for 10 minutes. The excess of fixative was quenched with 0.1 M glycine in PBS for 10 minutes. The cells were mounted in Mowiol and imaged using a multicolor laser scanning confocal microscope (the STED system described before).). For the immunostaining of Fig. 3D-G and Supp. Fig. 3, COS-7 cells were stained and blocked as described above. The 1.Abs were premixed with approximately two-fold molar excess of the 2.Nbs (either fluorescently labelled or unconjugated) for 30 minutes. The premixed complexes were in this case incubated simultaneously on the cells for the amount of time indicated. The cells were then washed three times for 5 min with PBS. Hoechst was added and rinsed after 5 minutes before they were mounted in Mowiol and imaged with STED microscopy.

Pre-mixing experiment Western Blot

A confluent plate of COS-7 cells was briefly washed with ice-cold PBS before lysing the cells on the plate sitting on ice with pre-chilled Lysis buffer (50 mM Tris/HCl, pH 7.5, 150 mM NaCl, 2 mM EDTA, 0.5% IgePAL, 0.5 % Sodium deoxycholate 33and freshly added DNAse, 1 mM PMSF and protease inhibitor cocktail (Roche). Cells were scrapped and passed through a syringe with needle gauge 26 several times avoiding foam. After max. speed centrifugation at 4°C in a table-top centrifuge for 15 minutes. Supernatant was taken and mixed with 2x loading dye (50 mM Tris-HCl, 4% sodium dodecyl sulfate (SDS), 0.01% Serva Blue G, 12% glycerol, pH 6.8, 50 mM DTT) and heated at 95°C for 10 minutes. Boiled samples were then loaded in 10% SDS-PAGE. Proteins in the gel were then transferred to a nitrocellulose membrane in wet trans-blot cell (Biorad). The membranes were blocked in blocking buffer (5% Nonfat Dried Milk in PBS + 0.1% Tween-20) for 1 hour at room temperature. 1.Abs were pre-mixed with the corresponding fluorescent 2.Nb

for 10 minutes and then added together on the blocked nitrocellulose membranes for 60 minutes at room temperature. Membranes were washed 5 times with large volumes of PBS for 5 minutes each and read with a LiCor Sytem Odyssey Clx.

Conjugating secondary nanobodies to ssDNA or fluorophores

Secondary nanobodies (obtained from NanoTag Biotechnologies GmbH) were coupled to docking oligonucleotide strands (Biomers GmbH, Ulm, Germany) functionalized with an azide group at the 5′-end and an Atto488 fluorophore at the 3′-end following the protocol described by Sograte-Idrissi et al[23]. In brief, the nanobody containing an extra C-terminal cysteine was reduced with 5 mM TCEP (Sigma-Aldrich, Cat. No. C4706) for 2 h on ice. TCEP was removed via 10 kDa molecular weight cut-off (MWCO) Amicon spin filters (Merck, Cat. No. UFC500324) and the nanobody was coupled through maleimide conjugation chemistry to a maleimide-DBCO crosslinker (Sigma-Aldrich, Cat. No. 760668). After removal of excess crosslinker through 10 kDa MWCO Amicon spin filters, the nanobody was coupled to the docking oligo containing an azide group at its 5´-end (Biomers) through a strain promoted azide-alkyne cycloaddition reaction. To avoid background signal, the excess of docking oligo was removed by a size exclusion chromatography column (Superdex® Increase 75, GE Healthcare) on an Äkta pure 25 system (GE Healthcare). The docking strand sequences were obtained from Agasti el al.[20] and can be found in Supp. Table 5.2.

Nanobodies bearing ectopic cysteines were first reduced with 10 mM of TCEP for 1-2h. After removing TCEP with a Nap5 column (GE Healthcare), reduced nanobodies were immediately exposed to ~3 molar excess of maleimide-functionalized fluorophore (e.g. CF633, Alexa488, Alexa546, Star635p) for 2 hours. Subsequently, the excess of dye was removed using a size exclusion chromatography column (Superdex® Increase 75, GE Healthcare) on an ÄKTA pure 25 system (GE Healthcare).

DNA-coupling of antibody

Donkey anti-mouse secondary antibody (Jackson Immunosearch, Cat. No. 715-005-151) was labelled with a DNA strand via a DBCO-sulfo-NHS ester linker according to the protocol as previously described[3]. Briefly, primary amines of the antibody were reacted with a DBCO-sulfo-

NHS ester cross-linker (Jena Bioscience, Cat. No. CLK-A124-10) for two hours at 4°C. Unreacted cross linker was then removed using a Zeba desalting column (40 kDa MWCO, Thermo-Fisher Scientific, Cat. No. 87766). The antibody-DBCO conjugate was then attached to a DNA strand functionalized with an azide group at the 5'-end via copper-free click chemistry. Excess DNA-strands were removed using 100 kDa MWCO Amicon spin filters (Merck Millipore, Cat. No. UFC510096). Docking strand sequences were obtained from Agasti el al.[20] and can be found in Supp. Table 2.

Stainings for DNA-PAINT

Cells for DNA PAINT imaging were plated on an 8-well chamber coverglass II (Sarstedt, Cat No: 94.6190.802 or ibidi, Cat. No. 80827 ibidi, Cat. No. 80827) and grown overnight. The next day, cells were fixed. COS-7 cells were fixed with pre-cooled methanol for 20 minutes at -20°C. The cells were then blocked with 3% (w/v) BSA for 20 minutes at room temperature and incubated with a primary mouse monoclonal anti-alpha tubulin antibody directly labelled with Atto647N (SySy, Cat No: 302 211) and diluted 1:25 in 1.5% BSA for 1 h at room temperature. Unbound 1.Ab was removed by washing the cells 3 times with PBS for 5 minutes each. They were then incubated with the 2.Nb or 2.Ab coupled to DNA-PAINT docking sequences. The cells were washed 3 times for 5 minutes with PBS.

Rat primary hippocampal neuron, were fixed by adding 4% PFA for 30 minutes on ice and 4% PFA for 30 additional minutes at room temperature. The neurons were blocked and permeabilized with 3% (w/v) BSA + 0.1% (v/v) Triton X-100 for 20 minutes at room temperature. The mouse monoclonal anti Bassoon (Enzo, Cat No: ADI-VAM-PS003-F) and the mouse monoclonal anti Homer (SySy, Cat No: 1600111) were pre-mixed in a 1:5 molar ratio with 2.Nb anti mouse coupled to P1 (5´- TTATACATCTATTTT-Atto488-3´) and P5 (5´-TTTCAATGTATTTTT-Atto488-3`) respectively. The pre-mixed anti Homer 1.Ab and its 2.Nb were added on the cells for 1 h with slow orbital shaking. The cells were then washed 3x 5 minutes each with PBS and 1x 5 minutes with PBS supplemented with 0.1 M NaCl. The 1.Ab-2Nb complex were briefly fixed by adding 4% PFA for 5 minutes. The fixative was removed and the remained quenched with 0.1 M glycine for 5 minutes. The pre-mixed anti Bassoon 1.Ab with its 2.Nb was added to the cells for 1 h at room temperature, and post-fixed and quenched as before. For drift correction purposes, cells were

incubated with a 1:10 dilution of 90 nm gold particles (cytodiagnostics, Cat. No. G-90-100) for 10 minutes, rinsed 4x with PBS and stored at 4°C until imaging was performed.

DNA-PAINT Imaging

The correspondent imager strand to the DNA-PAINT docking sites used on the nanobodies (Supp. Table 5.3), were equipped with a Cy3b fluorophore at their 3´-end. Imager strands were diluted in PBS supplemented with 500 mM NaCl and 1x Trolox (Sigma-Aldrich, Cat. No. 238813-1G). Imager strands were used at concentrations between 0.5 nM and 2 nM to optimize the number of binding events per time (see Supp. Table 4). The focal plane was found by searching in the 488 nm channel. Cells were then imaged in the 561 nm channel with a 100-200 ms exposure time per frame for 30.000-60.000 frames. When exchange of imager was performed, the chamber was washed 10 times with PBS supplemented with 0.5 M NaCl until no residual blinking was observed anymore. The reconstruction of the raw data and the drift correction with cross correlation and gold particles as fiducial markers was performed with Picasso Sotware[3]. Microtubule filament sizes were measured via exported regions and Gaussian fits in Origin on the localizations. Images were acquired as described below and raw data movies were reconstructed with the Picasso software suite. Drift correction and multicolor alignment was performed via redundant cross-correlation and 90 nm gold particles as fiducial markers. The Picasso software suite was also used to detect the localisation frequency events in Supp. Fig. 5.4A.

Cochlear staining

Mice C75Bl6/J of 3 weeks of age were euthanized by decapitation. Cochleae were harvested and fixed in 4% PFA for 45 minutes at room temperature. Afterwards, they were processed following the cochlea-adapted version of the iDISCO+ protocol (Keppeler and Duque-Afonso et al., in preparation). Briefly, they were decalcified in 10% EDTA in PBS, pH 8, for 2 days and treated with 25% N,N,N′,N′-Tetrakis(2-Hydroxypropyl)ethylenediamine in PBS for another 2 days, in order to remove endogenous fluorescence[34] at room temperature under constant rotation. The samples underwent the methanol-free pre-treatment of the iDISCO+ protocol[35], followed by the regular procedure for immunostaining and clearing. The pre-treatment consisted in subsequent incubations at 37°C under constant shaking of the following solutions: 0.2% Triton X-100 in PBS (2x1h), 0.2% Triton X-100/20% DMSO in PBS (1 day), 0.1% Triton X-100/20% DMSO/0.1%

Tween-20/0.1% Deoxycholate/0.1% IGEPAL CA-630 in PBS (1 day), Triton X-100 in PBS (2x1h). The immunostaining continued at 37°C, under constant shaking, with the incubation of the tissue in a Permeabilization solution (0.16%TritonX-100/20%DMSO/2.3% Glycine (0.3M) in PBS, 2 days) and in a Blocking Solution (0.16% TritonX-100/10%DMSO/3%BSA in PBS, 2 days). The 1.Ab (Guinea Pig antiserum anti-parvalbumin- α, 195 004, Synaptic System) was pre-mixed with the 2.Nb (Nanobody anti-guinea pig Alexa 546) using a molar ratio of 1:3 or 45 min, under constant rotation, at room temperature. The PTwH buffer contained 0.2% Tween-20/0.001% Heparin in PBS. The primary antibody was diluted in a solution containing 5%DMSO/1.5%BSA in PTwH with a concentration of 1:300. The 2.Ab (Goat-Anti Guinea pig 568, Invitrogen, A11075, 1:500) and the 1.Ab pre-mixed with the 2.Nb were diluted in a solution containing only 1.5%BSA in PTwH. The sample were incubated in 4 different ways (37°C, under shaking): 1) 6 days and 2) 14 days in the solution containing the 1.Ab premixed with the 2.Nb, 3) 3 days and 4) 7 days with the 1.Ab followed by a washing step of 1 day in PTwH at room temperature and the incubation of the 2.Ab for 3 and 7 days respectively. Before the clearing procedure, the samples were washed in PTwH for 1 day at room temperature. Finally, samples were dehydrated in an increasing methanol dilution series (20, 40, 60, 80, 100 and 100% Methanol in ddH2O, one hour each), incubated in 66% Dicloromethane/33% Methanol for 3 hours plus two consecutive incubation in 100% DCM for 15 minutes each for lipid extraction, and immerse in Dibenzylether, as a refractive index matching solution.

Cochlear probe penetration quantification

The original stack was resampled by a factor of 2.15x2.15x2 and converted to 8-bits in FIJI[36]. Then, the ganglion was coarsely segmented manually with TrakEM2[37] and imported to 3DSlicer[38,39]. There, a median filter with a kernel of 10x10x1 pixel was applied and the resulting image was threshold segmented, converted to a 3D closed surface or mesh and stored as a .stl file, as it is the input format needed for the following step. Centerlines of the ganglion were then calculated using the vmtkcenterline function of the open source software VMTK (the Vascular Modelling Toolkit, Orobix Srl) and then imported to MATLAB for further analysis. For every sample, the mesh, centerline and raw stack were imported to MATLAB. The centerline was fitted using spline interpolation and 100 position equally spaced were retrieved. In each of these

positions, 14 radii of 200 µm were positioned, 6 orthogonal to the rest. The chosen orientation was parallel to the apical-basal axis formed by the most apical and most basal coordinate of the centerline. Those radii that were inside of the mesh, checked by the function inpolyhedron, or outside of the original image space, were removed. Radii were mapped in the image space and the pixel values in their coordinates were used to obtain the line profiles. The minimum of each profiles was subtracted for each to have a comparable baseline.

Microscopy Setups

Fluorescent imaging of Supp Fig.5.1 was done with Nikon inverted epifluorescence microscope. The microscope was equipped with an HBO 100-W lamp and an IXON X3897 Andor Camera. For all samples, a 60X Plan apochromat oil immersion objective (NA 1.4) was used (from Nikon). The filter sets and time course (if applicable) used for imaging are shown in Table 3. Images were obtained using the image acquisition software NiS-Elements AR (Nikon). STED microscopy images were obtained using STED Expert line microscope (Abberior Instruments, Göttingen, Germany) composed of a IX83 inverted microscope (Olympus, Hamburg, Germany) with a UPLSAPO 100x 1.4 NA oil immersion objective (Olympus). Confocal images were obtained from the same setup without using the STED depletion laser. DNA-PAINT imaging was carried out on an inverted Nikon Eclipse Ti microscope (Nikon Instruments) with the Perfect Focus System, applying an objective-type TIRF configuration with an oil-immersion objective (Apo SR TIRF 100x, NA 1.49, Oil). Two lasers were used for excitation: 561nm (200 mW, Coherent Sapphire) or 488 nm (200 mW, Toptica iBeam smart). The laser beam was passed through a clean-up filter (ZET488/10x or ZET561/10x, Chroma Technology) and coupled into the microscope objective using a beam splitter (ZT488rdc or ZT561rdc, Chroma Technology). Fluorescence light was spectrally filtered with two emission filters (ET525/50m and ET500lp for 488 nm excitation and ET600/50 and ET575lp for 561 nm excitation, Chroma Technology) and imaged on a sCMOS camera (Andor Zyla 4.2) without further magnification, resulting in an effective pixel size of 130 nm after 2x2 binning. Camera Readout Sensitivity was set to 16-bit, Readout Bandwidth to 540 MHz. Light-sheet images of the cochleae were done using a light-sheet microscope (LaVision Biotec Ultramicroscope II). The laser power was constant for all the samples except for the sample incubated with 1.Ab-2.Ab for 14 days, which was 6.75 times lower (13.5% vs. 2%). The stacks were acquired with a total zoom of 8x (2x MVPLAPO Objective and 4x Optic Zoom microscope

body), a step size of 3 µm, with a light-sheet of 30% width and a thickness of 5 µm (NA: 0.148, unidirectional illumination and 11-12 steps of dynamic horizontal focus. The images were imported to FIJI[36] for calculating the maximum intensity projection image and to generate the RGB tif files with a mpl-magma look-up-table.

Acknowledgments

We thank Niklas Engels for providing Ramos cells. We thank Riccardo Testolin for the help in designing the hybrid plot graphs. We thank Eugenio F. Fornasiero, Sebastian Jaehne and Sven Truckenbrodt for reading and commenting the manuscript

This work was supported by the Deutsche Forschungsgemeinschaft (DFG) through Cluster of Excellence Nanoscale Microscopy and Molecular Physiology of the Brain (CNMPB) to F.O and by the Deutsche Forschungsgemeinschaft (DFG, German Research Foundation) under Germany's Excellence Strategy - EXC 2067/1- 390729940 to S.O.R. and T.MT.S. and S.S. acknowledge support from the DFG through the Graduate School of Quantitative Biosciences Munich (QBM). This work was further supported by the DFG through the Emmy Noether Program (DFG JU 2957/1-1), the SFB 1032 (Nanoagents for spatiotemporal control of molecular and cellular reactions, Project A11), the ERC through an ERC Starting Grant (MolMap, grant agreement no. 680241), the Max Planck Society, the Max Planck Foundation, and the Center for Nanoscience (CeNS) to R.J.

Author contributions

S.SI. designed and performed experiments, analyzed data, and wrote the manuscript, T.S. and S.S. designed and performed experiments, analyzed data and revised the manuscript. C.DA designed and performed experiments, analyzed data and revised the manuscript. M.A. created image analysis macros and revised the manuscript. T.M designed experiment and revised the manuscript. R.J. designed experiment and revised the manuscript. S.O.R. designed experiments, analyzed data and revised the manuscript F.O. designed and conceived the project, designed and performed experiments and wrote the manuscript.

5.5 References

1. Coons, A. H., Creech, H. J., Jones, R. N. & Berliner, E. the demonstration of pneumococcal antigen in tissues by the use of fluorescent antibody. J. Immunol. 45 (3), 159–170 (1942).

2. Haugland, R. P. Coupling of Monoclonal Antibodies with Fluorophores. in Monoclonal Antibody Protocols 205–222 (Humana Press, 1995). doi:10.1385/0-89603-308-2:205

3. Schnitzbauer, J., Strauss, M. T., Schlichthaerle, T., Schueder, F. & Jungmann, R. Super-resolution microscopy with DNA-PAINT. (2017). doi:10.1038/nprot.2017.024

4. Ries, J., Kaplan, C., Platonova, E., Eghlidi, H. & Ewers, H. A simple, versatile method for GFP-based super-resolution microscopy via nanobodies. Nat. Methods 9, 582–584 (2012).

5. Eilers, Y., Ta, H., Gwosch, K. C., Balzarotti, F. & Hell, S. W. MINFLUX monitors rapid molecular jumps with superior spatiotemporal resolution. Proc. Natl. Acad. Sci. U. S. A. 115, 6117–6122 (2018).

6. Pleiner, T. et al. Nanobodies: site-specific labeling for super-resolution imaging, rapid epitope-mapping and native protein complex isolation. Elife 4, e11349 (2015).

7. Peckys, D. B., Korf, U. & de Jonge, N. Local variations of HER2 dimerization in breast cancer cells discovered by correlative fluorescence and liquid electron microscopy. Sci. Adv. 1, e1500165 (2015).

8. Opazo, F. et al. Aptamers as potential tools for super-resolution microscopy. Nat. Methods 9, 938–9 (2012).

9. Strauss, S. et al. Modified aptamers enable quantitative sub-10-nm cellular DNA-PAINT imaging. Nat. Methods 15, 685–688 (2018).

10. Schlichthaerle, T. et al. Site-Specific Labeling of Affimers for DNA-PAINT Microscopy. Angew. Chemie Int. Ed. 57, 11060–11063 (2018).

11. Bedford, R. et al. Alternative reagents to antibodies in imaging applications. Biophys. Rev. 9, 299–308 (2017).

12. Pleiner, T., Bates, M. & Görlich, D. A toolbox of anti-mouse and anti-rabbit IgG secondary nanobodies. J. Cell Biol. 217, 1143–1154 (2018).

13. Maidorn, M., Rizzoli, S. O. & Opazo, F. Tools and limitations to study the molecular composition of synapses by fluorescence microscopy. Biochem. J. 473, 3385–3399 (2016).

14. Gomes de Castro, M. A., Höbartner, C. & Opazo, F. Aptamers provide superior stainings of cellular receptors studied under super-resolution microscopy. PLoS One 12, e0173050 (2017).

15. Fang, T. et al. Nanobody immunostaining for correlated light and electron microscopy with preservation of ultrastructure. Nat. Methods 15, 1029–1032 (2018).

16. Manning, L. & Doe, C. Q. Immunofluorescent antibody staining of intact Drosophila larvae. Nat. Protoc. 12, 1–14 (2017).

17. Ezaki, T. Antigen retrieval on formaldehyde-fixed paraffin sections: its potential drawbacks and optimization for double immunostaining. Micron 31, 639–649 (2000).

18. Mayor, S., Rothberg, K. G. & Maxfield, F. R. Sequestration of GPI-anchored proteins in caveolae triggered by cross-linking. Science 264, 1948–51 (1994).

19. Spiegel, S., Kassis, S., Wilchek, M. & Fishman, P. H. Direct visualization of redistribution and capping of fluorescent gangliosides on lymphocytes. J. Cell Biol. 99, 1575–81 (1984).

20. Agasti, S. S. et al. DNA-barcoded labeling probes for highly multiplexed Exchange-PAINT imaging. Chem. Sci. 8, 3080–3091 (2017).

21. Wade, O. K. et al. 124-Color Super-resolution Imaging by Engineering DNA-PAINT Blinking Kinetics. Nano Lett. acs.nanolett.9b00508 (2019). doi:10.1021/acs.nanolett.9b00508

22. Tanaka, K. A. K. et al. Membrane molecules mobile even after chemical fixation. Nat. Methods 7, 865–866 (2010).

23. Sograte-Idrissi, S. et al. Nanobody Detection of Standard Fluorescent Proteins Enables Multi-Target DNA-PAINT with High Resolution and Minimal Displacement Errors. Cells 8, 48 (2019).

24. Auer, A. et al. Nanometer-scale Multiplexed Super-Resolution Imaging with an Economic 3D-DNA-PAINT Microscope. ChemPhysChem 19, 3024–3034 (2018).

25. Richter, K. et al. Presynaptic cytomatrix protein bassoon is localized at both excitatory and inhibitory synapses of rat brain. J. Comp. Neurol. 408, 437–48 (1999).

26. Tao-Cheng, J.-H., Thein, S., Yang, Y., Reese, T. S. & Gallant, P. E. Homer is concentrated at the postsynaptic density and does not redistribute after acute synaptic stimulation. Neuroscience 266, 80–90 (2014).

27. Dani, A., Huang, B., Bergan, J., Dulac, C. & Zhuang, X. Super-resolution Imaging of Chemical Synapses in the Brain. Neuron 68, 843–856 (2010).

28. Truckenbrodt, S. et al. X10 expansion microscopy enables 25-nm resolution on conventional microscopes. EMBO Rep. 19, e45836 (2018).

29. Gomes de Castro, M. A. et al. Differential organization of tonic and chronic B cell antigen receptors in the plasma membrane. Nat. Commun. 10, 820 (2019).

30. Opazo, F. et al. Limited Intermixing of Synaptic Vesicle Components upon Vesicle Recycling. Traffic 11, 800–812 (2010).

31. Pereira, P. M. et al. Fix Your Membrane Receptor Imaging: Actin Cytoskeleton and CD4 Membrane Organization Disruption by Chemical Fixation. Front. Immunol. 10, 675 (2019).

32. Richter, K. N. et al. Glyoxal as an alternative fixative to formaldehyde in immunostaining and super-resolution microscopy. EMBO J. 37, 139–159 (2018).

33. Schlichthaerle, T., Ganji, M., Auer, A., Wade, O. K. & Jungmann, R. Bacterial-derived antibody binders as small adapters for DNA-PAINT microscopy. ChemBioChem (2018). doi:10.1002/cbic.201800743

34. Greenbaum, A. et al. Bone CLARITY: Clearing, imaging, and computational analysis of osteoprogenitors within intact bone marrow. Sci. Transl. Med. 9, eaah6518 (2017).

35. Renier, N. et al. Mapping of Brain Activity by Automated Volume Analysis of Immediate Early Genes. Cell 165, 1789–1802 (2016).

36. Schindelin, J. et al. Fiji: an open-source platform for biological-image analysis. Nat. Methods 9, 676–682 (2012).

37. Cardona, A. et al. TrakEM2 Software for Neural Circuit Reconstruction. PLoS One 7, e38011 (2012).

38. Kikinis, R., Pieper, S. D. & Vosburgh, K. G. 3D Slicer: A Platform for Subject-Specific Image Analysis, Visualization, and Clinical Support. in Intraoperative Imaging and Image-Guided Therapy 277–289 (Springer New York, 2014). doi:10.1007/978-1-4614-7657-3_19

39. Fedorov, A. et al. 3D Slicer as an image computing platform for the Quantitative Imaging Network. Magn. Reson. Imaging 30, 1323–41 (2012).

5.5 Supplementary Information

Circumvention of common labelling artefacts using secondary nanobodies

Shama Sograte-Idrissi[1,2,3,], Thomas Schlichthaerle[4,5], Carlos J. Duque-Afonso[6,7,8,9], Mihai Alevra[1], Sebastian Strauss[4,5], Tobias Moser[6,7,8,9], Ralf Jungmann[4,5], Silvio Rizzoli[1,2,8], Felipe Opazo[1,2,10 *]

[1]Institute of Neuro- and Sensory Physiology, University Medical Center Göttingen, 37073 Göttingen, Germany

[2]Center for Biostructural Imaging of Neurodegeneration (BIN), University of Göttingen Medical Center, 37075 Göttingen, Germany

[3] International Max Planck Research School for Molecular Biology, Göttingen, Germany

[4] Faculty of Physics and Center for Nanoscience, LMU Munich, 80539, Munich, Germany

[5] Max Planck Institute of Biochemistry, 82152, Martinsried, Germany

[6] Institute for Auditory Neuroscience and InnerEarLab, University Medical Center Göttingen, 37075 Göttingen, Germany.

[7] Max Planck Institute for Experimental Medicine, 37075 Göttingen, Germany

[8] Multiscale Bioimaging Cluster of Excellence (MBExC), Göttingen, Germany

[9]University of Göttingen, 37075 Göttingen, Germany

[10] NanoTag Biotechnologies GmbH, 37079, Göttingen, Germany

Key words: DNA-PAINT, STED microscopy, immunostaining artefacts, linkage error.

[*] Corresponding Author: fopazo@gwdg.de

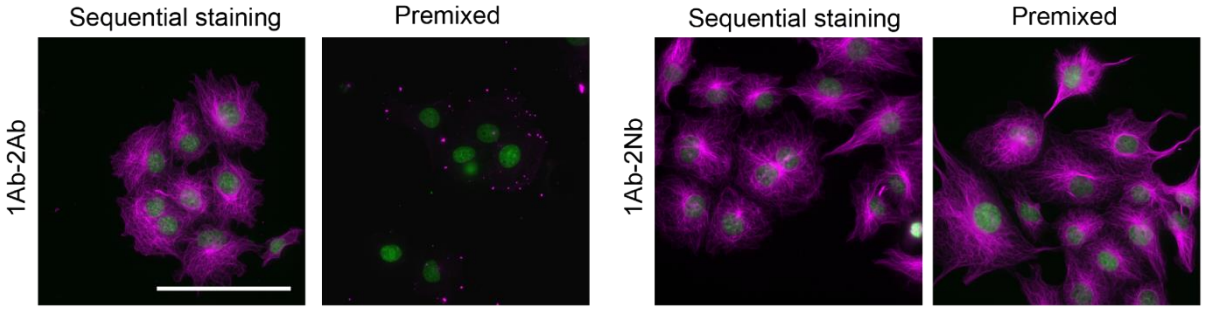

Supplementary Figure 5.1: Pre-mixing antibodies in a centrifuge tube prior incubation on the cell. Immunostaining is commonly done by sequential incubation of the primary probe and the secondary probe. Pre-mixing the two probe in a centrifuge tube prior incubation leads to no staining for 1.Ab-2.Ab while staining is maintained for 1.Ab-2.Nb. Hoechst staining (nucleus) in green, microtubule staining in magenta. Scale bar represents 50 µm.

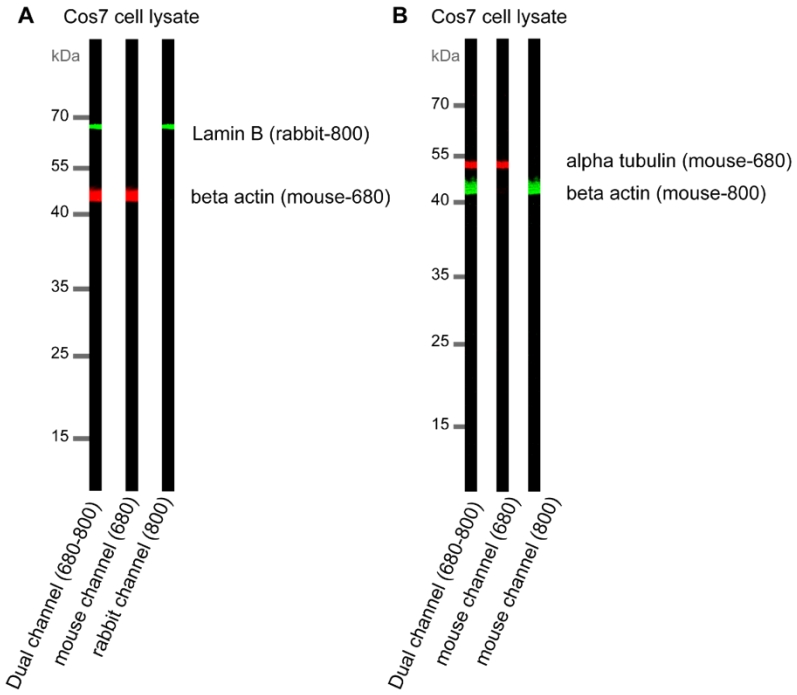

Supplementary Figure 5.2: Pre-mixing 1.Ab-2.Nb for Western Blot. COS-7 cell lysate blotted on nitrocellulose membrane. **A)** Pre-mixing allows shorter protocol by one single step staining. The membrane was stained with 1.Ab beta actin pre-mixed with 2.Nb anti Mouse coupled to IRDye680RD and 1.Ab anti Lamin B pre-mixed with 2.Nb anti Rabbit-IRDye800CW **B)** Pre-mixing allows use of same species antibodies in the same Western blot. The membrane was

stained with 1.Ab beta actin pre-mixed with 2.Nb anti Mouse-IRDye800CW and 1.Ab anti alpha tubulin pre-mixed with 2.Nb anti Mouse-IRDye680RD.

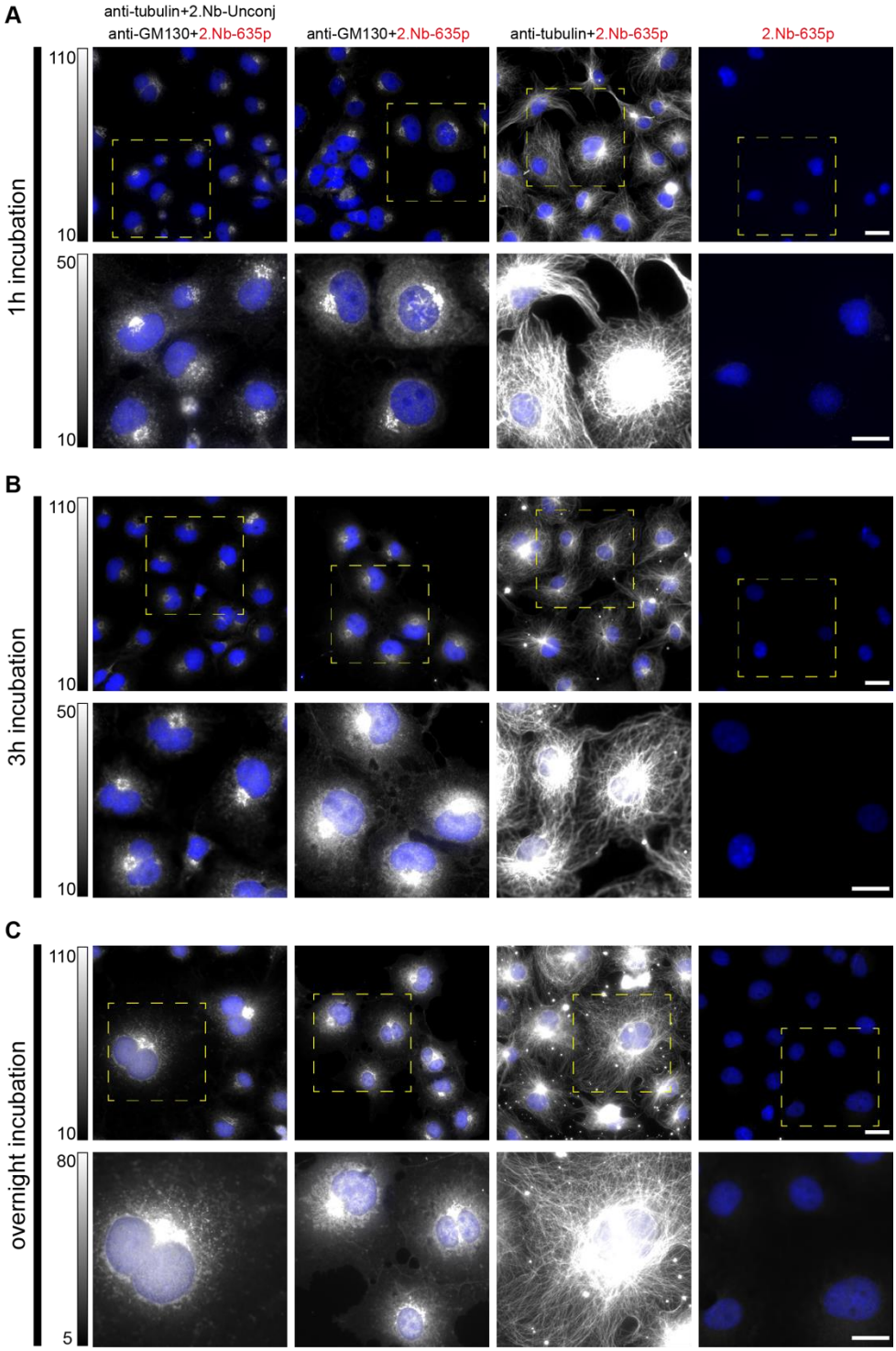

Supplementary Figure 5.3: Assessment of cross-contamination of 2.Nbs if pre-mixtures of same species are co-incubated on the sample simultaneously. (**A**) Top-left panel shows the epifluorescence images of COS-7 cells co-incubated for 1h at room temperature with the following pre-mixtures: anti-tubulin with unconjugated 2.Nb (2.Nb-Unconj), and anti-GM130

with 2.Nb-Star635p. The other top panels are controls. From left to right: anti-GM130 with 2.Nb-Star635p, without the anti-tubulin primary antibody; only anti-tubulin premixed with 2.Nb-Star635p; only the fluorescently labeled secondary nanobody (2.Nb-Star635p). The lower panels show the zoom areas depicted with dashed squares. Gray levels were equally set for all images (depicted with the gradient bar shown on the left). Scale bar for top and zoomed panels represents 20 µm. (**B, C**) same as A, with pre-mixtures incubated for 3h and overnight (~16h), respectively.

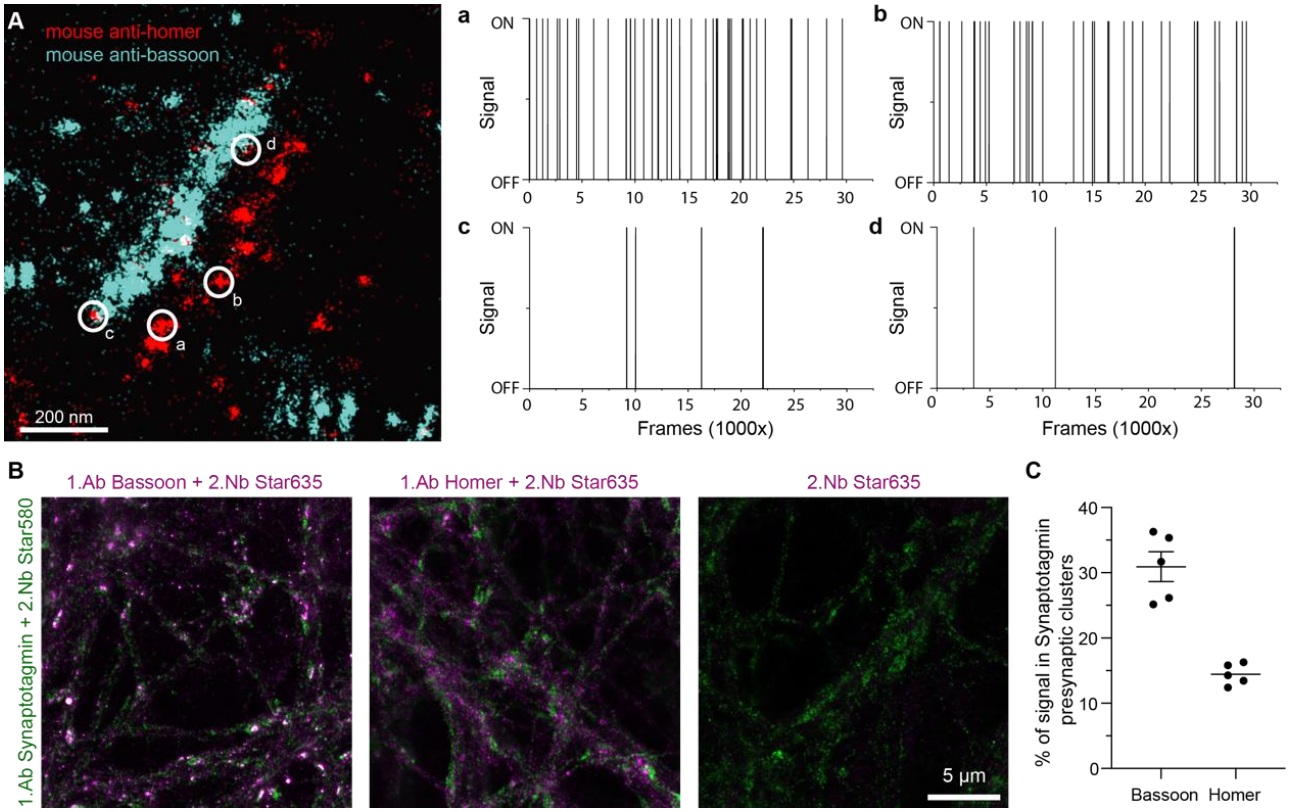

Supplementary Figure 5.4: The presence of homer signal in pre-synapses. (**A**) Example synapse taken from Fig. 3I. Analysis of homer DNA-PAINT localizations on the bassoon-rich localization area (pre-synapses) where the low frequency of visits by imager (shown in c & d) suggest that these "homer" localizations are non-specific events caused by the imager "stickiness". In contrast, homer localizations on the post-synaptic area can be clearly attributed to specific and repeated annealing of imager to the docking DNA strand present on the 2.Nb (a & b). (**B**) 2-Color STED microscopy images of primary hippocampal neurons stained with a guinea pig anti-Synaptotagmin1 antibody (pre-synaptic marker found in synaptic vesicles) and the same anti-homer or anti-bassoon used for the DNA-PAINT in Fig. 3H. (**C**) An analysis of B suggests that a substantial fraction of the primary antibody anti-homer (post-synaptic marker)

can be found within Syt1-marked pre-synapses. An average of ~14.45±1.6% (mean±SD) of the homer signal is present there. Bassoon, which is a bona fide pre-synaptic protein, shows a stronger correlation to Syt1-marked synaptic vesicles, as expected. The graph displays the mean±sem with an N = 5.

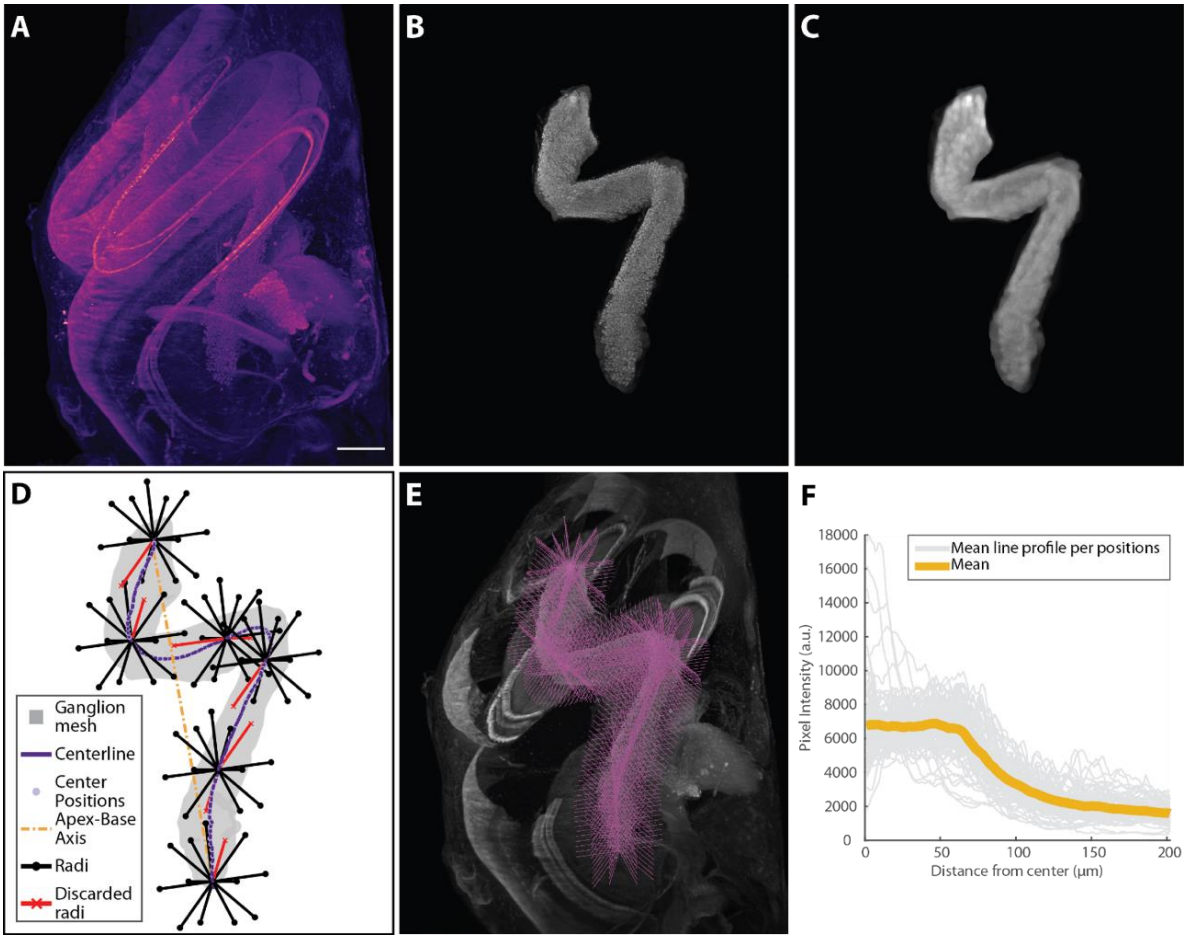

Supplemental Figure 5.5: Method to investigate the sample penetration of different labelling approaches in cochlear staining**. A)** Maximal intensity projection of a cleared cochlea stained with 1.Ab against parvalbumin-α premixed with 2.Nb anti-guinea pig. **B)** Coarse manual segmentation of the ganglion**. C)** Median filtered image of the ganglion (kernel: 10x10x1). **D)**. 2D projection of the mesh created from a threshold segmentation of C), its centerline, the apex-base axis, the center positions where the radii fan out and the used and discarded radii. Only 6 out of the 100 center positions and their corresponding radii used are displayed for clarity. **E)** Maximal intensity projections of a sub-stack of the slices that contains only the ganglion. In magenta, all the radii mapped back in the image space. **F)**. Mean line profile per position (n=100 positions) and mean line profile for this sample is plotted against the distance from the center position. Scale bars for A-C and E represent 200 µm each.

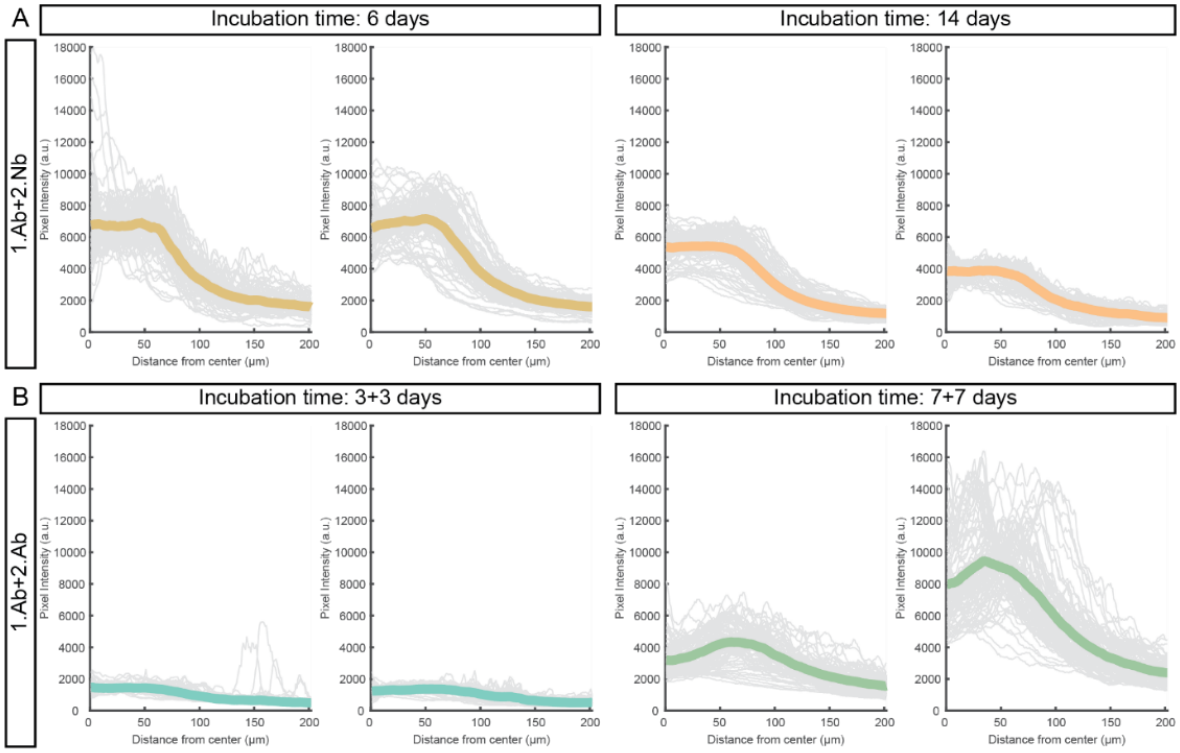

Supplemental Figure 5.6: Line profile from individual cochlear samples. Mean profile per position (n= 100 per sample, grey thin traces) and mean profile per sample (N=2 per staining method and incubation time, color thick traces) are displayed against distance from center position from **A)** Samples stained with a 1.Ab against parvalbumin-α premixed with 2.Nb against guinea pig, labeled with Alexa Fluor 546, and **B)** Samples stained with a 1.Ab against parvalbumin-α revealed by a 2.Ab against guinea pig, labeled with Alexa Fluor 568.

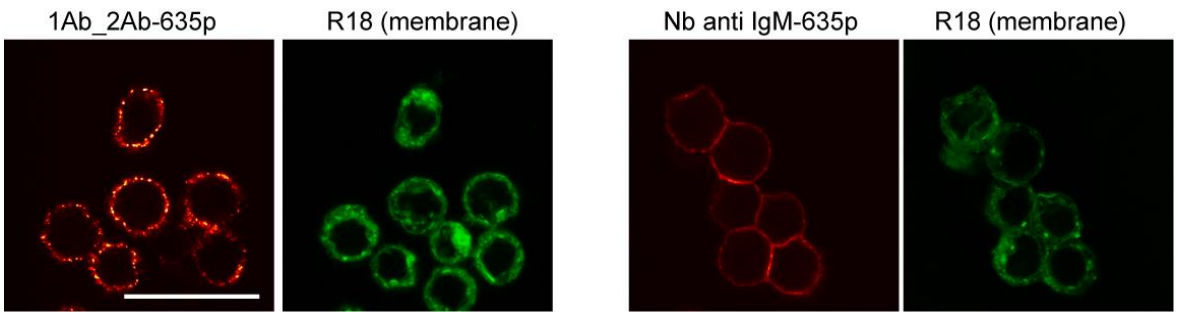

Supplementary Figure 5.7: Diffraction limited images (confocal microscope) of B cells stained with 1.Ab-2.Ab (left panel) or primary nanobody 1.Nb (right panel) targeting the IgM

of the BCR receptor. In green a membrane staining is performed (R18) to show the integrity of the membrane. Scale bar represents 50 µm

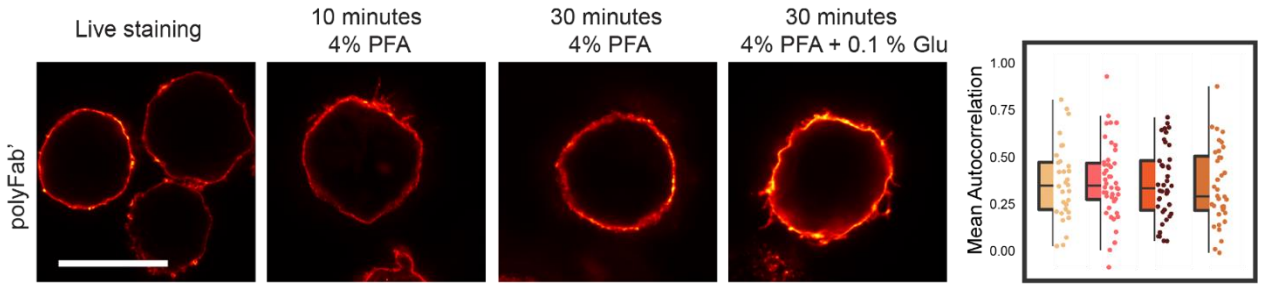

Supplementary Figure 5.8: B cells fixed in different conditions and subsequently stained with monovalent polyFab`. STED images and autocorrelation analysis as explained in Fig.5.

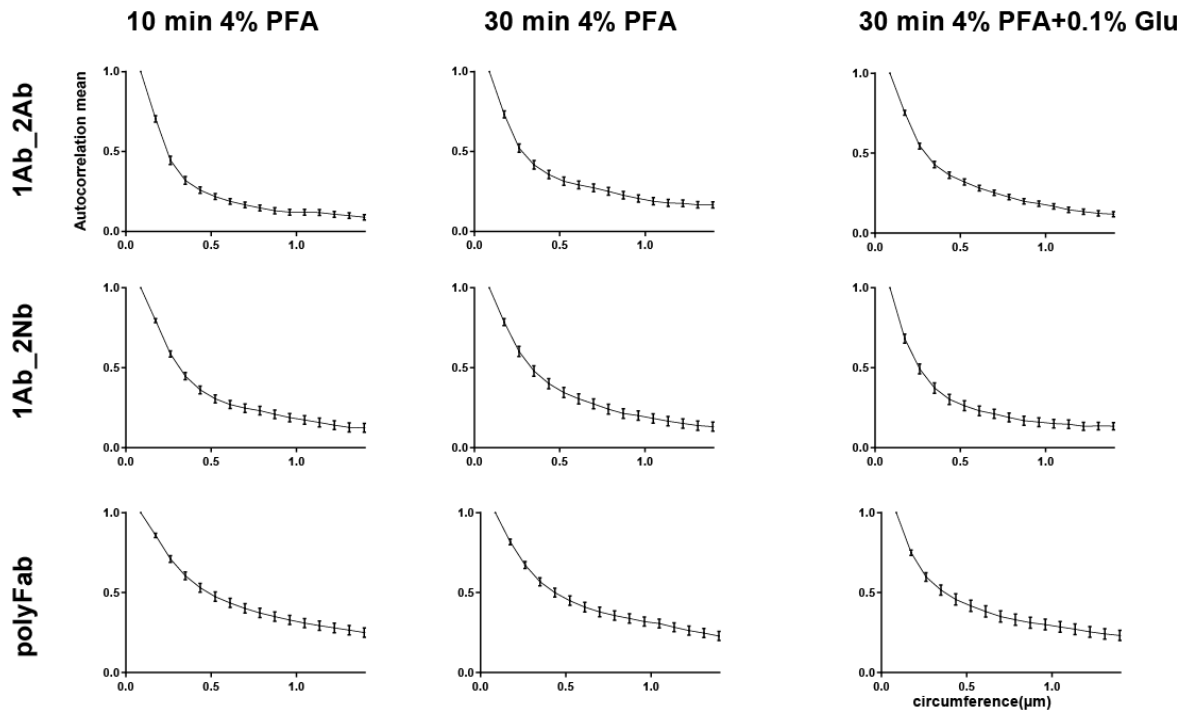

Supplementary Figure 5.9: Autocorrelation curve of B cells fixed prior staining with different fixation conditions. Selected images and analyses are in Fig.6 and Supp.Fig.6.

Supplementary Table 5.1 | Antibodies

Probe name	Company	Catalogue number	Dilution used
affibody® anti-IgM coupled to the Star635P	Abcam, Cambridge, UK	ab36088	1:25
Anti-IgM polyFab' coupled to the Star635P	Jackson ImmunoResearch, Cambridgeshire, UK	cleaved with Papain from 109-006-129	1:50
Monoclonal mouse anti-IgM	Abcam, Cambridge, UK	ab193159	1:200
Secondary donkey anti-rabbit-Star635P	Abberior, Göttingen, Germany	2-0012-007-2	1:200
FluoTag-X2 anti-rabbit Star635P	NanoTag Biotechnology, Göttingen, Germany	N1002-Ab635P	1:50
Monoclonal mouse anti-GM130	BD bioscience	610822	1:62,5
Monoclonal mouse anti-NPC	Abcam, Cambridge, UK	ab24609	1:200
Mouse monoclonal anti-alpha tubulin	Synaptic Systems, Göttingen, Germany	302211	1:500
FluoTag-X2 anti-Mouse kLC CF633, Alexa488, Alexa546, Star635P	NanoTag Biotechnologies, Göttingen, Germany	N1202	1:100
Secondary donkey anti-mouse antibody	Jackson ImmunoResearch, Cambridgeshire, UK	715-005-151	1:100
Monoclonal mouse anti-beta actin	Sigma-Aldrich, Missouri, USA	A1978	1:100
Polyclonal rabbit anti-Lamin B	Sigma-Aldrich, Missouri, USA	HPA050524)	1:100
FluoTag-X2 anti-Mouse kLC LiCor800CW	NanoTag Biotechnologies, Göttingen, Germany	N1202-Li800	1:500
FluoTag-X2 anti-Mouse kLC LiCor680RD	NanoTag Biotechnologies, Göttingen, Germany	N1202-Li680	1:500
FluoTag-X2 anti-rabbit LiCor800CW	NanoTag Biotechnologies, Göttingen, Germany	N1202-Li800	1:500
Polyclonal Guinea Pig anti-Synaptotagmin1	Synaptic Systems, Göttingen, Germany	105105	1:1000

Supplementary Table 5.2 | Handle sequences

Handle Name	Sequence	5'-mod	3'-mod	Company
P1	TTATACATCTATTTT	Azide	Atto488	Biomers.net
P3	TTTCTTCATTATTTT	Azide	Atto488	Biomers.net
P5	TTTCAATGTATTTTT	Azide	Atto488	Biomers.net

Supplementary Table 5.3 | Imager sequences

Imager name	Sequence	5'-mod	3'-mod	Company
P1*	CTAGATGTAT	None	Cy3b	Eurofins Genomics
P3*	GTAATGAAGA	None	Cy3b	Eurofins Genomics
P5*	CATACATTGA	None	Cy3b	Eurofins Genomics

Supplementary Table 5.4| Imaging parameters

Dataset	Parameters	Power @561 nm
Figure 2: DNA-PAINT Microtubule with 2.Nbs	200ms, 2D, 60k Frames, 2nM. P1*	1 kW/cm^2
Figure 2: DNA-PAINT Microtubule with 2.Abs	200ms, 2D, 60k Frames, 2nM. P1*	1kW/cm^2
Figure 3: bassoon	150ms, 3D, 30k Frames, 3nM, P5*	1 kW/cm^2
Figure 3: homer	150ms, 3D, 30k Frames, 6nM, P3*	1 kW/cm^2

Supplementary Table 5.5 | Statistics on BCR autocorrelation Analysis. One-way ANOVA with Tukey Multiple Comparison Test. ns= non-significant, *= $p \leq 0.05$, **= $p \leq 0.01$, ***= $p \leq 0.001$, ****= $p \leq 0.0001$

From Figure 5	**polyFab live**	**Affibody live**	**1.Ab+2.Ab live**	**1.Ab+2Nb live**
polyFab live		ns	****	**
Affibody live			****	ns
1.Ab+2.Ab live				***
From Figure 6a	**1.Ab+2.Ab live**	**1.Ab+2.Ab 10 min 4% PFA**	**1.Ab+2.Ab 30 min 4% PFA**	**1.Ab+2.Ab 30 min 4% PFA+ 0.1% GLU**
1.Ab+2.Ab live		ns	***	****
1.Ab+2.Ab 10 min 4% PFA			*	ns
1.Ab+2.Ab 30 min 4% PFA				ns
From Figure 6b	**1.Ab+2Nb live**	**1.Ab+2Nb 10 min 4% PFA**	**1.Ab+2Nb 30 min 4% PFA**	**1.Ab+2Nb 30 min 4% PFA+ 0.1% GLU**
1.Ab+2Nb live		ns	ns	ns
1.Ab+2Nb 10 min 4% PFA			ns	ns
1.Ab+2Nb 30 min 4% PFA				ns
From Supp. Figure 8	**polyFab live**	**polyFab 10 min 4% PFA**	**polyFab 30 min 4% PFA**	**polyFab 30 min 4% PFA+ 0.1% GLU**
polyFab live		ns	ns	ns
polyFab 10 min 4% PFA			ns	ns
polyFab 30 min 4% PFA				ns

6. General discussion

Over the last few years, the advent of super resolution microscopy enabled imaging objects beyond the diffraction limit, such as sub-cellular elements in the neuronal synapse. However, the difficulty of imaging several targets in super resolution within the same synapse persists and synaptic proteins are usually addressed separately in different samples. In addition, conventional immunostaining approaches use antibodies that are a source of artefacts such as target induced clustering, fluorophore delocalization and lack of sample penetration (Maidorn et al., 2016). Hence, there is a need of artefact-free affinity binders for different synaptic targets working in a highly multiplexed super resolution microscopy technique. In my doctoral research, I developed and optimized a set of tools to image multiple targets in super resolution microscopy using alternative probes. First, I established a pipeline for the production and validation of nanobodies targeting different proteins in the synapse. Then, I characterized and showed the advantages of using secondary nanobodies as an alternative to secondary antibodies in imaging applications. Finally, I developed a robust protocol to couple nanobodies to a single-stranded DNA for Exchange PAINT.

An optimized pipeline for the generation of multiple synaptic nanobodies

Nanobodies have proven to be a superior alternative to conventional antibodies. Their smaller size enables reduced fluorophore delocalization in microscopy, enhanced sample penetration and access to cryptic epitopes (Ingram, Schmidt, & Ploegh, 2018). They are composed of a single domain with no posttranslational modifications, except for one or two disulfide bridges. They can be easily produced as a recombinant protein in prokaryotes, enabling cheap and animal independent production, and guarantying batch to batch uniformity (Muyldermans, 2013). However, in comparison to conventional antibodies, the diversity in available nanobodies is low. The Institute collection and analysis of nanobodies (Ican) database counts 2391 nanobodies from which 2131 appear in patents and 260 in publications. Out of those, 1863 are used in clinical practice and 130 in basic research mainly targeting fluorescent and tag proteins. (Zuo et al., 2017). Hence, there is an urgent need for a fast and simple selection procedure of nanobodies against endogenous mammalian targets, to target the synaptic proteins for example. In this thesis, I achieved this by first minimizing the amount of immunizations required for generating nanobodies against different antigens. By immunizing alpacas with a full synaptosome preparation, I enabled the potential identification of nanobodies against many

different synaptic targets (Chapter 3). To investigate if the animal produced hcAbs against a particular target, I created the preELISA (Fig. 3.1). preELISA enables to assess the possibility of finding nanobodies against a specific synaptic target before starting the selection process. This approach of immunization of a camelid with a cocktail of immunogen combined with the preELISA would allow the generation of many nanobodies in a shorter time. This approach could be applied to any other kind of preparation. For example, a whole cellular organelle could be purified and injected in the camelid and the preELISA used to assess which protein of this organelle generated hcAbs.

Another caveat in nanobodies identification is the laborious and extensive validation of the nanobodies clone candidates obtained by the selection. In fact, every type of selection (phage display, NGS-MS approach, etc.) leads to many nanobody candidates that needs to be validated for their specificity to their target and for the applicability in the method they are required for. In this thesis, I established a validation pipeline to validate to test the specificity of the nanobody directly in the phagemid without needing further subcloning at early steps. I assessed at an early stage the binding ability of the nanobody candidates in immunofluorescence by using the bacterial cell lysate and indirect immunostaining of 3xFLAG tag present on the phagemid (Fig. 3.4). I established a rampELISA estimating the affinity of the nanobody to its antigen (Fig. 3.5, 3.6). This approach drastically reduces the number of nanobodies to be processed in the downstream validation steps.

Phage display versus other techniques

From synaptosome-immunized alpacas, I created a nanobody library and screened for nanobodies against endogenous synaptic targets using phage display technique (Smith, 1985) (Chapter 3). This method is a simple technique and is the most used approach for the selection of nanobodies (Arbabi Ghahroudi et al., 1997; Li et al., 2017; Maidorn et al., 2019). In this technique, the nanobody library is infected with helper phages leading to the production of fully formed phages displaying the nanobody on their surface. Phages are then extracted by PEG precipitation and the selection of antigen specific nanobodies is done by “panning” the phages onto an immobilized antigen. Two to three panning rounds are usually performed to enrich the binding clones. The ability of the clones to bind to the antigens is verified by phageELISA and further validation process. The positive clones are then sequenced to derive their aminoacidic composition (Pardon et al., 2014). Using phage display I successfully obtained nanobodies against different synaptic targets with different affinity reaching pM affinities (Fig. 3.6).

Low affinity nanobodies could be useful for certain therapeutic applications because of their fast clearance and elution (Liu et al., 2018). However, immunofluorescence, requires binders with high affinity to withstand the washings necessary in immunostaining protocol for guarantying low background staining. Therefore, some protein engineering approach could be used to enhance the affinity of the nanobodies. Affinity maturation has been performed by others by random and site directed mutagenesis of the CDR of the nanobody increasing up to 100 fold the affinity of the nanobodies (Koide et al., 2007; Yau et al., 2005). However, the mutagenesis and consecutive display methods necessary are laborious and require validation of many candidates. To circumvent this, *in silico* affinity maturation has been proven a valuable tool. Both *ab initio* (Mahajan et al., 2018) and homology modeling were used to increase the nanobody affinities (Cheng et al., 2019).

In this project, we tested another screening method that supposedly allows the rapid generation of high affinity nanobody using a combination of NGS and MS (Fridy et al., 2014). As discussed in Chapter 3, this method is too expensive and laborious and was not successful for the identification of high affinity binding nanobodies from a complex immunogen. Alternative screening methods for nanobodies are the one using cell surface display (Ueda et al 2016). Instead of using a filamentous phage to display the nanobody, yeast or bacteria cell surface is used (Fleetwood et al., 2013; Ryckaert, Pardon, Steyaert, & Callewaert, 2010). The advantage here compared to a phage display approach, is that flow cytometry detection of the cell is possible, due to its bigger size than the phage. Therefore, fluorescence-based analysis and sorting of displayed libraries can be performed (Boder & Wittrup, 1997; Daugherty, Chen, Olsen, Iverson, & Georgiou, 1998). This also allows to measure the binding affinity of the nanobodies selected by measurement with flow cytometry without the need of subcloning and further processing (Adams, Mora, Walczak, & Kinney, 2016; Chao et al., 2006). Compared to our method, this achieve the same result obtained using the rampELISA established in this thesis (Fig. 3.1), giving an estimation of the binding affinity of the nanobody clone by subjecting it to different amount of antigen.

Yeast display compared to phage display, guarantees proper folding and secretion of nanobodies which might not be able to be expressed in prokaryotes (Ryckaert et al., 2010). However, as it is the case for the NGS and MS approach, the yeast display does not involve a prokaryotic step. Therefore, nanobodies might be selected that might not be properly expressed in prokaryotic systems that is the ultimate cheap and fast goal for production. The bacterial

display techniques seem, therefore, a better alternative. However, displaying the nanobodies on the surface of Gram-negative bacteria such as *E. coli* requires overcoming the nanobody challenge of translocation to the surface. The nanobody needs to cross different areas of the bacteria: the inner membrane, the periplasm and the outer membrane (Dalbey & Kuhn, 2012). This is why this approach, even if combining the advantages of yeast display and phage display, has not been, up to this date, leading to the selection of many nanobodies (Salema & Fernández, 2017). To circumvent the difficult crossing of the outer membrane, bacterial display has also been performed by using Gram-positive bacteria that are composed of a simple cell envelope. This has allowed for example the generation of a library of 10^7 clones displayed on *Staphylococcus carnosus* and selection of nanobodies against GFP (Kronqvist, Lofblom, Jonsson, Wernerus, & Stahl, 2008).

The limited transfection/transformation efficiency of those cells (yeast and Gram positive bacteria) compared to the transformation efficiency of *E. coli* limits the size of the resulting library (Salema & Fernández, 2017). The size of the library has been shown to correlate to the diversity of the nanobodies represented but also to the affinity of the nanobody selected (Vaughan et al., 1996; Waterhouse, Griffiths, Johnson, & Winter, 1993). In this regard *E. coli* remains a good alternative, exhibiting library size of up to 10^9 clones (Galán et al., 2016). The synaptosome library I generated by Gibson cloning into the “minimal phagemid” has a library size of 10^7 clones (Fig. 3.3). The estimation of the library diversity in phage display is conventionally done by calculating the colonies of *E. coli* obtained after transformation of the library (Pardon et al., 2014). However, this estimate assumes that there is no more than one inserted gene in each *E. coli* colony and that every colony contains a different DNA sequence coding for a different nanobody. Indeed, the NGS of the nanobodies resulted in 10^6 non-redundant nanobodies, confirming that counting colonies is not precise for the diversity determination of the library (Fig. 3.2).

Our synaptosome library led to the identification of nanobodies against five different synaptic targets (Chapter 3). This library can be stored for years at -80 degree and used for selection of nanobodies against other synaptic targets.

Probes for multiplexed super resolution microscopy

Due to the lack of available nanobodies targeting endogenous proteins in immunofluorescence, I have tested alternative approaches to avoid using the standard primary-secondary complex. First, I have successfully used nanobodies available against common fluorescent proteins

(Chapter 4) to target recombinant protein fused to fluorescent proteins and use them in DNA-PAINT. Next, I have tested secondary nanobodies as an alternative to secondary antibodies in microscopy (Chapter 5). I observed that the use of secondary nanobodies reduces the linkage error in STED microscopy and DNA PAINT (Fig. 5.1, 5.2). Those results confirm the one obtained using secondary nanobodies in STORM microscopy (Pleiner, Bates, & Görlich, 2018). Smaller linkage error corresponds to better attainable resolution. I have for example imaged microtubules with DNA-PAINT using secondary nanobodies and obtained a diameter size of 30 nm, close to the microtubule size of 25 nm reported in the literature (Ledbetter & Porter, 1964). I have also shown that premixing the primary antibody to the secondary nanobody prior incubation on the sample (Fig 5.3) reduces the incubation necessary in thick biological samples and guarantee homogenous staining (Fig 5.4). Finally, I have shown how antigen clustering induced by the affinity probe in live and poorly chemically fixed samples can be rescued by the use of secondary nanobodies (Fig 5.5 and Fig. 5.6). The advantages obtained using secondary antibodies could also be obtained by direct labelling of the primary antibody and no use of a secondary probe (Mikhaylova et al., 2015). However, the available labelling chemistry of antibody is not site directed and can hence interfere with the binding capability of the antibody. On the other hand, secondary nanobodies have the convenience to be purchased and working for a big majority of primary antibodies.

After characterizing the probes to be used for the imaging of the synapse, I focused on the microscopy technique. As discussed in the introduction, Exchange-PAINT is the method of choice for imaging multiple targets in super resolution microscopy (Jungmann et al., 2014). This method relies on the sequential imaging of orthogonal imager strands binding to different docking strands attached to different targets through affinity probes (Jungmann et al., 2014). In this thesis, a protocol was established to link the nanobodies to docking strands (Fig. 4.2). I used a click and thiol-based strategy to couple an azide-DNA to an ectopic C terminal cysteine of the nanobody through a maleimide-DBCO cross-linker. In comparison to a previously published approach labelling the amino group of the nanobody (Agasti et al., 2017), our protocol allows a site-directed coupling to only the C-terminus of the nanobody. In addition, the purification of the labelled nanobody by size exclusion chromatography (Fig. 4.2 C) guarantees no free-floating docking strand that could increase signal background during imaging. Towards completion of this project, a similar site directed coupling approach was published by Fabricius et al.. In their approach, they use a SortaseA-mediated conjugation to couple an azide-DNA to the C terminus of the nanobody through an ammine-DBCO cross linker (Fabricius, Lefèbre, Geertsema, Marino, & Ewers, 2018). Their approach requires the

production of Sortase A, which for standard imaging laboratories might need to be outsourced. Our approach instead uses commercially available components, which however are comparably expensive. Another advantage of their approach is the possibility to assess the correct occurrence of the first step of the reaction (coupling of the nanobody to the cross-linker) by size reduction of the nanobody losing the SortaseA signal visible on SDS-PAGE.

Future work: characterization of the synapse in super resolution

I have successfully generated a Stg1 nanobody working in immunostaining (Fig. 3.7). The affinity of the nanobodies selected against VAMP2, Homer and Bassoon (Fig. 3.3, 3.4, 3.5) will be in the future enhanced with approaches described above to make them suitable for immunostaining as well. These newly selected nanobodies might enable by imaging the discovery of structural organization which was not known before, as it was done by previously identified nanobodies against Syntaxin 1a (stx1a) and SNAP25 (Maidorn et al., 2019). Those two nanobodies identified population of stx1a and SNAP25 outside of the synaptic area that could not be revealed by antibody staining and that the extra-synaptic stx1a population was recruited to the synapse upon neuronal stimulation (Maidorn et al., 2019). To stain synaptic proteins for which no functional nanobodies in immunofluorescence yet exist, I will use primary antibodies already validated and commercially available. The primary antibodies will be detected by the secondary nanobodies that have been shown in Chapter 5 to be a better alternative than the secondary antibodies. As shown in Chapter 5 (Fig. 5.3), multiple primary antibodies originating from the same animal species can now be used in the same sample by premixing to secondary nanobodies conjugated to a reporter. Therefore, the species limit is lifted and the number of targets that can be imaged is no longer limited by the use of secondary probes. All those nanobodies can be coupled to a single strand DNA by using the site targeted labeling method developed in Chapter 4. Using the custom-built microfluidic setup I described in Fig. 4.3, I will be able to perform Exchange-PAINT in an automatized fashion with injection and removal of liquid with up to 24 inlet channels. Altogether, our tools will enable the imaging of multi-synaptic targets in the same synapse in super resolution. These tools will help, for example, to characterize the spatial organization of the different synaptic and their relative position to one another. This can be done by the analysis of the size, shape, intensity and distance between molecules and can be automatized with statistical methods such as Statistical Object Distance Analysis (SODA). SODA analyses the morphology and performs coupling probability for every single pair of objects. It was used to analyze images obtained by Structural

illuminated microscopy and 3D STORM and showed for the first time that two postsynaptic markers, PSD95 and Homer, are arranged in different nanodomains and form an asymmetric triangle with the presynaptic protein Synapsin (Lagache et al., 2018).

An additional common question that can be answered using the tools developed in this thesis is how the synapse rearrange their molecular components during plasticity. A recent study has shown how pre and postsynaptic proteins are arranged in nanomodules and that those rearrange during plasticity (Hruska, Henderson, Le Marchand, Jafri, & Dalva, 2018). However, those findings were obtained with 3-color STED microscopy, limiting the amounts of proteins to be analyzed in the same synapse.
Our approach could, therefore, be used to expand that knowledge to the reorganization of other synaptic proteins respectively. Hippocampal neurons in basal condition could be compared to high frequency stimulated neurons (chemical or electrical), or exposed to synaptic activity blocked by neurotoxins such as Tetrodotoxin.

A further important question, which could be answered using our tools, is how the protein reorganization during synaptic plasticity is associated with gene expression. Local translation at the nerve terminal has been shown to exist (Scarnati, Kataria, Biswas, & Paradiso, 2018). However, it has not been shown in concomitance related to protein localization and amounts. Using Exchange- PAINT and the tools developed in this thesis, this could be easily achievable. DNA-PAINT has been successfully applied to single molecule mRNA by using fluorescent in situ hybridization (FISH) probes containing docking sites for imager strand (Wade et al., 2019). Staining the synapse with both FISH probes and protein binders (nanobodies and secondary nanobodies) would give a description of how gene expression and protein activity are related in the synapse. Quantification of the molecules, both protein and mRNA, can be performed using quantitative PAINT imaging (qPAINT) (Jungmann et al., 2016). qPAINT determines the number of molecules imaged by using the predictable binding kinetics between the imager and docking strand. It has been shown that qPAINT is able to quantify molecules separated by as little as 3 nm which corresponds to the size of the DNA strand used (M. A. B. Baker et al., 2019).

However, one limitation of our approach is that each target imaged in DNA PAINT image to reach high resolution, requires at least 20’000 frames corresponding to a minimum of 30 min at least of acquisition time (Fig. 4.4). Therefore, imaging both protein target and mRNA could take a long time, and considering that many synapses needs to be imaged to have a representative picture, this approach might be very time-consuming. In fact, synapses are

variable in their composition and morphology. For example, the synaptic vesicle volume has been shown to vary up to 5 folds between neighboring synapse in rat hippocampal neurons (Hu, Qu, & Schikorski, 2008). To circumvent the image acquisition time, multiple targets could be acquired at the same time by using different fluorophores on different imager strands present in the solution at the same time (Gómez-García, Garbacik, Otterstrom, Garcia-Parajo, & Lakadamyali, 2018). Another approach would be spectral barcoding, meaning using the same imager strand binding to different targets with different binding kinetics (Wade et al., 2019).

Finally, it is of capital importance to expand the variety of high affinity nanobodies available against synaptic proteins but also against other targets. This year a nanobody was approved for the first time by the FDA as drug against acquired thrombotic thrombocytopenic purpura, (Morrison, 2019), opening the doors to the therapeutic market. Considering the abilities of the nanobodies to reach cryptic epitopes and potentially to cross the blood brain barrier, there will be excellent complement to the currently available diagnostic and therapeutic tools (Jank et al., 2019).

7. References

Abbe, E. (1873). Beiträge zur Theorie des Mikroskops und der mikroskopischen Wahrnehmung. *Archiv Für Mikroskopische Anatomie*, *9*(1), 413–418. https://doi.org/10.1007/BF02956173

Adams, R. M., Mora, T., Walczak, A. M., & Kinney, J. B. (2016). Measuring the sequence-affinity landscape of antibodies with massively parallel titration curves. *ELife*, *5*. https://doi.org/10.7554/eLife.23156

Agasti, S. S., Wang, Y., Schueder, F., Sukumar, A., Jungmann, R., & Yin, P. (2017). DNA-barcoded labeling probes for highly multiplexed Exchange-PAINT imaging. *Chemical Science*, *8*(4), 3080–3091. https://doi.org/10.1039/C6SC05420J

Arbabi Ghahroudi, M., Desmyter, A., Wyns, L., Hamers, R., & Muyldermans, S. (1997). Selection and identification of single domain antibody fragments from camel heavy-chain antibodies. *FEBS Letters*, *414*(3), 521–526. https://doi.org/10.1016/s0014-5793(97)01062-4

Baker, M. (2015). Reproducibility crisis: Blame it on the antibodies. *Nature*, *521*(7552), 274–276. https://doi.org/10.1038/521274a

Baker, M. A. B., Nieves, D. J., Hilzenrat, G., Berengut, J. F., Gaus, K., & Lee, L. K. (2019). Stoichiometric quantification of spatially dense assemblies with qPAINT. *Nanoscale*, *11*(26), 12460–12464. https://doi.org/10.1039/C9NR00472F

Balzarotti, F., Eilers, Y., Gwosch, K. C., Gynnå, A. H., Westphal, V., Stefani, F. D., … Hell, S. W. (2017). Nanometer resolution imaging and tracking of fluorescent molecules with minimal photon fluxes. *Science (New York, N.Y.)*, *355*(6325), 606–612. https://doi.org/10.1126/science.aak9913

Benson, D. L., Watkins, F. H., Steward, O., & Banker, G. (1994). Characterization of GABAergic neurons in hippocampal cell cultures. *Journal of Neurocytology*, *23*(5), 279–295. https://doi.org/10.1007/BF01188497

Betzig, E. (2015). Single Molecules, Cells, and Super-Resolution Optics (Nobel Lecture). *Angewandte Chemie International Edition*, *54*(28), 8034–8053. https://doi.org/10.1002/anie.201501003

Boder, E. T., & Wittrup, K. D. (1997). Yeast surface display for screening combinatorial polypeptide libraries. *Nature Biotechnology*, *15*(6), 553–557. https://doi.org/10.1038/nbt0697-553

Bradbury, A., & Plückthun, A. (2015). Reproducibility: Standardize antibodies used in research. *Nature*, *518*(7537), 27–29. https://doi.org/10.1038/518027a

Chaikuad, A., Keates, T., Vincke, C., Kaufholz, M., Zenn, M., Zimmermann, B., … Müller, S. (2014). Structure of cyclin G-associated kinase (GAK) trapped in different conformations using nanobodies. *The Biochemical Journal*, *459*(1), 59–69. https://doi.org/10.1042/BJ20131399

Chalfie, M., Tu, Y., Euskirchen, G., Ward, W. W., & Prasher, D. C. (1994). Green fluorescent protein as a marker for gene expression. *Science (New York, N.Y.)*, *263*(5148), 802–805. https://doi.org/10.1126/science.8303295

Chao, G., Lau, W. L., Hackel, B. J., Sazinsky, S. L., Lippow, S. M., & Wittrup, K. D. (2006). Isolating and engineering human antibodies using yeast surface display. *Nature Protocols*,

1(2), 755–768. https://doi.org/10.1038/nprot.2006.94

Cheng, X., Wang, J., Kang, G., Hu, M., Yuan, B., Zhang, Y., & Huang, H. (2019). Homology Modeling-Based in Silico Affinity Maturation Improves the Affinity of a Nanobody. *International Journal of Molecular Sciences*, *20*(17), 4187. https://doi.org/10.3390/ijms20174187

D'Huyvetter, M., Xavier, C., Caveliers, V., Lahoutte, T., Muyldermans, S., & Devoogdt, N. (2014). Radiolabeled nanobodies as theranostic tools in targeted radionuclide therapy of cancer. *Expert Opinion on Drug Delivery*, *11*(12), 1939–1954. https://doi.org/10.1517/17425247.2014.941803

Dai, M. (2017). DNA-PAINT Super-Resolution Imaging for Nucleic Acid Nanostructures. In *Methods in molecular biology (Clifton, N.J.)* (Vol. 1500, pp. 185–202). https://doi.org/10.1007/978-1-4939-6454-3_13

Dalbey, R. E., & Kuhn, A. (2012). Protein Traffic in Gram-negative bacteria – how exported and secreted proteins find their way. *FEMS Microbiology Reviews*, *36*(6), 1023–1045. https://doi.org/10.1111/j.1574-6976.2012.00327.x

Dani, A., Huang, B., Bergan, J., Dulac, C., & Zhuang, X. (2010). Super-resolution Imaging of Chemical Synapses in the Brain. *Neuron*, *68*(5), 843–856. Retrieved from https://www.ncbi.nlm.nih.gov/pmc/articles/PMC3057101/pdf/nihms259099.pdf

Daugherty, P. S., Chen, G., Olsen, M. J., Iverson, B. L., & Georgiou, G. (1998). Antibody affinity maturation using bacterial surface display. *Protein Engineering*, *11*(9), 825–832. Retrieved from http://www.ncbi.nlm.nih.gov/pubmed/9796833

Desmyter, A., Farenc, C., Mahony, J., Spinelli, S., Bebeacua, C., Blangy, S., … Cambillau, C. (2013). Viral infection modulation and neutralization by camelid nanobodies. *Proc Natl Acad Sci U S A*, *110*(15), E1371-9. https://doi.org/10.1073/pnas.1301336110

Fabricius, V., Lefèbre, J., Geertsema, H., Marino, S. F., & Ewers, H. (2018). Rapid and efficient C-terminal labeling of nanobodies for DNA-PAINT. *Journal of Physics D: Applied Physics*, *51*(47), 474005. https://doi.org/10.1088/1361-6463/aae0e2

Fleetwood, F., Devoogdt, N., Pellis, M., Wernery, U., Muyldermans, S., Ståhl, S., & Löfblom, J. (2013). Surface display of a single-domain antibody library on Gram-positive bacteria. *Cellular and Molecular Life Sciences : CMLS*, *70*(6), 1081–1093. https://doi.org/10.1007/s00018-012-1179-y

Fornasiero, E. F., Mandad, S., Wildhagen, H., Alevra, M., Rammner, B., Keihani, S., … Rizzoli, S. O. (2018). Precisely measured protein lifetimes in the mouse brain reveal differences across tissues and subcellular fractions. *Nature Communications*, *9*(1), 4230. https://doi.org/10.1038/s41467-018-06519-0

Fridy, P. C., Li, Y., Keegan, S., Thompson, M. K., Nudelman, I., Scheid, J. F., … Rout, M. P. (2014). A robust pipeline for rapid production of versatile nanobody repertoires. *Nature Methods*, *11*(12), 1253–1260. https://doi.org/10.1038/nmeth.3170

Fukuda, M., Moreira, J. E., Liu, V., Sugimori, M., Mikoshiba, K., & Llinás, R. R. (2000). Role of the conserved WHXL motif in the C terminus of synaptotagmin in synaptic vesicle docking. *Proceedings of the National Academy of Sciences of the United States of America*, *97*(26), 14715. https://doi.org/10.1073/PNAS.260491197

Galán, A., Comor, L., Horvatić, A., Kuleš, J., Guillemin, N., Mrljak, V., & Bhide, M. (2016). Library-based display technologies: where do we stand? *Molecular BioSystems*, *12*(8), 2342–2358. https://doi.org/10.1039/C6MB00219F

Gallagher, S. R. (2012). SDS-Polyacrylamide Gel Electrophoresis (SDS-PAGE). In *Current Protocols Essential Laboratory Techniques* (Vol. 6, pp. 7.3.1-7.3.28). Hoboken, NJ, USA: John Wiley & Sons, Inc. https://doi.org/10.1002/9780470089941.et0703s06

Gibson, D. G., Young, L., Chuang, R.-Y., Venter, J. C., Hutchison, C. A., & Smith, H. O. (2009). Enzymatic assembly of DNA molecules up to several hundred kilobases. *Nature Methods*, *6*(5), 343–345. https://doi.org/10.1038/nmeth.1318

Gibson, T. J., Seiler, M., & Veitia, R. A. (2013). The transience of transient overexpression. *Nature Methods*, *10*(8), 715–721. https://doi.org/10.1038/nmeth.2534

Gomes de Castro, M. A., Wildhagen, H., Sograte-Idrissi, S., Hitzing, C., Binder, M., Trepel, M., … Opazo, F. (2019). Differential organization of tonic and chronic B cell antigen receptors in the plasma membrane. *Nature Communications*, *10*(1), 820. https://doi.org/10.1038/s41467-019-08677-1

Gómez-García, P. A., Garbacik, E. T., Otterstrom, J. J., Garcia-Parajo, M. F., & Lakadamyali, M. (2018). Excitation-multiplexed multicolor superresolution imaging with fm-STORM and fm-DNA-PAINT. *Proceedings of the National Academy of Sciences of the United States of America*, *115*(51), 12991–12996. https://doi.org/10.1073/pnas.1804725115

Götzke, H., Kilisch, M., Martínez-Carranza, M., Sograte-Idrissi, S., Rajavel, A., Schlichthaerle, T., … Frey, S. (2019). A rationally designed and highly versatile epitope tag for nanobody-based purification, detection and manipulation of proteins. *BioRxiv*, 640771. https://doi.org/10.1101/640771

Greenberg, A. S., Avila, D., Hughes, M., Hughes, A., McKinney, E. C., & Flajnik, M. F. (1995). A new antigen receptor gene family that undergoes rearrangement and extensive somatic diversification in sharks. *Nature*, *374*(6518), 168–173. https://doi.org/10.1038/374168a0

Gupta, S., Thirstrup, D., Jarvis, T. C., Schneider, D. J., Wilcox, S. K., Carter, J., … Baird, G. S. (2011). Rapid Histochemistry Using Slow Off-rate Modified Aptamers With Anionic Competition. *Applied Immunohistochemistry & Molecular Morphology*, *19*(3), 273–278. https://doi.org/10.1097/PAI.0b013e3182008c29

Hamers-Casterman, C., Atarhouch, T., Muyldermans, S., Robinson, G., Hamers, C., Songa, E. B., … Hamers, R. (1993). Naturally occurring antibodies devoid of light chains. *Nature*, *363*(6428), 446–448. https://doi.org/10.1038/363446a0

Hardman, R. (2006). A Toxicologic Review of Quantum Dots: Toxicity Depends on Physicochemical and Environmental Factors. *Environmental Health Perspectives*, *114*(2), 165–172. https://doi.org/10.1289/ehp.8284

Hayashi, M. K., Tang, C., Verpelli, C., Narayanan, R., Stearns, M. H., Xu, R.-M., … Hayashi, Y. (2009). The Postsynaptic Density Proteins Homer and Shank Form a Polymeric Network Structure. *Cell*, *137*(1), 159–171. https://doi.org/10.1016/J.CELL.2009.01.050

Hell, S. W., & Wichmann, J. (1994). Breaking the diffraction resolution limit by stimulated emission: stimulated-emission-depletion fluorescence microscopy. *Optics Letters*, *19*(11), 780–782. Retrieved from http://www.ncbi.nlm.nih.gov/pubmed/19844443

Helma, J., Cardoso, M. C., Muyldermans, S., & Leonhardt, H. (2015). Nanobodies and recombinant binders in cell biology. *The Journal of Cell Biology*, *209*(5), 633–644. https://doi.org/10.1083/jcb.201409074

Hruska, M., Henderson, N., Le Marchand, S. J., Jafri, H., & Dalva, M. B. (2018). Synaptic nanomodules underlie the organization and plasticity of spine synapses. *Nature Neuroscience*, *21*(5), 671–682. https://doi.org/10.1038/s41593-018-0138-9

Hu, Y., Qu, L., & Schikorski, T. (2008). Mean synaptic vesicle size varies among individual excitatory hippocampal synapses. *Synapse*, *62*(12), 953–957. https://doi.org/10.1002/syn.20567

Huston, J. S., Levinson, D., Mudgett-Hunter, M., Tai, M. S., Novotny, J., Margolies, M. N., … Crea, R. (1988). Protein engineering of antibody binding sites: recovery of specific activity in an anti-digoxin single-chain Fv analogue produced in Escherichia coli. *Proceedings of the National Academy of Sciences*, *85*(16), 5879–5883. https://doi.org/10.1073/pnas.85.16.5879

Ingram, J. R., Schmidt, F. I., & Ploegh, H. L. (2018). Exploiting Nanobodies' Singular Traits. *Annual Review of Immunology*, *36*(1), 695–715. https://doi.org/10.1146/annurev-immunol-042617-053327

Ivanova, D., Dirks, A., Montenegro-Venegas, C., Schöne, C., Altrock, W. D., Marini, C., … Fejtova, A. (2015). Synaptic activity controls localization and function of Ct BP 1 via binding to B assoon and P iccolo. *The EMBO Journal*, *34*(8), 1056–1077. https://doi.org/10.15252/embj.201488796

Jank, L., Pinto-Espinoza, C., Duan, Y., Koch-Nolte, F., Magnus, T., & Rissiek, B. (2019). Current Approaches and Future Perspectives for Nanobodies in Stroke Diagnostic and Therapy. *Antibodies*, *8*(1), 5. https://doi.org/10.3390/antib8010005

Jinek, M., Chylinski, K., Fonfara, I., Hauer, M., Doudna, J. A., & Charpentier, E. (2012). A Programmable Dual-RNA-Guided DNA Endonuclease in Adaptive Bacterial Immunity. *Science*, *337*(6096), 816–821. https://doi.org/10.1126/science.1225829

Jungmann, R., Avendaño, M. S., Dai, M., Woehrstein, J. B., Agasti, S. S., Feiger, Z., … Yin, P. (2016). Quantitative super-resolution imaging with qPAINT. *Nature Methods*, *13*(5), 439–442. https://doi.org/10.1038/nmeth.3804

Jungmann, R., Avendaño, M. S., Woehrstein, J. B., Dai, M., Shih, W. M., & Yin, P. (2014). Multiplexed 3D cellular super-resolution imaging with DNA-PAINT and Exchange-PAINT. *Nature Methods*. https://doi.org/10.1038/nmeth.2835

Jungmann, R., Steinhauer, C., Scheible, M., Kuzyk, A., Tinnefeld, P., & Simmel, F. C. (2010). Single-Molecule Kinetics and Super-Resolution Microscopy by Fluorescence Imaging of Transient Binding on DNA Origami, *10*, 43. https://doi.org/10.1021/nl103427w

Köhler, G., & Milstein, C. (1975). Continuous cultures of fused cells secreting antibody of predefined specificity. *Nature*, *256*(5517), 495–497. Retrieved from http://www.ncbi.nlm.nih.gov/pubmed/1172191

Koide, A., & Koide, S. (2007). Monobodies: antibody mimics based on the scaffold of the fibronectin type III domain. *Methods in Molecular Biology (Clifton, N.J.)*, *352*, 95–109. https://doi.org/10.1385/1-59745-187-8:95

Koide, A., Tereshko, V., Uysal, S., Margalef, K., Kossiakoff, A. A., & Koide, S. (2007). Exploring the Capacity of Minimalist Protein Interfaces: Interface Energetics and Affinity Maturation to Picomolar KD of a Single-domain Antibody with a Flat Paratope. *Journal of Molecular Biology*, *373*(4), 941–953. https://doi.org/10.1016/j.jmb.2007.08.027

Kronqvist, N., Lofblom, J., Jonsson, A., Wernerus, H., & Stahl, S. (2008). A novel affinity protein selection system based on staphylococcal cell surface display and flow cytometry. *Protein Engineering Design and Selection*, *21*(4), 247–255. https://doi.org/10.1093/protein/gzm090

Kumaran, J., MacKenzie, C. R., & Arbabi-Ghahroudi, M. (2012). Semiautomated Panning of

Naive Camelidae Libraries and Selection of Single-Domain Antibodies Against Peptide Antigens. In *Single Domain Antibodies* (Vol. 911, pp. 105–124). Totowa, NJ: Humana Press. https://doi.org/10.1007/978-1-61779-968-6_7

Lagache, T., Grassart, A., Dallongeville, S., Faklaris, O., Sauvonnet, N., Dufour, A., … Olivo-Marin, J.-C. (2018). Mapping molecular assemblies with fluorescence microscopy and object-based spatial statistics. *Nature Communications*, *9*(1), 698. https://doi.org/10.1038/s41467-018-03053-x

Lam, A. Y., Pardon, E., Korotkov, K. V, Hol, W. G. J., & Steyaert, J. (2009). Nanobody-aided structure determination of the EpsI:EpsJ pseudopilin heterodimer from Vibrio vulnificus. *Journal of Structural Biology*, *166*(1), 8–15. https://doi.org/10.1016/j.jsb.2008.11.008

Lauwereys, M., Ghahroudi, M. A., Desmyter, A., Kinne, J., Hölzer, W., De Genst, E., … Muyldermans, S. (1998). Potent enzyme inhibitors derived from dromedary heavy-chain antibodies. *EMBO Journal*, *17*(13), 3512–3520. https://doi.org/10.1093/emboj/17.13.3512

Ledbetter, M. C., & Porter, K. R. (1964). Morphology of Microtubules of Plant Cell. *Science (New York, N.Y.)*, *144*(3620), 872–874. https://doi.org/10.1126/science.144.3620.872

Lee, Y. J., & Jeong, K. J. (2015). Challenges to production of antibodies in bacteria and yeast. *Journal of Bioscience and Bioengineering*, *120*(5), 483–490. https://doi.org/10.1016/J.JBIOSC.2015.03.009

Li, T., Vandesquille, M., Bay, S., Dhenain, M., Delatour, B., & Lafaye, P. (2017). Selection of similar single domain antibodies from two immune VHH libraries obtained from two alpacas by using different selection methods. *Immunology Letters*, *188*, 89–95. https://doi.org/10.1016/j.imlet.2017.07.001

Limsakul, P., Peng, Q., Wu, Y., Allen, M. E., Liang, J., Remacle, A. G., … Wang, Y. (2018). Directed Evolution to Engineer Monobody for FRET Biosensor Assembly and Imaging at Live-Cell Surface. *Cell Chemical Biology*, *25*(4), 370-379.e4. https://doi.org/10.1016/j.chembiol.2018.01.002

Lipman, N. S., Jackson, L. R., Trudel, L. J., & Weis-Garcia, F. (2005). Monoclonal Versus Polyclonal Antibodies: Distinguishing Characteristics, Applications, and Information Resources. *ILAR Journal*, *46*(3), 258–268. https://doi.org/10.1093/ilar.46.3.258

Liu, W., Song, H., Chen, Q., Yu, J., Xian, M., Nian, R., & Feng, D. (2018). Recent advances in the selection and identification of antigen-specific nanobodies. *Molecular Immunology*, *96*, 37–47. https://doi.org/10.1016/j.molimm.2018.02.012

Longo, P. A., Kavran, J. M., Kim, M.-S., & Leahy, D. J. (2013). Transient mammalian cell transfection with polyethylenimine (PEI). *Methods in Enzymology*, *529*, 227–240. https://doi.org/10.1016/B978-0-12-418687-3.00018-5

Lvov, A., Greitzer, D., Berlin, S., Chikvashvili, D., Tsuk, S., Lotan, I., & Michaelevski, I. (2009). Rearrangements in the Relative Orientation of Cytoplasmic Domains Induced by a Membrane-anchored Protein Mediate Modulations in Kv Channel Gating. *Journal of Biological Chemistry*, *284*(41), 28276–28291. https://doi.org/10.1074/jbc.M109.028761

Mahajan, S. P., Meksiriporn, B., Waraho-Zhmayev, D., Weyant, K. B., Kocer, I., Butler, D. C., … DeLisa, M. P. (2018). Computational affinity maturation of camelid single-domain intrabodies against the nonamyloid component of alpha-synuclein. *Scientific Reports*, *8*(1), 17611. https://doi.org/10.1038/s41598-018-35464-7

Maidorn, M., Olichon, A., Rizzoli, S. O., & Opazo, F. (2019). Nanobodies reveal an extra-

synaptic population of SNAP-25 and Syntaxin 1A in hippocampal neurons. *MAbs*, *11*(2), 305–321. https://doi.org/10.1080/19420862.2018.1551675

Maidorn, M., Rizzoli, S. O., & Opazo, F. (2016). Tools and limitations to study the molecular composition of synapses by fluorescence microscopy. *The Biochemical Journal*, *473*(20), 3385–3399. https://doi.org/10.1042/BCJ20160366

Mattson, G., Conklin, E., Desai, S., Nielander, G., Savage, M. D., & Morgensen, S. (1993). A practical approach to crosslinking. *Molecular Biology Reports*, *17*(3), 167–183. https://doi.org/10.1007/BF00986726

Mikhaylova, M., Cloin, B. M. C., Finan, K., van den Berg, R., Teeuw, J., Kijanka, M. M., … Kapitein, L. C. (2015). Resolving bundled microtubules using anti-tubulin nanobodies. *Nature Communications*, *6*, 7933. https://doi.org/10.1038/ncomms8933

Modi, S., Higgs, N. F., Sheehan, D., Griffin, L. D., & Kittler, J. T. (2018). Quantum dot conjugated nanobodies for multiplex imaging of protein dynamics at synapses. *Nanoscale*, *10*(21), 10241–10249. https://doi.org/10.1039/C7NR09130C

Morrison, C. (2019). Nanobody approval gives domain antibodies a boost. *Nature Reviews Drug Discovery*, *18*(7), 485–487. https://doi.org/10.1038/d41573-019-00104-w

Muyldermans, S. (2013). Nanobodies: Natural Single-Domain Antibodies. *Annual Review of Biochemistry*, *82*(1), 775–797. https://doi.org/10.1146/annurev-biochem-063011-092449

Nilsson, F. Y., & Tolmachev, V. (2007). Affibody molecules: new protein domains for molecular imaging and targeted tumor therapy. *Current Opinion in Drug Discovery & Development*, *10*(2), 167–175. Retrieved from http://www.ncbi.nlm.nih.gov/pubmed/17436552

Pardon, E., Laeremans, T., Triest, S., Rasmussen, S. G. F., Wohlkönig, A., Ruf, A., … Steyaert, J. (2014). A general protocol for the generation of Nanobodies for structural biology. *Nature Protocols*, *9*(3), 674–693. https://doi.org/10.1038/nprot.2014.039

Pleiner, T., Bates, M., & Görlich, D. (2018). A toolbox of anti-mouse and anti-rabbit IgG secondary nanobodies. *The Journal of Cell Biology*, *217*(3), 1143–1154. https://doi.org/10.1083/jcb.201709115

Pleiner, T., Bates, M., Trakhanov, S., Lee, C.-T., Schliep, J. E., Chug, H., … Görlich, D. (2015). Nanobodies: site-specific labeling for super-resolution imaging, rapid epitope-mapping and native protein complex isolation. *ELife*, *4*, e11349. https://doi.org/10.7554/eLife.11349

Plückthun, A. (2015). Designed ankyrin repeat proteins (DARPins): binding proteins for research, diagnostics, and therapy. *Annual Review of Pharmacology and Toxicology*, *55*, 489–511. https://doi.org/10.1146/annurev-pharmtox-010611-134654

Porter, R. R. (1959). The hydrolysis of rabbit y-globulin and antibodies with crystalline papain. *The Biochemical Journal*, *73*, 119–126. Retrieved from http://www.pubmedcentral.nih.gov/articlerender.fcgi?artid=1197021&tool=pmcentrez&rendertype=abstract

Qu, L., Akbergenova, Y., Hu, Y., & Schikorski, T. (2009). Synapse-to-synapse variation in mean synaptic vesicle size and its relationship with synaptic morphology and function. *The Journal of Comparative Neurology*, *514*(4), 343–352. https://doi.org/10.1002/cne.22007

Ries, J., Kaplan, C., Platonova, E., Eghlidi, H., & Ewers, H. (2012). A simple, versatile method for GFP-based super-resolution microscopy via nanobodies. *Nature Methods*, *9*(6), 582–

584. https://doi.org/10.1038/nmeth.1991

Rizzoli, S. O. (2014). Synaptic vesicle recycling: steps and principles. *The EMBO Journal*, *33*(8), 788–822. https://doi.org/10.1002/embj.201386357

Rust, M. J., Bates, M., & Zhuang, X. (2006). Sub-diffraction-limit imaging by stochastic optical reconstruction microscopy (STORM). *Nature Methods*, *3*(10), 793–796. https://doi.org/10.1038/nmeth929

Ryckaert, S., Pardon, E., Steyaert, J., & Callewaert, N. (2010). Isolation of antigen-binding camelid heavy chain antibody fragments (nanobodies) from an immune library displayed on the surface of Pichia pastoris. *Journal of Biotechnology*, *145*(2), 93–98. https://doi.org/10.1016/j.jbiotec.2009.10.010

Sakamoto, Y., Tanaka, N., Ichimiya, T., Kurihara, T., & Nakamura, K. T. (2005). Crystal Structure of the Catalytic Fragment of Human Brain 2′,3′-Cyclic-nucleotide 3′-Phosphodiesterase. *Journal of Molecular Biology*, *346*(3), 789–800. https://doi.org/10.1016/J.JMB.2004.12.024

Salema, V., & Fernández, L. Á. (2017). Escherichia coli surface display for the selection of nanobodies. *Microbial Biotechnology*, *10*(6), 1468–1484. https://doi.org/10.1111/1751-7915.12819

Scarnati, M. S., Kataria, R., Biswas, M., & Paradiso, K. G. (2018). Active presynaptic ribosomes in the mammalian brain, and altered transmitter release after protein synthesis inhibition. *ELife*, *7*. https://doi.org/10.7554/eLife.36697

Schenck, S., Kunz, L., Sahlender, D., Pardon, E., Geertsma, E. R., Savtchouk, I., … Dutzler, R. (2017). Generation and Characterization of Anti-VGLUT Nanobodies Acting as Inhibitors of Transport. *Biochemistry*, *56*(30), 3962–3971. https://doi.org/10.1021/acs.biochem.7b00436

Schermelleh, L., Ferrand, A., Huser, T., Eggeling, C., Sauer, M., Biehlmaier, O., & Drummen, G. P. C. (2019). Super-resolution microscopy demystified. *Nature Cell Biology*, *21*(1), 72–84. https://doi.org/10.1038/s41556-018-0251-8

Schlichthaerle, T., Eklund, A. S., Schueder, F., Strauss, M. T., Tiede, C., Curd, A., … Jungmann, R. (2018). Site-Specific Labeling of Affimers for DNA-PAINT Microscopy. *Angewandte Chemie International Edition*, *57*(34), 11060–11063. https://doi.org/10.1002/anie.201804020

Schnitzbauer, J., Strauss, M. T., Schlichthaerle, T., Schueder, F., & Jungmann, R. (2017). Super-resolution microscopy with DNA-PAINT. *Nature Protocols*, *12*(6), 1198–1228. https://doi.org/10.1038/nprot.2017.024

Schueder, F., Lara-Gutiérrez, J., Beliveau, B. J., Saka, S. K., Sasaki, H. M., Woehrstein, J. B., … Jungmann, R. (2017). Multiplexed 3D super-resolution imaging of whole cells using spinning disk confocal microscopy and DNA-PAINT. *Nature Communications*, *8*(1), 2090. https://doi.org/10.1038/s41467-017-02028-8

Seitz, K. J., & Rizzoli, S. O. (2019). GFP nanobodies reveal recently-exocytosed pHluorin molecules. *Scientific Reports*, *9*(1), 7773. https://doi.org/10.1038/s41598-019-44262-8

Shashkova, S., & Leake, M. C. (2017). Single-molecule fluorescence microscopy review: shedding new light on old problems. *Bioscience Reports*, *37*(4). https://doi.org/10.1042/BSR20170031

Skerra, A. (2008). Alternative binding proteins: anticalins - harnessing the structural plasticity of the lipocalin ligand pocket to engineer novel binding activities. *The FEBS Journal*,

275(11), 2677–2683. https://doi.org/10.1111/j.1742-4658.2008.06439.x

Smith, G. (1985). Filamentous fusion phage: novel expression vectors that display cloned antigens on the virion surface. *Science*, *228*(4705), 1315–1317. https://doi.org/10.1126/science.4001944

Soler, M. A., Fortuna, S., de Marco, A., & Laio, A. (2018). Binding affinity prediction of nanobody–protein complexes by scoring of molecular dynamics trajectories. *Physical Chemistry Chemical Physics*, *20*(5), 3438–3444. https://doi.org/10.1039/C7CP08116B

Stack, E. C., Wang, C., Roman, K. A., & Hoyt, C. C. (2014). Multiplexed immunohistochemistry, imaging, and quantitation: A review, with an assessment of Tyramide signal amplification, multispectral imaging and multiplex analysis. *Methods*, *70*(1), 46–58. https://doi.org/10.1016/J.YMETH.2014.08.016

Takei, K., Mundigl, O., Daniell, L., & De Camilli, P. (1996). The synaptic vesicle cycle: a single vesicle budding step involving clathrin and dynamin. *The Journal of Cell Biology*, *133*(6), 1237–1250. https://doi.org/10.1083/jcb.133.6.1237

Terry-Lorenzo, R. T., Torres, V. I., Wagh, D., Galaz, J., Swanson, S. K., Florens, L., … Garner, C. C. (2016). Trio, a Rho Family GEF, Interacts with the Presynaptic Active Zone Proteins Piccolo and Bassoon. *PLOS ONE*, *11*(12), e0167535. https://doi.org/10.1371/journal.pone.0167535

Thastrup, O., Tullin, S., Kongsbak Poulsen, L., & Bjørn, S. (n.d.). Fluorescent proteins. US patent 6172188. Retrieved from https://worldwide.espacenet.com/publicationDetails/biblio?CC=US&NR=6172188&KC=&FT=E&locale=en_EP#

Tiede, C., Tang, A. A. S., Deacon, S. E., Mandal, U., Nettleship, J. E., Owen, R. L., … McPherson, M. J. (2014). Adhiron: a stable and versatile peptide display scaffold for molecular recognition applications. *Protein Engineering, Design and Selection*, *27*(5), 145–155. https://doi.org/10.1093/protein/gzu007

Vaks, L., & Benhar, I. (2014). Production of Stabilized scFv Antibody Fragments in the E. coli Bacterial Cytoplasm (pp. 171–184). Humana Press, Totowa, NJ. https://doi.org/10.1007/978-1-62703-586-6_10

Vangindertael, J., Camacho, R., Sempels, W., Mizuno, H., Dedecker, P., & Janssen, K. P. F. (2018). An introduction to optical super-resolution microscopy for the adventurous biologist. *Methods and Applications in Fluorescence*, *6*(2), 022003. https://doi.org/10.1088/2050-6120/aaae0c

Vaughan, T. J., Williams, A. J., Pritchard, K., Osbourn, J. K., Pope, A. R., Earnshaw, J. C., … Johnson, K. S. (1996). Human Antibodies with Sub-nanomolar Affinities Isolated from a Large Non-immunized Phage Display Library. *Nature Biotechnology*, *14*(3), 309–314. https://doi.org/10.1038/nbt0396-309

Von Pawel-Rammingen, U., Johansson, B. P., & Björck, L. (2002). IdeS, a novel streptococcal cysteine proteinase with unique specificity for immunoglobulin G. *EMBO Journal*, *21*(7), 1607–1615. https://doi.org/10.1093/emboj/21.7.1607

Wade, O. K., Woehrstein, J. B., Nickels, P. C., Strauss, S., Stehr, F., Stein, J., … Jungmann, R. (2019). 124-Color Super-resolution Imaging by Engineering DNA-PAINT Blinking Kinetics. *Nano Letters*, acs.nanolett.9b00508. https://doi.org/10.1021/acs.nanolett.9b00508

Walling, M. A., Novak, J. A., & Shepard, J. R. E. (2009). Quantum dots for live cell and in vivo

imaging. *International Journal of Molecular Sciences*, *10*(2), 441–491. https://doi.org/10.3390/ijms10020441

Waterhouse, P., Griffiths, A. D., Johnson, K. S., & Winter, G. (1993). Combinatorial infection and *in vivo* recombination: a strategy for making large phage antibody repertoires. *Nucleic Acids Research*, *21*(9), 2265–2266. https://doi.org/10.1093/nar/21.9.2265

Weng, J., & Ren, J. (2006). Luminescent quantum dots: a very attractive and promising tool in biomedicine. *Current Medicinal Chemistry*, *13*(8), 897–909. Retrieved from http://www.ncbi.nlm.nih.gov/pubmed/16611074

Wiedenmann, J., Oswald, F., & Nienhaus, G. U. (2009). Fluorescent proteins for live cell imaging: Opportunities, limitations, and challenges. *IUBMB Life*, *61*(11), 1029–1042. https://doi.org/10.1002/iub.256

Wilhelm, B. G., Mandad, S., Truckenbrodt, S., Kröhnert, K., Schäfer, C., Rammner, B., … Rizzoli, S. O. (2014). Composition of isolated synaptic boutons reveals the amounts of vesicle trafficking proteins. *Science (New York, N.Y.)*, *344*(6187), 1023–1028. https://doi.org/10.1126/science.1252884

Xu, C., Yang, Y., Liu, L., Li, J., Liu, X., Zhang, X., … Liu, X. (2018). Microcystin-LR nanobody screening from an alpaca phage display nanobody library and its expression and application. *Ecotoxicology and Environmental Safety*, *151*, 220–227. https://doi.org/10.1016/j.ecoenv.2018.01.003

Yan, J., Li, G., Hu, Y., Ou, W., & Wan, Y. (2014). Construction of a synthetic phage-displayed Nanobody library with CDR3 regions randomized by trinucleotide cassettes for diagnostic applications. *Journal of Translational Medicine*, *12*(1), 343. https://doi.org/10.1186/s12967-014-0343-6

Yau, K. Y. F., Dubuc, G., Li, S., Hirama, T., MacKenzie, C. R., Jermutus, L., … Tanha, J. (2005). Affinity maturation of a VHH by mutational hotspot randomization. *Journal of Immunological Methods*, *297*(1–2), 213–224. https://doi.org/10.1016/J.JIM.2004.12.005

Zimmermann, I., Egloff, P., Hutter, C. A., Arnold, F. M., Stohler, P., Bocquet, N., … Seeger, M. A. (2018). Synthetic single domain antibodies for the conformational trapping of membrane proteins. *ELife*, *7*. https://doi.org/10.7554/eLife.34317

Zrazhevskiy, P., & Gao, X. (2013). Quantum dot imaging platform for single-cell molecular profiling. *Nature Communications*, *4*(1), 1619. https://doi.org/10.1038/ncomms2635

Zuo, J., Li, J., Zhang, R., Xu, L., Chen, H., Jia, X., … Xie, W. (2017). Institute collection and analysis of Nanobodies (iCAN): a comprehensive database and analysis platform for nanobodies. *BMC Genomics*, *18*(1), 797. https://doi.org/10.1186/s12864-017-4204-6

8. List of abbreviations

Ab	Antibody
Amp	Ampicillin
(k)bp	(kilo)base pair
(k)Da	(kilo)Dalton
DNA	Deoxyribonucleic acid
DTT	Dithiothreitol
GFP	Green fluorescent protein
hcAb	Heavy chain antibody
HEPES	4-(2-hydroxyethyl)-1-piperazineethanesulfonic acid
HILO	Highly inclined and laminated optical sheet
HRP	Horseradish peroxidase
Kan	Kanamycin
kD	Equilibrium dissociation constant
min	Minutes
Nb	Nanobody
nm	Nanometer
PAINT	Point Accumulation for Imaging in Nanoscale Topography
PALM	Photo-activated localization microscopy
PBS	Phosphate-buffered saline
PMSF	Phenylmethylsulfonylfluorid
RESOLFT	Reversible Saturable optical Fluorescence Transitions
RNA	Ribonucleic acid
rpm	Revolutions per minute
RT	Room temperature
SDS	Sodium dodecyl sulfate
s.d	Standard deviation
s.e.m	Standard error of the mean
sdAb	Single domain Antibody
SMLM	Single molecule localization microscopy

STED	Stimulated emission depletion microscopy
STORM	Stochastic optical reconstruction microscopy
TIR(F)	Total internal reflection (fluorescence)
Tmp	Trimethoprim

9. Acknowledgements

First, I would like to thank my two supervisors Prof. Silvio Rizzoli and Dr. Felipe Opazo. Silvio, thank you for giving me the opportunity to work in this project, for the instructive advice on how to build a scientific career and navigate through the academic world. Felipe, thank you for your supervision, for sharing your knowledge and experience and giving me a great environment for my PhD, I could not have hoped for a better supervisor.

I would like to extend my gratitude to Prof. Peter Rehling and Prof. Blanche Schwappach-Pignataro for their time and advice throughout my whole PhD. I would like to thank the IMPRS Molbio and the GGNB office shaping us as scientists and beyond and giving us such incredible opportunities Thank you Kerstin Grüniger and Kirsten Pöhlker for their help and availability. A special thank you goes to Dr. Steffen Burkhardt without his presence, the graduate program would not be the same. Thank you for being a great mentor and taking great care of us.

I would also like to thank my collaborators Dr. Roman Tzukanov and Nazar Oleksiievets for putting together and realizing a great project, Prof. Ralf Jungmann and Thomas Schlichthaerle for welcoming me in their team and being great collaborators, Dr. Steffen Frey for his help and Carlos Duque Afonso for his creative and good work.

I would like to thank all the lab members. In particular, Dr. Manuel Maidorn for his invaluable initial training and constant support throughout the years. I would also like to thank Dr. Eugenio Fornasiero and Dr. Martin Helm for being extremely helpful and giving me great advices. I would like to thank Dr. Sebastian Jähne for his help in proofreading and microscopy expertise. I would like to thank Dr. Mihai Alevra for his help with data analysis.

Thanks to Dr. Selda Kabatas, for her constant support in every lab and life challenge. I could not have wished for a better office mate. I would like to thank Sinem Sertel for her constant moral support, encouragement and friendship.

I would like to thank Dr. Carlo Breda and Prof. Flaviano Giorgini for being the best first supervisors one could wish for. Thank you for making it such a pleasant first dive in the academic world and thank you for believing in me.

Grazie a Professoressa Lucia Palmieri, che educandomi e crescendomi, mi ha trasmesso la passione per la scienza e l'infastidimento per le cose illlogiche.

For all my beloved people, who supported me and loved me throughout this work and beyond. Thank you.

10. List of pubblications

Sograte-Idrissi S. *et al.* "Circumvention of common labelling artefacts using secondary nanobodies" *Nanoscale***,**12, 10226-1023 (2020).

Götzke H, Kilisch M, Martínez-Carranza M, **Sograte-Idrissi S** et *al*. "The ALFA-tag is a highly versatile tool for nanobody-based bioscience applications". *Nature Communications* 10, 4403 (2019).

Sograte-Idrissi S. *et al.* "Nanobody Detection of Standard Fluorescent Proteins Enables Multi-Target DNA-PAINT with High Resolution and Minimal Displacement Errors". *Cells mdpi* **8**, 48 (2019).

Gomes de Castro M.A, Wildhagen H, **Sograte-Idrissi S.** et *al*. "Differential organization of tonic and chronic B cell antigen receptors in the plasma membrane". *Nature Communications.* 10, 820 (2019).

Breda C., Sathyasaikumar K.V, **Sograte Idrissi S.** et *al*. "Tryptophan-2,3-dioxygenase (TDO) inhibition ameliorates neurodegeneration by modulation of kynurenine pathway metabolites". *Proceedings of the National Academy of Sciences of the United States of America*, 113(19), 5435–5440 (2016).